Department of Precision and Microsystems Engineering

Evaporation control of femtoliter droplets to obtain less than 500 nm vitreous ice for high resolution CryoEM

Jelle Johannes Mens

Report no : 2024.066
Coach : dr. V.U. Shastri
Professor : dr. M.K. Ghatkesar
Specialisation : Mechatronic System Design
Type of report: Master thesis
Date : 14-08-2024

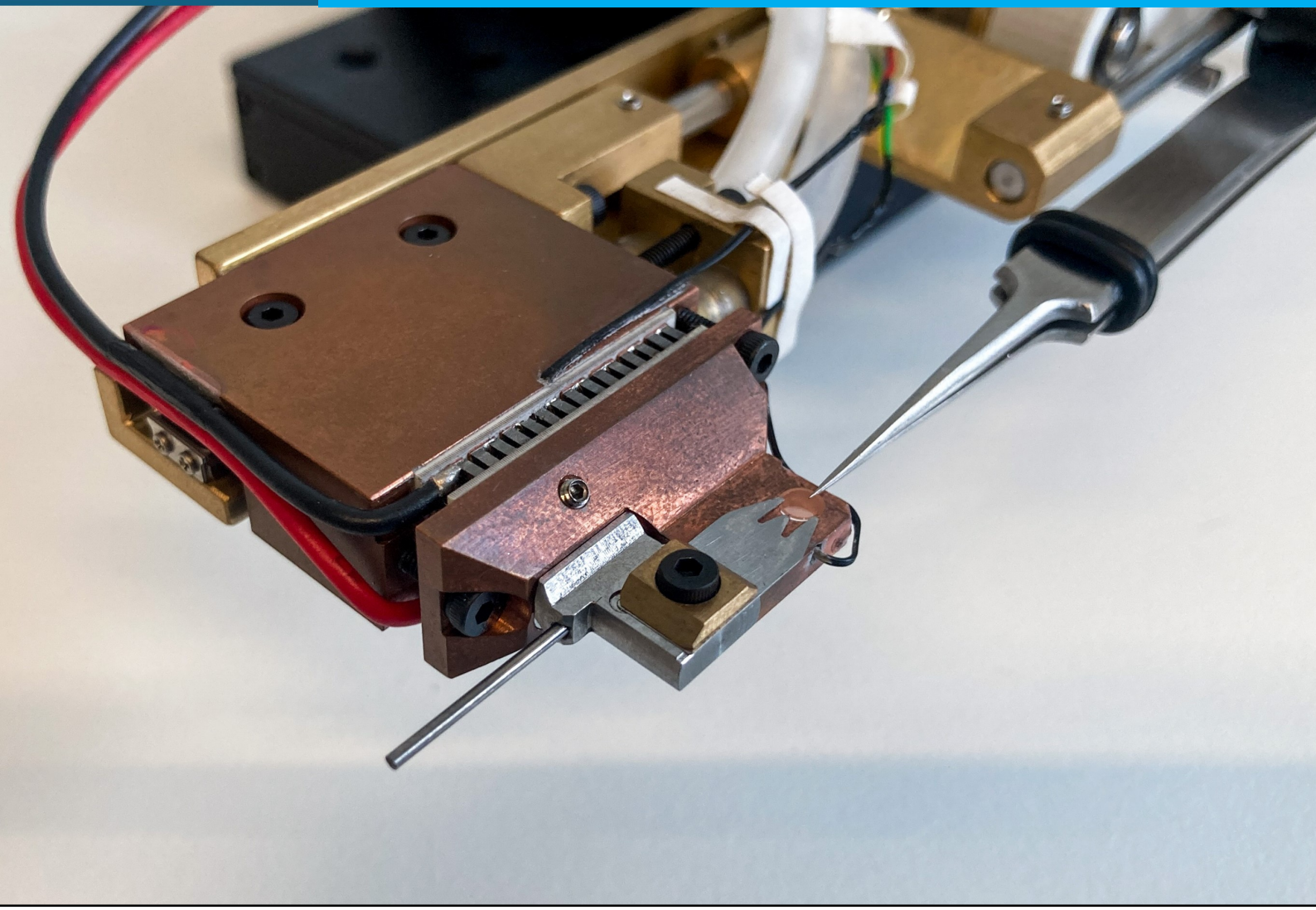

TU Delft Delft University of Technology

Challenge the future

Evaporation control of femtoliter droplets to obtain less than 500nm vitreous ice for high resolution CryoEM

by

Jelle Mens

To obtain the degree of Master of Science
at the Delft University of Technology,
To be defended publicly on Wednesday August 21, 2024 at 12:00 AM.

Student number:	4594584	
Supervisor:	dr. M. K. Ghatkesar,	TU Delft
Daily supervisor:	dr. V. U. Shastri,	TU Delft
Collaborator:	dr. A. Jacobi,	TU Delft

TU Delft

Contents

Part I

Thesis Paper

Evaporation control of femtoliter droplets to obtain less than 500nm vitreous ice for high resolution CryoEM

Abstract

Subcellular biopsy (SCB) using atomic force microscopy (AFM) with a microfluidic cantilever enables the extraction of biological samples from living cells. Traditional cryo-electron microscopy (cryo-EM) sample preparation methods are unsuitable for the small volumes from SCB. This study presents a novel method to prepare cryo-EM samples directly from SCB samples, integrating dispensing, thickness measurement, and local temperature control to minimize evaporation. The method uses a microfluidic AFM cantilever for dispensing, a Mach-Zehnder interferometer for real-time thickness measurement, and plunge freezing for vitrification. The system successfully demonstrated dispensing picoliter droplets, with potential for femtoliter volumes. The temperature-controlled grid holder reduced evaporation rates, allowing sufficient time for real-time thickness measurement. The system has demonstrated the required transition speed and plunge velocity. Initial cryo-EM thickness measurements demonstrate the method's potential. In conclusion, a novel system for subcellular biopsy sample preparation for cryo-EM was designed, fabricated, and tested. It maintains picoliter sample volumes on a temperature-controlled EM grid, enabling real-time thickness measurement and immediate plunge freezing.

1. Introduction

Subcellular biopsy (SCB) is performed using an atomic force microscope equipped with a microfluidic cantilever to obtain biological samples from living cells. Cryo-electron microscopy (cryo-EM) is the main technique for producing high-resolution 2D and 3D sub-nanometer structures, utilizing a transmission electron microscope (TEM). TEM samples are thin vitreous ice layers, less than $500\,\mathrm{nm}$ thick, containing the bio-material of interest, with the ice layer being only slightly thicker than the bio molecules within it. Sample preparation for cryo-EM involves several steps: dispersing biological material in an aqueous solution on a TEM-specific sample grid, controlling thickness (e.g., blotting using commercial machines like Vitrobot from ThermoFisher [14]), and plunging the grid into liquid ethane at temperatures below $100\,\mathrm{K}$ to achieve the cooling rates necessary for vitreous ice. However, this preparation method requires a starting sample volume in microliters, with more than $99\,\%$ lost during blotting. SCB samples, with volumes in fL or pL, cannot be prepared using these methods. This work presents a new sample preparation method, allowing SCB samples to be directly dispensed on the EM grid with a microfluidic AFM cantilever post-SCB procedure. The thickness is measured using a Mach-Zehnder interferometer, and thickness reduction is managed through controlled evaporation until the desired thickness is achieved. The sample is then vitrified using plunge freezing. This method connects SCB with microfluidic AFM, real-time thickness measurement, and plunge-freezing, aiming to reduce processing time and sample evaporation, ensuring sufficient time for each step. Previous work (AFM4cryoEM)[12] used global humidity and local temperature control to reduce evaporation but did not include a method to check sample thickness before plunge freezing, complicating successful preparation assessment prior to CryoEM analysis. Knowing the ice layer thickness before CryoEM analysis would improve system reliability and throughput. The new method presented in this work integrates all necessary process steps within AFM4cryoEM, including real-time thickness measurement.

2. System design

2.1. Requirements

The new system must integrate three processes: dispensing, thickness control, and vitrification. Each part of the process takes time, so a method to slow down sample evaporation after dispensing is essential. Under normal ambient conditions, the evaporation of a pL volume sample would occur in less than a second after being dispensed on the EM grid. The general requirements for the system are as follows:

1. Dispense a femtoliter sample on an EM grid.
2. Limit the evaporation of the sample.
3. Perform real-time thickness measurement on the sample.
4. Reduce sample thickness to less than $500\,\mathrm{nm}$.
5. Vitrify the sample directly after a predetermined thickness is measured.

Different methods can be implemented, with the choice and order of operations determined by the specific requirements and constraints of each process.

During the dispensing step, the AFM is stationary and positioned on a microscope that views the process from below. The space between the AFM cantilever and the microscope objective is very limited, with only $3\,\mathrm{mm}$ of clearance at the narrowest part, determined by the microscope objective's focal length, as shown in Figure 2.1. The maximum allowed relative humidity around the AFM is $70\,\%$, and dispensing must be done on a horizontal EM grid.

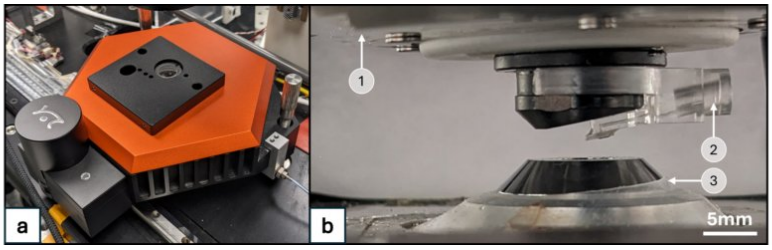

Figure 2.1: a: Atomic force microscope. **b:** Available space between 1: The bottom of the AFM, 2: The microfluidic cantilever, and 3: The microscope objective.

The measurement technique is a direct implementation of the method developed by [2] in previous work. It relies on retrieving the shape and thickness of a sample droplet from the fringe pattern produced by a Mach-Zehnder interferometer. To ensure sufficient data for analysis, the sample droplet should be placed in the middle of the grid square without touching the surrounding grid bars. Space is needed on both sides of the EM grid for optical elements to direct the laser beam through the sample. Consequently, the dispense location cannot be the same as the measurement location, as the microscope objective and optical elements of the interferometer occupy the same space. The field of view for this measurement method is approximately $150\,\mu\mathrm{m}$ x $200\,\mu\mathrm{m}$, which is sufficient to view one entire grid square.

Vitrification is typically achieved through plunge freezing. If the water layer on the grid is thin enough and the entry velocity into the liquid ethane exceeds $1.5\,\mathrm{m\,s^{-1}}$, a cooling rate of more than $10^4\,\mathrm{K\,s^{-1}}$ can be reached [4], which is necessary to create vitreous ice. The ethane cup is stationary, and the plunging motion is performed with a vertically oriented EM grid.

Evaporation control is primarily achieved by altering environmental conditions to keep the sample temperature close to the dew point temperature of its surroundings, theoretically stopping evaporation.

The dew point depends on temperature and relative humidity, both of which can be controlled to reduce sample evaporation. One method involves using a process chamber to bring relative humidity close to $100\,\%$, matching room temperature with the dew point and minimizing evaporation. Another method is locally cooling the sample to the dew point temperature, achieving local $100\,\%$ relative humidity. Humidity control requires a process chamber around the sample preparation device, but at $100\,\%$ relative humidity, most electronics, optics, and movement mechanisms perform poorly, imposing stricter requirements on these components. The main challenge with local temperature control is the limited space between the AFM and the microscope objective. Good thermal contact between the EM grid and the temperature controller is essential. Additionally, the mechanical transfer of the EM grid from the temperature controller to the plunge freeze operation exposes the grid to ambient conditions, as there is no global control with a process chamber. In this work, local temperature control is used to avoid additional humidity requirements on major components.

2.2. Temperature controlled grid holder

Figure 2.2 shows a schematic overview of all the major components needed for the temperature controller or dew point stage (DP stage). A thermoelectric cooler (TEC) is used as the temperature control element. It performs heat transport when a control current is applied. The side that gets cold is mounted towards the grid holder, while the side that gets hot is mounted to a water block that can transport the excess heat away from the temperature controller. Water cooling was chosen over forced convective cooling for two reasons. First, the limited space makes it difficult to implement a cooling element large enough to allow for forced convective cooling. Second, the excessive airflow resulting from this method could disturb the dispensing operation and the sample after dispensing. The temperatures on the hot and cold sides are measured with NTC sensors. The TEC controller reads these temperature sensors and uses a PID control loop to maintain an accurate temperature on the cold side of the TEC. The dew point is measured with an off-the-shelf dew point sensor that measures temperature, absolute humidity, and relative humidity, and sends this information via USB to a computer. Based on these data, the set point is determined for the temperature of the grid holder.

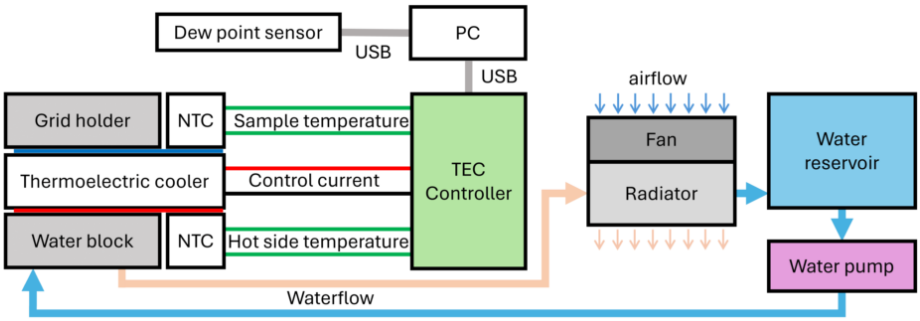

Figure 2.2: Schematic system overview of all relevant components required for a functional DP stage.

DP stage design

The physical dimensions of the dew point stage are determined by the available space. The final design is shown in Figure 2.3. Major components include a copper water block **1**, TEC **2**, copper grid holder **3**, and grid clip **6**. The grid holder is $2.5\,\mathrm{mm}$ thick at the section between the AFM and objective, with a $2.5\,\mathrm{mm}$ hole below the EM grid, relieved with a $45°$ taper to clear the microscope's optical path. The temperature sensor **10**, shown enlarged in Figure D, has a diameter of $0.8\,\mathrm{mm}$ and is positioned $0.3\,\mathrm{mm}$ from the EM grid edge to measure the temperature close to the sample. The EM grid is secured with a $0.1\,\mathrm{mm}$ thick spring steel clip with three fingers holding the grid at the edge. The water block's inlet **8** and outlet **9** are positioned to keep the inlet closest to the heat source, with the hot side temperature measured by sensor **11**. The selected TEC is the largest element that fits in the confined space, ensuring a fast thermal response for cooling to a target temperature, though not needed for steady-state operations. A detailed explanation of part selection and design considerations can be found in Supplementary 1.

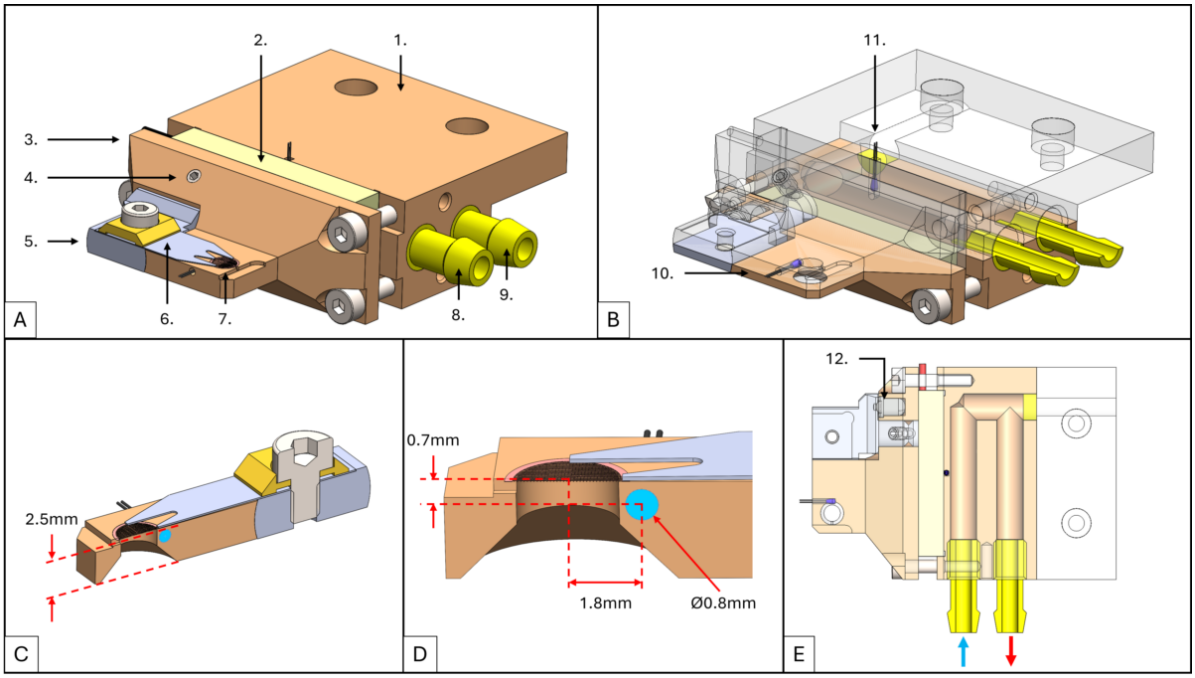

Figure 2.3: A: 1: Water block, **2:** TEC, **3:** Grid holder, **4:** Lock screw, **5:** Clip carrier, **6:** Grid clip, **7:** EM grid, **8:** Water inlet, **9:** Water outlet. **B: 10:** Grid temperature sensor, **11:** Hot side temperature sensor. **C:** Section view through the middle of the EM grid. **D:** Zoom in of Section view C, showing the relative position between the temperature sensor and the EM grid. **E:** Section view to show the flow path through the water block.

2.3. Motion sequence scheme

The system must integrate dispensing, thickness measurement, and plunge freezing operations with specific requirements. The transition time must be less than $300\,\mu s$, and the plunge freeze speed should exceed $1.5\,m\,s^{-1}$.

The main constraints include the requirement that dispensing must be done on a horizontal grid, and that thickness measurement cannot occur at the dispensing position. Additionally, plunge freezing is performed with a vertical EM grid. Several process steps need to be considered. The grid needs to rotate at some point, and thickness measurement can be done either before or after this rotation. The release of the EM grids from the temperature controller can also be performed before or after rotation. Measuring before rotation benefits from keeping the droplet in the same XY plane as the dispensing step, simplifying droplet location. However, measuring after rotation complicates locating the droplet again and positioning it in the interferometer's field of view, requiring an additional motion axis. Releasing the EM grid from the dew point stage before rotating reduces mechanical complexity but necessitates rotation to occur in ambient conditions.

The EM grid is held in the tweezers throughout the entire process. Literature examples, such as AFM4cryoEM [12], vitrojet [13], and the Linkham plunger [9], use complex pick-and-place motions with the EM grid and tweezers, aiding automation and improving throughput. See literature study 2.7, 2.5, and 2.6 for their detailed system descriptions. However, for this proof of concept, automation and improving throughput are not yet considered, and the EM grid is placed in the tweezers before loading into the system.

An additional challenge is that the EM grid requires horizontal XY motion freedom during dispensing and measurement, and it needs to be vertical and attached to the plunger for plunge freezing. One solution, described by [1], is the CryoWriter, which also involves a horizontal sample retrieval and dispensing method transitioning to vertical plunge freeze motion. Their solution to this problem is implemented with their Cryodrop system. A detailed explanation of the system can be found in literature study 2.4. It has a stationary plunger and attaches the tweezers to the plunger after measurement and after releasing the EM grid from the DP stage. This is done by retracting the tweezers to release the EM grid and dropping

the tweezers near the stationary plunger, which attracts and catches the tweezers with a magnet.

There are, however, other ways to solve this practical problem. A complete analysis that evaluated all possible system configurations was performed to find a solution with the lowest system complexity; see Appendix A for the complete analysis. The solution implemented in this work relies on two requirements: the total movement range needed to position the sample in the field of view of the thickness measurement, which is $\pm\ 1.5\,\mathrm{mm}$ in X and Y, and the minimum position accuracy needed to position the plunger above the ethane cup, which has a $20\,\mathrm{mm}$ internal diameter. To avoid touching the walls during plunging, the plunging area is limited to an $8\,\mathrm{mm}$ diameter in the center. Since the plunging area is larger than the movement range needed for thickness measurement, the plunger can be mounted directly to the XY stage used for positioning, with tweezers attached on a hinge pin. This setup allows the plunger to be in the correct position for plunging at any measurement, with the tweezers only needing to rotate $90°$ to move the grid to the plunge start position, eliminating the need for additional motion in X and Y after thickness measurement. Release of the EM grid and tweezers from the dew point stage can be achieved by moving the dew point stage in one axis instead of moving the EM grid. Figure 2.4 shows the complete motion description.

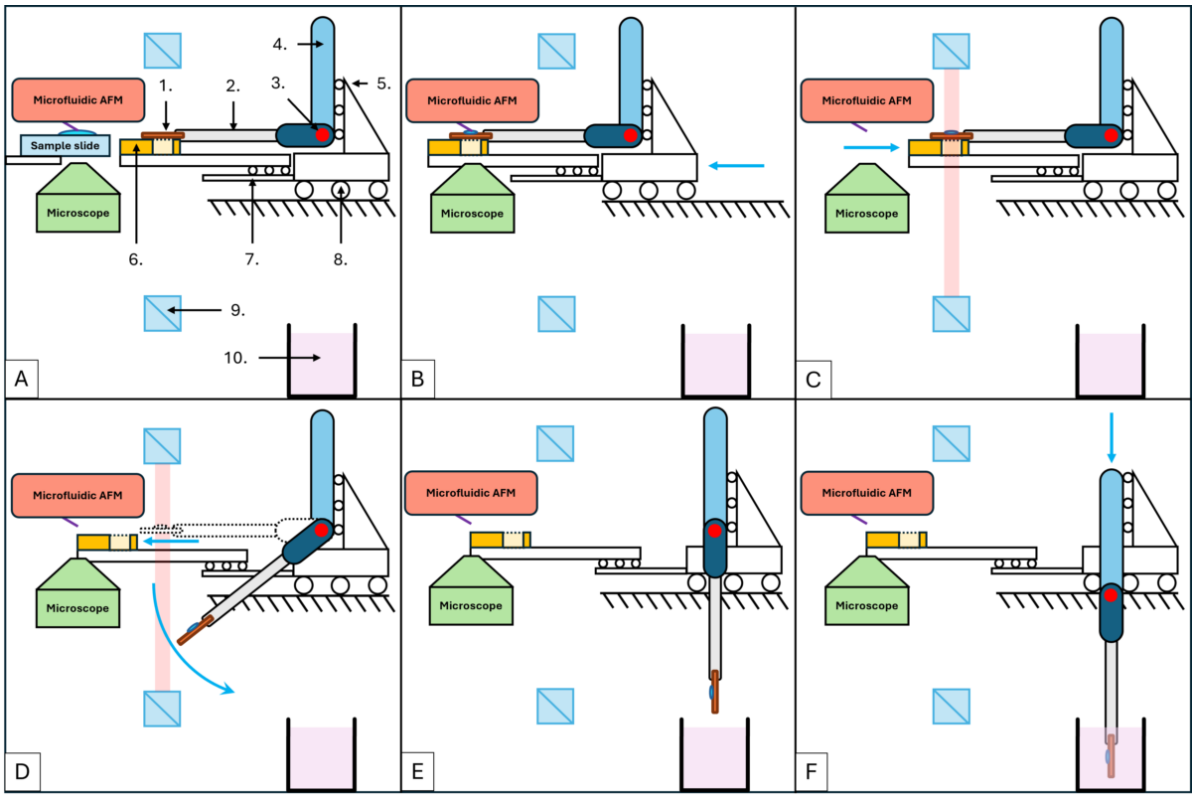

Figure 2.4: A: SCB step, components: **1:** EM grid, **2:** Tweezers, **3:** Hinge pin, **4:** Plunger, **5:** Linear guide for plunger, **6:** DP stage, **7:** Linear guide for DP stage, **8:** XY motion stage for positioning the grid throughout the process, **9:** Mach-Zehnder interferometer, **10:** Ethane cup. **B:** The mechanism is positioned between the AFM and the microscope to dispense on the EM grid. **C:** The XY motion stage transports the EM grid to the measurement location; thickness is measured in real time until a thickness below a predetermined threshold is reached. **D:** The DP stage is actuated sideways to release the EM grid and tweezers; the tweezers rotate down due to gravity. **E:** The EM grid ends up in the plunge start position without the need for additional positioning with the XY motion stage. **F:** The plunger is activated, and the sample is vitrified.

Plunge mechanism design

The physical design of the plunge freeze mechanism is illustrated in Figure 2.5. Four image sequences highlight its main functionalities. Sequence C1-3 demonstrates the EM grid release. Sequence D1-3 describes the mechanism responsible for this action. Sequence E1-3 depicts the rotation and plunging motion, and Sequence F1-3 illustrates the plunge release mechanism. A more detailed description of the design process can be found in Supplementary 2. Video (1) shows an animation of the mechanism.

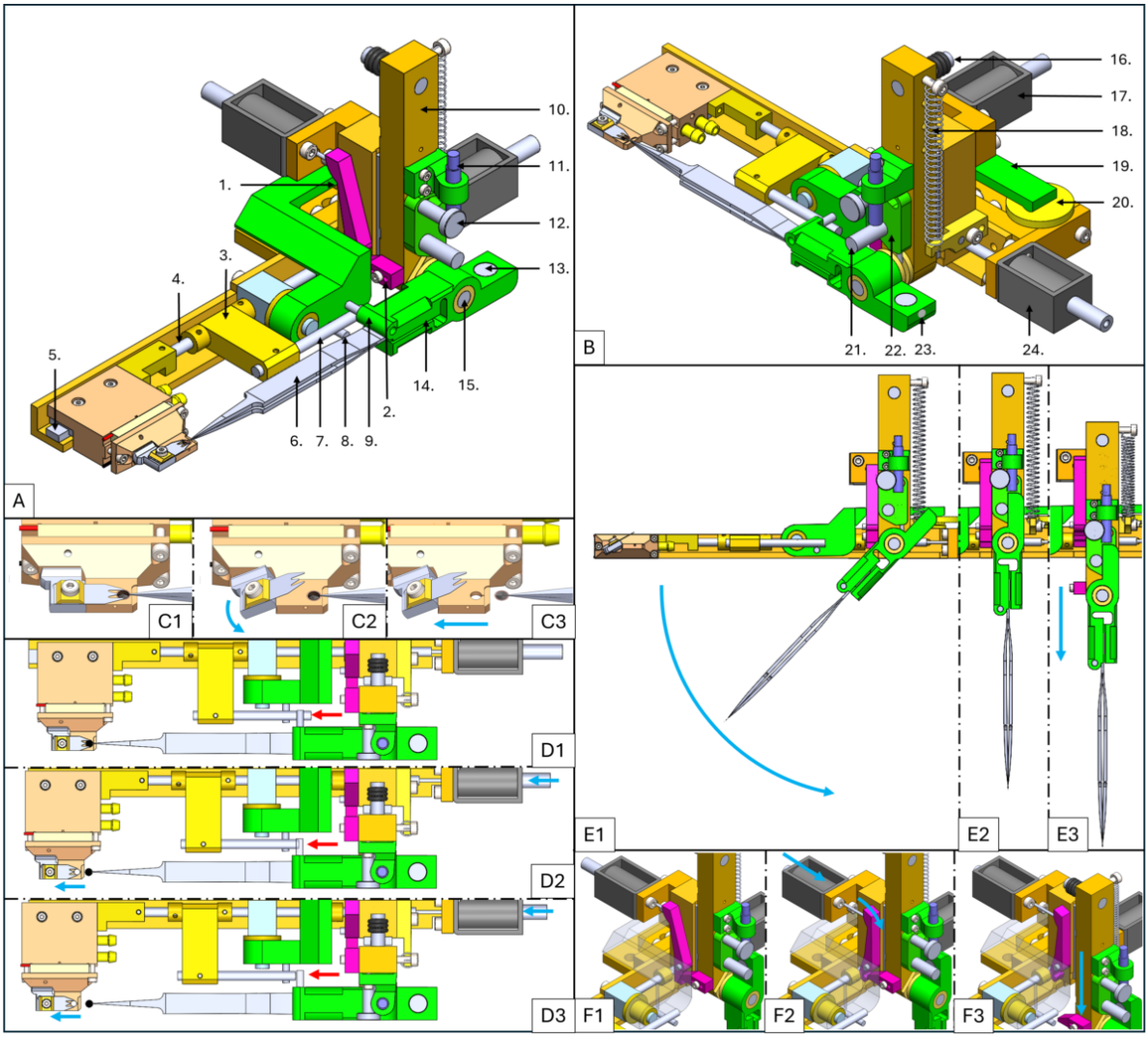

Figure 2.5: **A** and **B** show the entire mechanism, all relevant parts are numbered. **Sequence C1-3** shows the EM grid release: the grid clip rotates up, and the dew point stage moves to the left to clear the EM grid before rotation. Rotation starts only after the DP stage is completely removed from below the EM grid. **Sequence D1-3** explains the responsible mechanism. The release motion is actuated by solenoid **24**, which pushes against control rod **4**. This rod is directly connected to the water block that slides on linear rails **5**. A transfer lever **3** can rotate around the control rod and is linearly constrained with two shaft collars. On the other side of the transfer lever is the release pin **7**, which rests on the height adjust pin **8**. The height adjust pin can move up and down by rotating the height adjust knob **20**, which supports the height adjust arm **19**. The pendulum support pin **9** rests on the release pin. When the release is activated, the release pin slides out from under the pendulum support pin, as indicated by the red arrows in D2. This releases the pendulum base **14**, which rotates around the rotation pin **15**, mounted in the plunger **10**. **Sequence E1-3** shows the rotation and plunging motion. After rotating $90°$, the pendulum base hits the stop pin **21** and attaches to it with a magnet **13**. This is the plunge start position shown in E2. Set screw **23** aligns with an inductive proximity sensor **11**, which triggers the plunge release mechanism depicted in **sequence F1-3**. Solenoid **17** pushes against the trigger lever **1**, releasing the trigger toe **2**, mounted to the side of the plunger. Movement is indicated by blue arrows. Spring **18** actuates the plunger downwards until it hits the plunge stop **16** after approximately $30\,\mathrm{mm}$ of travel.

3. Materials and methods

A test setup was designed to evaluate the performance of the dew point controller, thickness measurement, and plunge freezing mechanism. The setup allows partial integration testing of dispensing, thickness measurement, and plunge freezing in a single sequence. This enables validation of thickness measurements performed with the interferometer against cryoEM measurements of the ice thickness in vitrified samples.

3.1. Test Setup

Dispensing is done with a microfluidic AFM cantilever mounted to a manual XY stage for positioning. The functional ability of the AFM is not needed for these validation tests, so it is omitted to reduce system complexity. A USB microscope views from the top, eliminating the need for a stationary microscope and an active XY motion stage. This setup simplifies positioning and transport between dispensing and measuring locations. All relevant components are schematically shown in Figure 3.1.

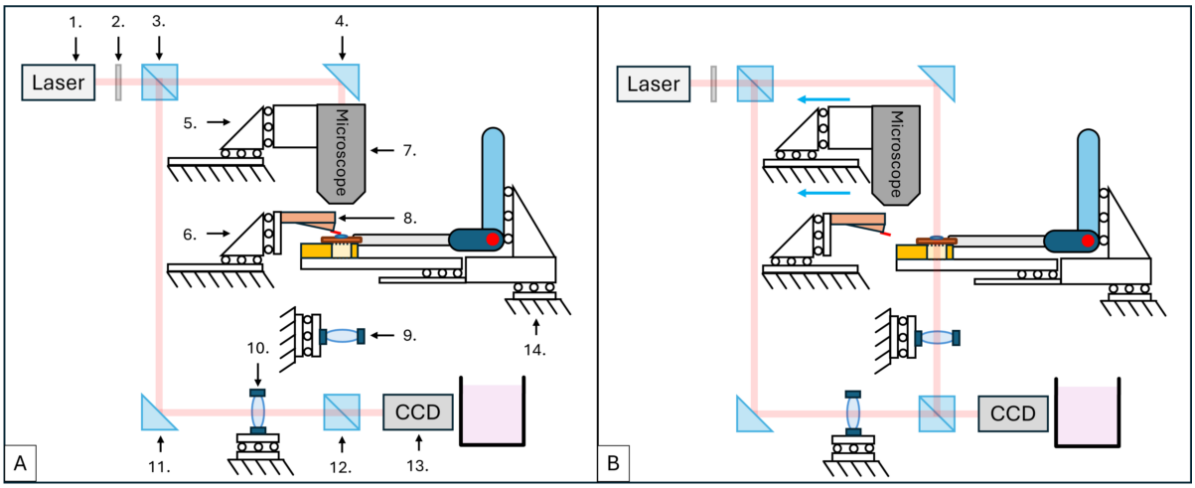

Figure 3.1: A: Dispensing step. **B:** Thickness measurement step. The Mach-Zehnder interferometer consists of a laser **1**, ND filter **2**, two beam splitters **3**, two $45°$ mirrors **4**, **11**, two lenses **9**, **10**, and a CCD **13**. The microscope **7** and the hollow cantilever **8** each have their own manual XY stages **5**, **6** for positioning and moving them in and out of the laser path between the $45°$ mirror **4** and beam splitter **12**. The DP stage and plunge mechanism are mounted on a manual XY stage to position the EM grid with a specific grid square in the CCD's field of view.

3.2. Integrated Test Procedure

The dispensing process is performed with a fluid FM micro pipette from Cytosurge, featuring an $8\,\mu\mathrm{m}$ aperture and a $2\,\mathrm{N\,m^{-1}}$ spring constant. The EM grid used is an R2/2 CU100f1 finder grid with $100\,\mu\mathrm{m}$ grid spacing, $10\,\mu\mathrm{m}$ grid bars, and a carbon film with a $1\,\mu\mathrm{m}$ hole pattern and $2\,\mu\mathrm{m}$ spacing. Dispensing is activated by a pressure controller (CYTOSURGE fluidFM MFCS V2) that can produce $1000\,\mathrm{mbar}$ overpressure and $-800\,\mathrm{mbar}$ underpressure. The micro pipette is filled with MilliQ water from the back and submerged with underpressure to load the hollow cantilever with liquid. The hollow cantilever is attached to a Thorlabs XYZ stage with a custom mount after loading it with MilliQ water.

Real-time thickness measurements are performed using a method directly implemented from previous work [2]. The theoretical background of the measurement principle is described in Supplementary 6.4. It was demonstrated that it is possible to measure the thickness of low contact angle droplet shapes on a glass surface, and this method was validated with white light interferometry. Additional testing confirmed the method's effectiveness when glycerol droplets were placed on an EM grid with a carbon film. Thickness measurements were further validated by plunge freezing the EM grid and performing

cryoEM measurements.

The measurement method works only for low contact angles because it assumes that the effects of the droplet acting like a lens due to Snell's law are small and can be neglected. It also does not consider the effect of internal reflection on the interference pattern due to the Fresnel equations. The low contact angle assumption made it difficult to measure the thickness of droplets on a hydrophobic grid; therefore, experiments were performed on both hydrophobic and plasma-cleaned hydrophilic grids.

The plunge freezing mechanism described earlier is used, involving tweezers (DUMONT swissmade 0209-5-PO) and a Vitrobot ethane cup to hold the cryogenic liquid. The plunge sequence follows the same steps as shown in Figure 2.4. Additional information can be found in Supplementary 6.

3.3. Temperature Controller Validation

The performance of the DP stage was tested before the partial integration test. The evaporation rate of approximately $100\,\mathrm{nm}$ sized droplets on a glass surface mounted in the grid holder was measured at different setpoint temperatures of the dew point stage. The dew point is obtained with a sensor (SENSOR-TEC UFT75-ST2) that calculates the dew point internally based on the measured temperature and humidity. The temperature of the dew point stage was set manually to an offset temperature ΔT with respect to the measured dew point. Droplets were dispensed with a modified $5\,\mathrm{mL}$ syringe and a $0.1\,\mathrm{mm}$ needle, with a differential screw arrangement designed to control the syringe plunger's travel precisely, resulting in a minimum droplet size of approximately $40\,\mathrm{nL}$. Data collection was done with two USB cameras (1600x1200 resolution), one from above and one from the side, using a fixed $15\,\mathrm{s}$ interval time-lapse. Frames were manually processed by placing points on the corners of the droplet shape in the side view and one on the top of the droplet. The volume was calculated assuming the droplet has the shape of a spherical cap. See Supplementary 4 for more details.

4. Results

4.1. Evaluation of System Construction and Performance

Figure 4.1 shows images of the fabricated and assembled mechanism. Figure 4.2 provides an overview of the test setup used to perform the integrated test procedure. A complete process description can be found in the user manual in Appendix D.

The motion profile of the tweezers tip was analyzed using slow-motion footage. Video (2) and (3) show the plunge action at full speed and in slow motion. Figure 4.3 shows the position of the tweezers over time, divided into three sections. The entire process, from releasing the EM grid from the temperature controller to a plunge-frozen EM grid, takes around $260\,\mathrm{ms}$, meeting the requirement of less than $300\,\mathrm{ms}$. An enlarged view of Section **c.** shows the plunger position again with the associated speed below in **d.**, indicating a maximum speed just above $1.5\,\mathrm{m\,s^{-1}}$, satisfying the entry velocity requirement into the cryogen.

4.2. Evaluation of Dew Point Stage Performance

To evaluate the performance of the DP stage, the effect of sample temperature offset relative to the measured dew point on the evaporation rate of $100\,\mathrm{nL}$ sized droplets on a glass surface was measured. Figure 4.4 shows the volume of nine droplets over time at different temperature offsets. During these tests, the ambient temperature varied between $18.8\,^{\circ}\mathrm{C}$ and $19.1\,^{\circ}\mathrm{C}$, with relative humidity between $57\,\%$ and $60\,\%$. The setpoint temperature of the controller was manually adjusted before each test to account for changes in the measured dew point. The graph shows results from the point each droplet reached $35\,\mathrm{nL}$. The average evaporation rate measured is shown in the right graph. A test with a $9\,^{\circ}\mathrm{C}$ temperature offset, equal to ambient temperature, served as a baseline, showing an evaporation rate of $223.0 \pm 97.3\,\mathrm{pL\,s^{-1}}$. The evaporation rate at $0\,^{\circ}\mathrm{C}$ temperature offset was $29.5 \pm 55.8\,\mathrm{pL\,s^{-1}}$, with the standard deviation larger than the measured value, highlighting a limit of the data acquisition method. Some data points gave a negative evaporation rate due to manual errors in placing points, leading to inaccuracies. See Supplementary 4 for more details . The evaporation of the $0\,^{\circ}\mathrm{C}$ droplet can be

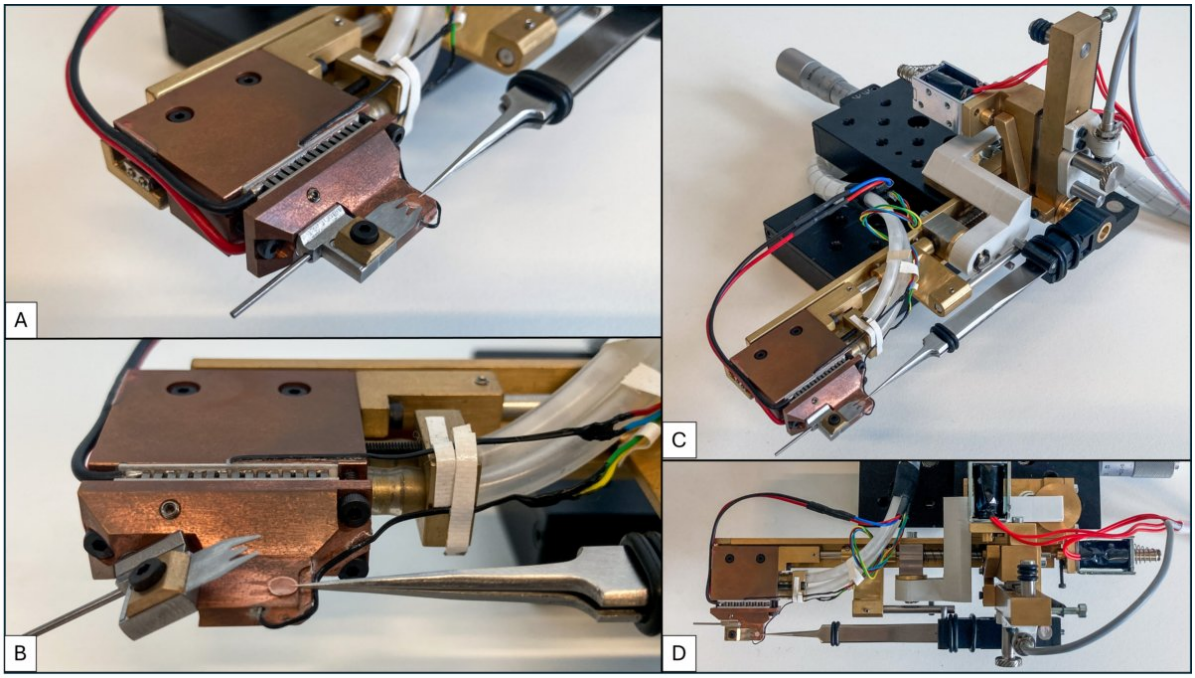

Figure 4.1: **A:** Isometric view of the assembled DP stage. **B:** Side view of the DP stage with the grid clip in the open position. **C:** Isometric view of the entire assembled mechanism. **D:** Top view of the assembled mechanism.

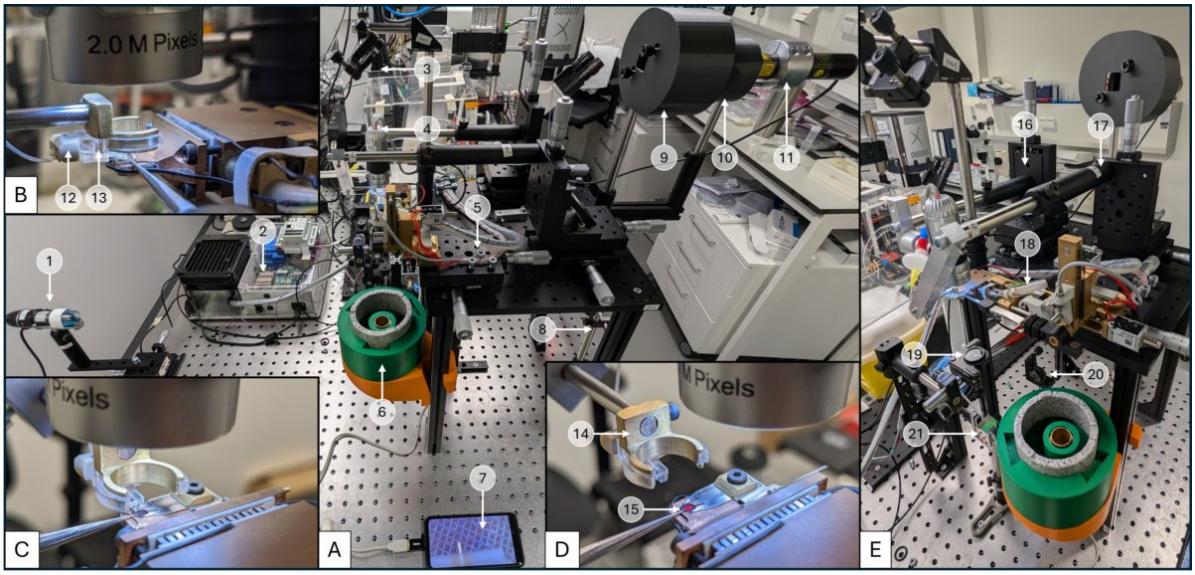

Figure 4.2: **A:** Side view of the entire test setup. **B:** Close-up of the cantilever from the side during dispensing. **C:** Close-up of the cantilever and EM grid from the front during dispensing. **D:** Close-up of the EM grid from the front during real-time thickness measurement, note the red dot from the laser on the EM grid. **E:** Front view of the test setup to show the position of the new mechanism. Labels: 1) CCD, 2) DP stage electronics and water cooling, 3) $45°$ mirror of the beam path that passes through the EM grid, 4) USB microscope, used during dispensing, 5) XY stage to position the EM grid in the field of view of the interferometer, 6) Ethane cup, 7) Smartphone connected to the USB microscope to view and record the dispensing process, 8) $45°$ mirror of the beam path that does not pass through the EM grid, 9) Laser safety cover with the first beam splitter inside, 10) Laser safety cover with the ND filter inside, 11) $1\,\mathrm{mW}$, $632\,\mathrm{nm}$ laser source, 12) Pressure line attachment, 13) Cytoclip with microfluidic cantilever, 14) Custom Cytoclip mount, 15) EM grid, 16) XYZ stage to position the USB microscope, 17) XYZ stage to position the microfluidic cantilever during dispensing, 18) New mechanism, 19) Lens below the EM grid that is used to get the droplet image in focus in the interferometer, 20) Lens in the beam path that does not pass through the EM grid, 21) Second beamsplitter that recombines the two beam paths.

viewed in Video (4).

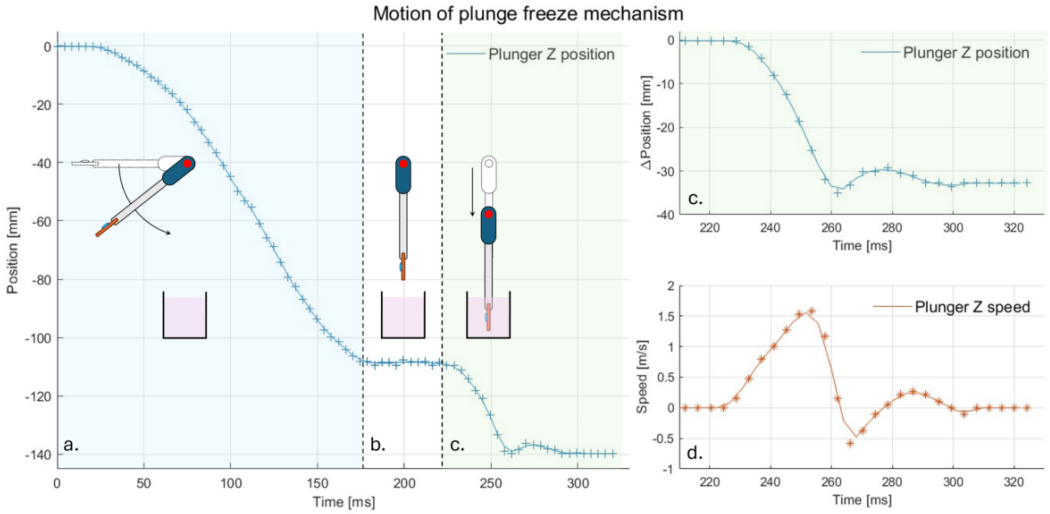

Figure 4.3: **a:** Rotation of the tweezers to the plunge start position. **b:** Activation of the plunge trigger mechanism. **c:** Plunging action. **d:** Speed of the plunging action.

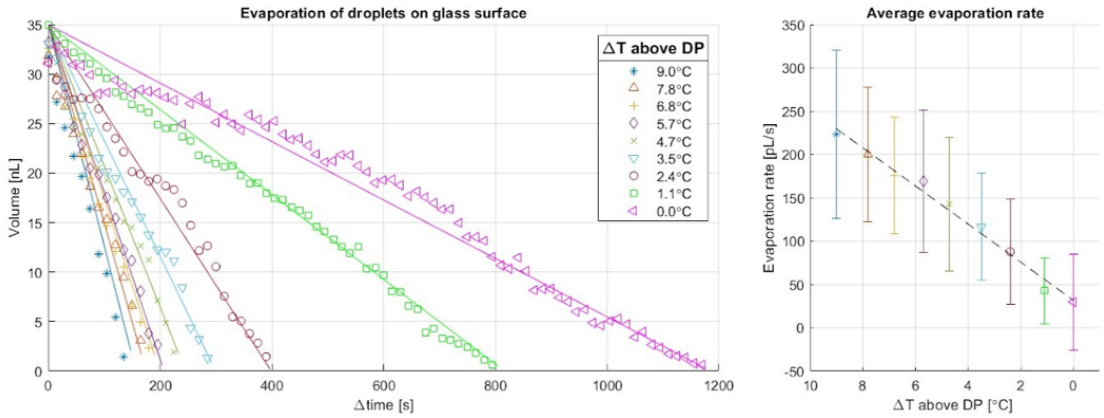

Figure 4.4: Results from nine evaporation tests on a glass surface at different temperature offsets relative to the measured dew point.

The evaporation of pL-sized droplets on an untreated hydrophobic EM grid was also tested. Droplets were dispensed in the middle of a grid square on the carbon film and measured with the interferometer setup as shown in Figure 4.5. All temperature set points were at the dew point or below. The evaporation rate of a droplet on an EM grid with a temperature $1\,^{\circ}\mathrm{C}$ above the measured dew point was too fast to start a thickness measurement. Video (5) shows this evaporation rate.

Reliable thickness measurements were not possible for most of the droplet's evaporation due to the hydrophobic surface. The droplets showed evaporation behavior that reduced the diameter before reaching a contact angle low enough for the interferometer to measure. The starting volume was estimated from the diameter measured just after dispensing, based on a 70° contact angle observed on nL-sized droplets dispensed on a hydrophobic EM grid, see Supplementary 4. Remarkably, evaporation almost entirely stopped before the droplet completely disappeared, reaching a stable state with a final diameter between $10\,\mu\mathrm{m}$ and $13\,\mu\mathrm{m}$, independent of the dew point offset. Final measurements with the interferometer were used to estimate the final volume of the droplets. Video (6) and (7) show the dispensing and fringe pattern data of the $-3\,^{\circ}\mathrm{C}$ droplet. The average evaporation rate was estimated based on the volume reduction and total evaporation time, shown in Figure 4.6. The error bars show the standard deviation of the data acquisition method used, not the deviation between multiple experiments. More information on these results can be found in Supplementary 5.

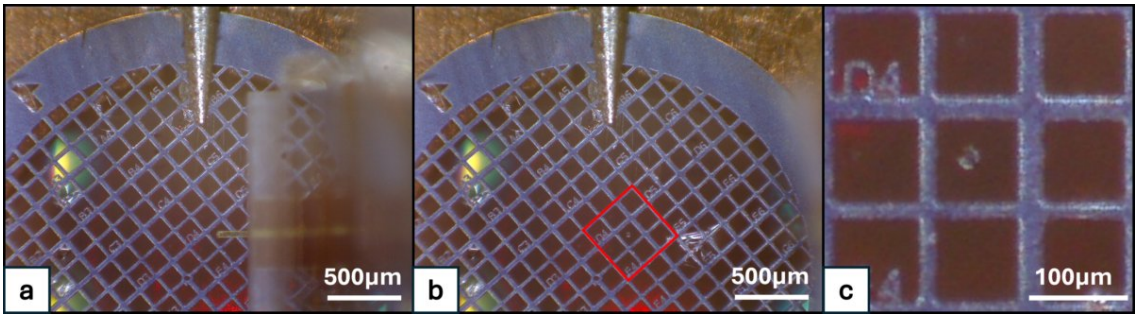

Figure 4.5: These photos show the droplet of $2.74 \pm 0.46\,\mathrm{pL}$, dispensed at $-1\,^{\circ}\mathrm{C}$ temperature offset to DP. **a:** Microfluidic cantilever touching the carbon film in the middle of one grid square during dispensing. **b:** Overview of the EM grid just after dispensing, red square indicates the zoom-in area of **c**. **c:** Close-up of the dispensed droplet.

ΔT below DP temp.	Start Diameter (µm)	Start Volume (pL)	End Diameter (µm)	End Volume (fL)	Time (s)	Average Evaporation Rate (fL/s)
-0°C	35.26 ± 1.65	7.06 ± 0.97	12.26 ± 1.18	4.81 ± 1.06	20.7s	340.63 ± 44.80
-1°C	25.70 ± 1.50	2.74 ± 0.46	10.50 ± 0.90	3.33 ± 0.58	15.1s	181.28 ± 29.02
-2°C	33.27 ± 1.07	5.91 ± 0.55	9.91 ± 0.49	6.11 ± 1.00	38.7s	152.45 ± 13.61
-3°C	28.51 ± 0.95	3.72 ± 0.37	11.86 ± 0.96	8.17 ± 1.46	50.7s	73.16 ± 6.93
-4°C	41.04 ± 3.14	11.23 ± 2.48	12.99 ± 1.53	6.09 ± 1.63	134.6s	83.40 ± 17.54

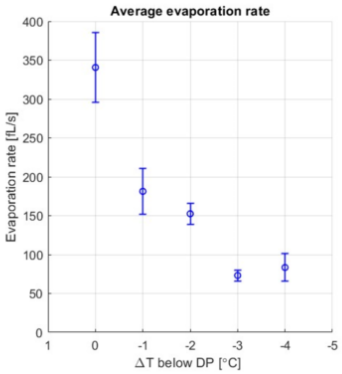

Figure 4.6: Results from measuring the average evaporation rate of five droplets on a hydrophobic EM grid at different temperature offsets below the measured dew point.

4.3. Partial Integration Test Results

Evaporation tests on untreated hydrophobic grids showed an upper limit on the droplet shape measurable with the interferometer. Without plasma cleaning, the shape never reached a state below this limit until the end of the experiments. To lower the contact angle, the grids were plasma treated. This resulted in droplets touching the edge of the grid square, making them only partially visible in the field of view. However, the droplets reached a state with a low enough contact angle for thickness measurement. Results from these measurements are shown in Figure 4.7. The dispensing and fringe pattern data of this measurement can be seen in Video (8) and (9). A complete test procedure can be seen in Video (10).

The data is from a droplet dispensed at a ΔT of $-3\,^{\circ}\mathrm{C}$. After $55\,\mathrm{s}$, the temperature was raised to $-2\,^{\circ}\mathrm{C}$ to increase the evaporation rate. The graph shows the $16\,\mathrm{s}$ of a $144\,\mathrm{s}$ evaporation period. Image **a** shows the dispensed droplet at $t = 1\,\mathrm{s}$ just after dispensing. Image **b** shows the fringe pattern at $t = 128.5\,\mathrm{s}$. Note that the fringe lines are not continuous and appear to have steps, possibly due to internal reflections, which do not result in good thickness measurements with the current algorithm. Frame **c** at $t = 133\,\mathrm{s}$ shows a fringe pattern clear enough to calculate a thickness. From $t = 133\,\mathrm{s}$ to **d** $t = 137\,\mathrm{s}$, a linear decay in measured thickness is observed from $650\,\mathrm{nm}$ to around $450\,\mathrm{nm}$. The real-time thickness measurement data, displayed during the experiment, was used to determine the thickness was below the threshold of $500\,\mathrm{nm}$, and the plunge action was initiated. The first section of data points in green is excluded due to vibrations induced by the manual rotation of the spring clip. The last section of data points is excluded due to vibrations caused by the manual actions involved in the plunge freezing process. The thickness of this sample could be measured with cryoEM to validate the interferometer thickness measurement just before plunge freezing.

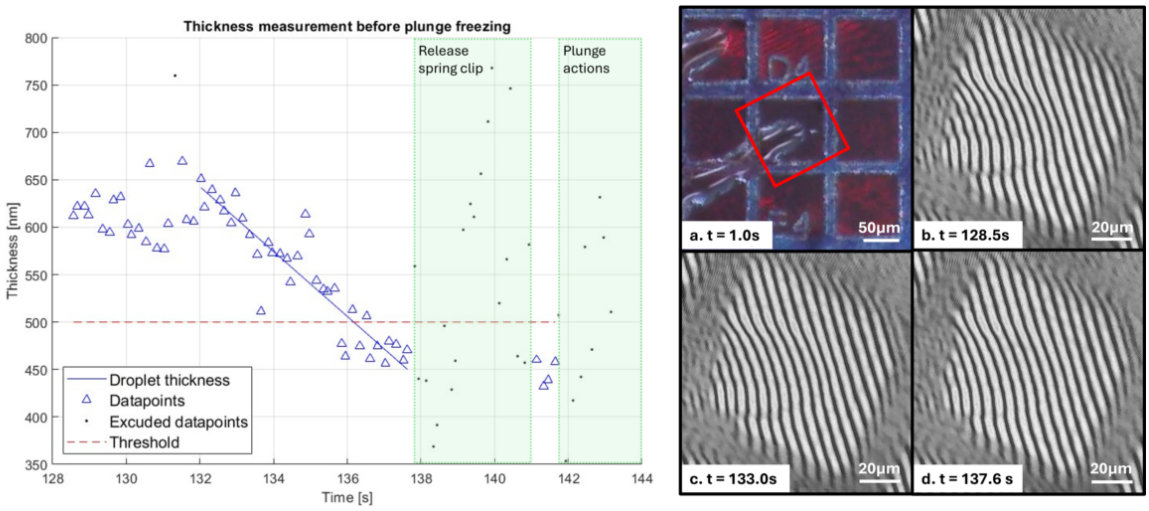

Figure 4.7: Fringe pattern data and the corresponding measured height of a droplet on a hydrophilic EM grid.

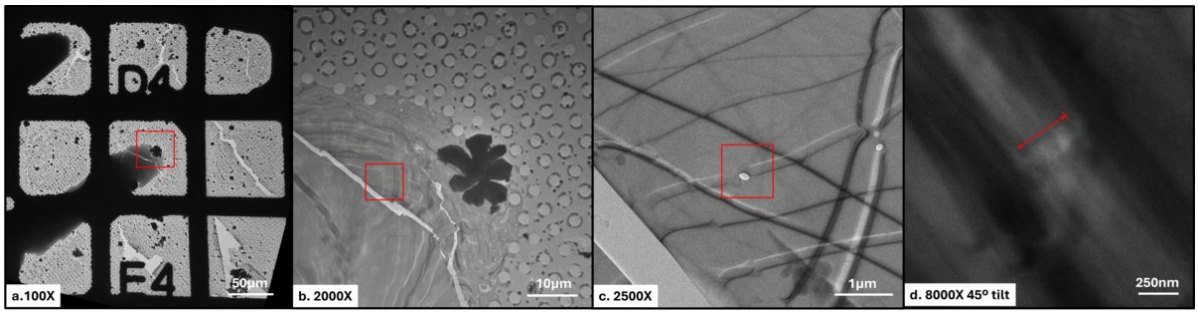

Figure 4.8: CryoEM results used to validate the real-time thickness measurement just before plunge freezing.

Figure 4.8 **a** shows a cryoEM image at 100x magnification of the grid squares where the droplet was dispensed. Image **b** shows the part of the droplet that had its height measured at 2000x magnification. The ice is crystalline and not amorphous, likely due to the ethane not being cold enough during plunge freezing. The ice is partially transparent to the electron beam, allowing thickness measurement. Image **c** shows a hole drilled with the electron beam, and **d** shows a $45°$ side view of the created channel. The length of the channel measured between $320\,\mathrm{nm}$ and $390\,\mathrm{nm}$. The start and end points are somewhat difficult to determine, so the total thickness estimate lies between $450\,\mathrm{nm}$ and $550\,\mathrm{nm}$ using trigonometry.

5. Discussion

A set of specific requirements was outlined at the beginning of this work. Most of these requirements have been met based on the test results or have shown potential to be achieved.

One major requirement was to dispense a fL-sized sample on an EM grid. The smallest droplet size achieved was $2.74 \pm 0.46\,\mathrm{pL}$, or approximately $2800\,\mathrm{fL}$. This is on the lower end of the pL range but not yet true fL droplets. Dispensing on the EM grid with a microfluidics cantilever was successfully demonstrated. With a smaller aperture ($600\,\mathrm{nm}$ instead of $8\,\mu\mathrm{m}$) and a broader pressure controller range, it could be possible to dispense droplets of several hundred fL on a hydrophilic grid without touching the grid bars.

Another requirement was controlling the evaporation rate. The grid needed to be maintained at a constant temperature with good thermal contact with the EM grid and a fast thermal response from the

temperature controller. Validation of the temperature controller showed it effectively slowed the evaporation rate of pL-sized droplets, extending the available process time to over two minutes. This duration is sufficient to transport the sample to the measurement location and perform real-time thickness measurements.

Reducing ice thickness to less than $500\,\mathrm{nm}$ was also required. The final functionality would be to reduce the thickness to just above the size of the expected particles in the liquid, resulting in the least amount of ice to image through. Thickness measurements can be done on droplets with a sufficiently low contact angle, and the final decrease in thickness is slow enough to manually identify, react to, and activate the plunge sequence. This demonstrates the potential of this sample preparation method. However, further refinement in process automation is needed to reduce manual steps, and the measurement algorithm must be improved to better interpret fringe lines and handle droplets that cover multiple grid squares or partially lie on grid bars.

Vitrification immediately after achieving the required thickness was another goal. The transition from measurement to frozen sample needed to occur in less than $300\,\mathrm{ms}$, and the plunge speed had to be at least $1.5\,\mathrm{m\,s^{-1}}$. The results showed that both requirements were satisfied. However, the ice not being vitreous is likely due to insufficient temperature control of the ethane used for plunge freezing, requiring additional testing to validate this.

The thickness measurement method was based on previous work [2]. Obtaining clean measurements is challenging due to disturbances from manual steps between taking the reference image and starting the measurement. Additionally, sensitivity to vibrations caused by the boiling of the cryogenic liquid and other external factors complicates interpreting the height profile during the experiment. Automating some of the manual steps and a more rigid interferometer setup would mitigate some of these problems.

The final design was based on a comprehensive system analysis found in Appendix A and B, exploring all possible configurations to find the least complex system. Notably, the CryoWriter sample preparation method [1] shows some clear similarities with the mechanism presented in this work, making it necessary to highlight both the similarities and the differences in the intended tasks and their execution. At a high level, both systems perform similar tasks: preparing and dispensing samples on a horizontal EM grid and measuring sample thickness in real-time before transitioning to a horizontal plunge freezing operation. However, the execution of each process step differs. The CryoWriter uses a micro capillary to dispense a sample volume of $3\,\mathrm{nL}$ to $20\,\mathrm{nL}$, covering multiple grid squares and creating a homogeneous water layer. In contrast, the new AFM4CryoEM system dispenses pL or fL volumes with a microfluidic cantilever within a specific grid square.

The new AFM4CryoEM system is specifically designed to fit in the confined space between the AFM and microscope, while the CryoWriter does not have such design restrictions. Additionally, the CryoWriter includes a temperature controller to cool the tweezers, which so far appears not to be necessary for the AFM4CryoEM system.

The CryoWriter measures water layer thickness by the transmission intensity of a laser through the water. As the water layer reduces, transmission intensity changes due to internal reflections. A condition for this method is that the water layer must be larger than the laser spot size. Conversely, the interferometer measures droplets smaller than the laser spot size. Each technique uses fundamentally different methods and cannot measure the samples for which the other system was designed.

Both systems require mechanical transport of the EM grid from the measurement location to the plunge start position since both dispense in the horizontal plane and aim to plunge freeze vertically. The CryoWriter uses the CryoDrop 2.4 mechanism as a solution, but this problem can be solved in other ways, one of which has been demonstrated in this work.

The results from the partial integration test indicate that the execution of the intended functionality is possible. The limited results obtained with cryo-EM seem to validate the thickness measurement before plunge freezing. However, more data points are needed to gain a better understanding of system performance.

6. Conclusion

A novel system has been designed, fabricated, and tested toward subcellular biopsy sample preparation for cryo-electron microscopy. The system is capable of sustaining sample volumes of less than $3\,\mathrm{pL}$ on a temperature-controlled EM grid for more than two minutes after dispensing with a microfluidic cantilever. It has been demonstrated that sample droplet thicknesses below $700\,\mathrm{nm}$ can be measured using a Mach-Zehnder interferometry setup, utilizing fringe pattern recognition to determine its thickness within this time frame. The sample can be transported through ambient conditions in less than $300\,\mathrm{ms}$ to be plunge-frozen immediately after a predetermined thickness threshold is crossed. Validation with Cryo-EM shows no significant sample loss during transport and sample thicknesses comparable to measurements before vitrification. Based on the limited results obtained so far to validate each aspect of the system, this proof-of-principle test setup shows the potential of this system approach. Automating parts of the system procedure will greatly improve the repeatability of testing by eliminating many manual steps currently required for a complete test sequence. A full integration test setup is necessary to validate dispensing with an actual AFM. To achieve fL sample sizes, more control over the dispensing procedure is needed, and further research into optimal surface conditions and treatments on the grid is required to facilitate subcellular biopsy sample preparation and understand their effects on the preparation process. The system presented shows clear potential to be further developed into a fully functional sample preparation method for studying subcellular biopsy material with high-resolution cryo-electron microscopy.

7. Recommendations

This chapter summarizes all recommendations made in this work. Each chapter in the supplementary material ends with a recommendation section in the context of the discussed topic. Some recommendations may be given multiple times but with different reasoning depending on the context. The page references point to the explanation and reasoning behind each recommendation.

7.1. Recommendations on the Current Version

These recommendations would improve testing with the current setup and may also apply to a future version of the test setup.

Mechanism Design

1. Change to a better version of the tweezers. (**p.**32), (**p.**47)
2. Use a different method to attach the tweezers to the mechanism. (**p.**32)
3. Improve the tweezer XY position adjustment mechanism. (**p.**94)
4. Automate opening the grid clip. (**p.**27), (**p.**32)

Test Setup

1. Use a smaller aperture microfluidic cantilever. (**p.**47)
2. Implement a pressure controller with the ability to trigger a predetermined dispense time. (**p.**47)
3. Add a quick retract style motion to the X-axis of the cantilever XYZ stage. (**p.**94)

Measurements

1. Use a CCD without automatic brightness adjustment. (**p.**47), (**p.**94)
2. Find the actual low contact angle limit of the measurement method. (**p.**47)
3. Calibrate the thickness measurement method with solid transparent reference droplets. (**p.**47)
4. Calibrate the DP stage temperature measurement with a known good temperature reference. (**p.**47)

Software

1. Rewrite the MATLAB code to include a user interface with simple buttons. (**p.**94)
2. Rewrite the MATLAB script to timestamp the raw data instead of recording the time passed since the start of the measurement. (**p.**94)

7.2. Recommendations for Future Versions

These recommendations apply when designing a next version of the test setup.

Mechanism Design

1. Conduct an optimization study on the combination of the grid holder, TEC, and water block. (**p.**27)
2. Investigate if the shape of the grid holder affects evaporation due to passive convective cooling airflow. (**p.**27)
3. Redesign or replace the trigger release mechanism. (**p.**32)
4. Mitigate the undamped resonance of the tweezer pendulum and the linear motion of the plunger. (**p.**32)
5. Use different solenoids or another actuator type. (**p.**32)

6. Consider other production methods during the design process of a future version. (**p.**32)

Test Setup

1. Add some vibration isolation between the interferometer and the ethane cup. (**p.**47)
2. Implement active temperature control of the liquid ethane. (**p.**47)

Measurements

1. Eliminate the need for a reference frame. (**p.**47)
2. Use a CCD with higher resolution. (**p.**47)
3. Improve the measurement algorithm to make it possible to measure droplets that cover more than one square of the grid. (**p.**47)

Software

1. Develop LabVIEW software to couple the dew point sensor and the TEC controller. (**p.**27)

7.3. Recommendations on Test Methods

A set of recommendations on the test method to validate the DP stage can be found here (**p.**40). These are only relevant when testing with nL size droplets is necessary.

A set of recommendations on the test method to determine the evaporation rate of pL droplets on an EM grid can be found here (**p.**43).

Part II

Supplementary Material

1. Design of DP Stage

This work describes the design process of the DP stage. The design method used was specifically focused on constructing a working proof of principle within the timespan of a master thesis. This approach differs from the design and construction of a prototype in that, for most of the many design considerations and decisions that had to be made, the approach was not to find the ”best” possible solution in terms of optimized design but to find solutions that are good enough to demonstrate the minimum required intended functionality and can be realized in a relatively short timespan. The main selection criteria are:

1. Solutions that are based on well-known working principles.
2. Solutions that make use of components that are directly available from known suppliers.
3. Off-the-shelf solutions that include the functionality of entire subsystems (e.g., do not program a custom control loop if you can buy a controller with an ”auto tune” button for a specific process).
4. Solutions that allow implementation of production techniques with short lead times (like 3D printing) and are not dependent on external production partners (design for conventional machining instead of CNC if possible).

1.1. Requirements

The DP stage has to:

1. Keep the EM grid at a constant set temperature.
2. Have a fast thermal response.
3. Have good thermal contact with the EM grid.
4. Fit between the AFM and microscope objective.

1.2. Design

All major components needed to build a DP stage are listed in Figure 1.1.

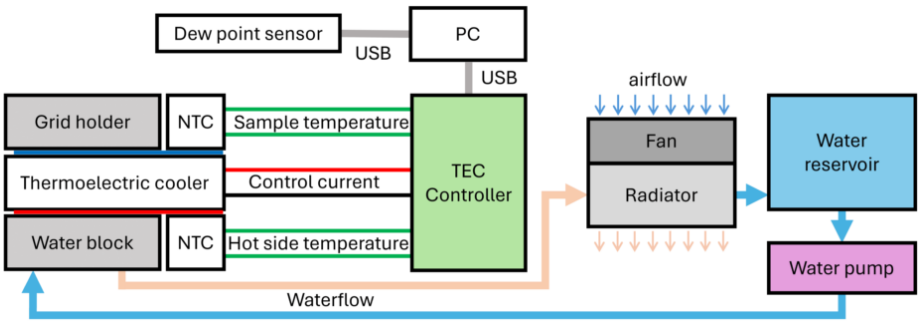

Figure 1.1: Schematic system overview of all relevant components required for a functional DP stage.

A preliminary design for the grid holder and waterblock was made that fits inside the confined space between the AFM and microscope objective. See Figure 1.2. This model was used to calculate some heat transfer requirements in COMSOL that could be used to start the TEC selection process. The detailed design of the grid holder and waterblock was done after parts selection.

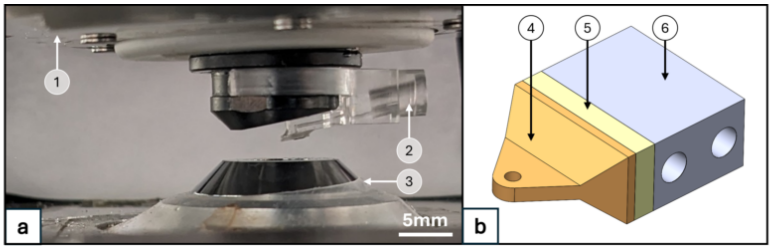

Figure 1.2: a. 1. Bottom of the AFM, 2. Cytoclip with AFM cantilever, 3. Microscope objective. **b.** Preliminary 3D model of DP stage that fits in the confined space between cantilever and microscope objective. 4. Grid holder, 5. Thermo-electric cooler (TEC), 6. Water cooling block.

Parts Selection

TEC

Heat transfer calculations were performed in COMSOL on a preliminary design of the DP stage. A model based on passive convective cooling was used to estimate the steady-state heat transport needed to keep the grid holder at a constant temperature $10\,^{\circ}\mathrm{C}$ below ambient temperature. See Figure 1.3 for some simulation results. The steady-state heat rate is approximately $0.04\,\mathrm{W}$.

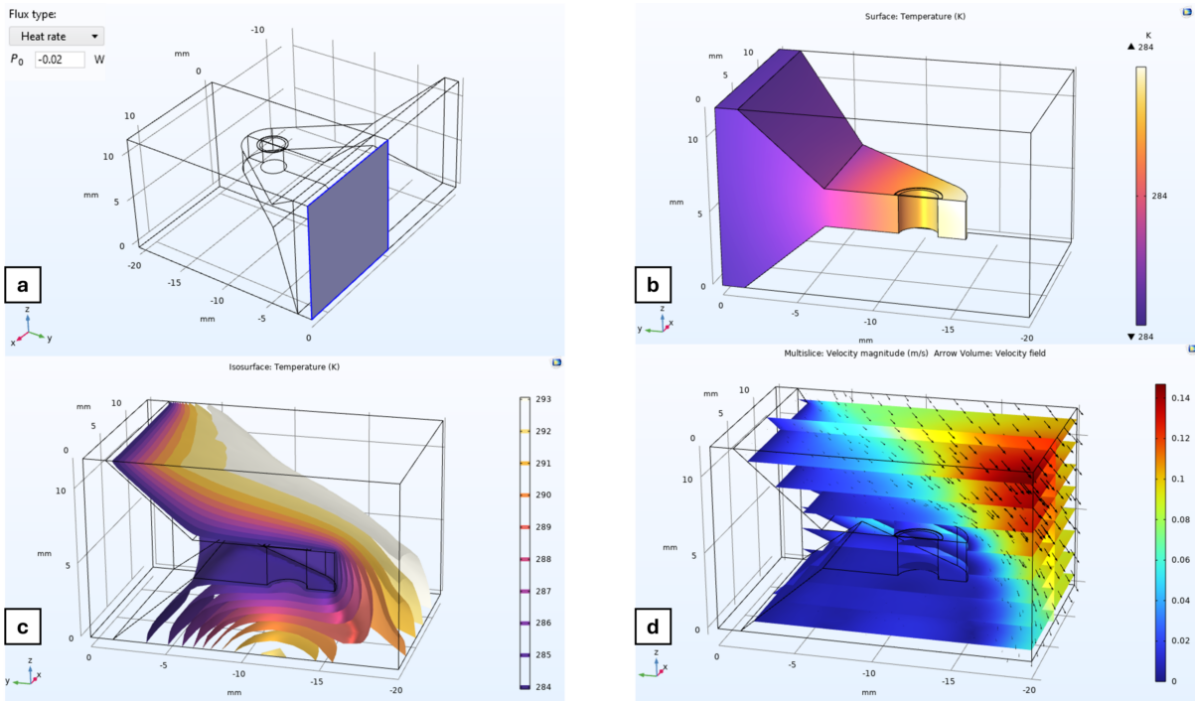

Figure 1.3: a. Surface area with a constant negative heat rate of $-0.2\,\mathrm{W}$ applied, the model complexity was reduced by using symmetry. **b.** Temperature gradient in the grid holder at steady state. Ambient temperature was modeled at $293\,\mathrm{K}$. **c.** Isothermic temperature distribution in the air around the grid holder. **d.** Velocity field in the air around the grid holder, induced by passive convective cooling.

The heat transfer capacity needed for a fast thermal response was estimated based on the total mass of material and the amount of energy that needs to be extracted from it to reach a temperature $10\,^{\circ}\mathrm{C}$ below ambient temperature. The total energy in joules divided by the desired response time gives an estimate of the required heat transport capacity. This simplified approximation ignores any resistance to heat transport in the material. The amount of heat that needs to be extracted from the grid holder to drop $10\,^{\circ}\mathrm{C}$ is estimated to be $20\,\mathrm{J}$. Heat transport needed for a fast thermal response is approximately $4\,\mathrm{W}$ to cool down in $5\,\mathrm{s}$. The thermal response and settling time of the previous AFM4CryoEM system presented in [12] was around $30\,\mathrm{min}$. The $5\,\mathrm{s}$ may be too ambitious of a performance metric to aim for, but if the actual response of the system stays below $30\,\mathrm{s}$, it could be considered fast and a major improvement over the previous system.

The cooling capacity of the waterblock was also modeled in COMSOL. See Figure 1.4. Different heat loads were tested at a constant water flow, and the resulting temperature rise above ambient was measured. The cooling capacity is approximately $25\,\mathrm{W}$ for a temperature rise of $10\,^{\circ}\mathrm{C}$ at the interface with the TEC. The water temperature is increased by $1\,^{\circ}\mathrm{C}$ at the outflow port.

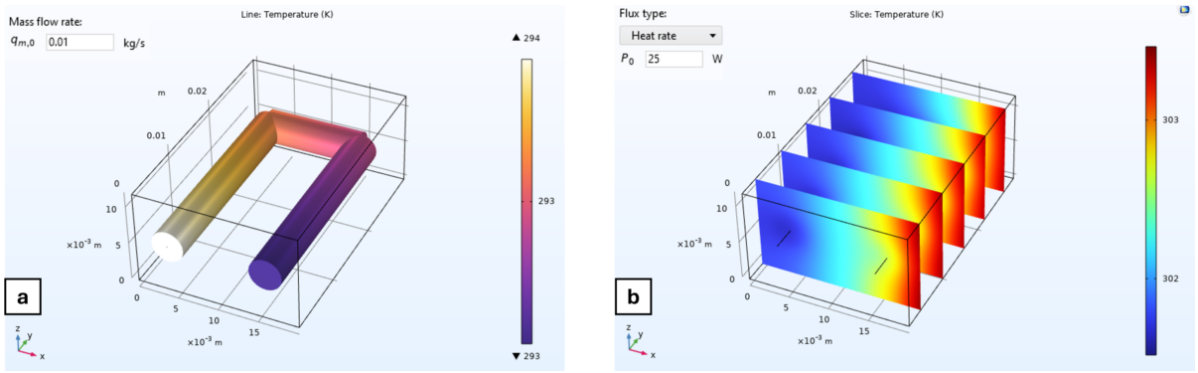

Figure 1.4: a. Temperature increase of the water flowing through the waterblock. **b.** Temperature gradient in the waterblock resulting from a heat rate input on the side surface of $25\,\mathrm{W}$.

The selection of a suitable TEC was based on the values mentioned above and the following criteria: it had to be a standard part, in stock at RS Components.

The heat transport required and the available space were the main selection criteria. The chosen TEC has the following specifications:

- Imax: $2.2\,\mathrm{A}$
- Vmax: $7.8\,\mathrm{V}$
- Pc max: $10.4\,\mathrm{W}$

Note that the Pmax is more than twice as high as specified. This is because this value is only valid if both sides are at the same temperature, which is only true at the start of cooling. After that, the maximum heat transport capacity drops significantly.

Some performance graphs from the data sheet can be seen in Figure 1.5. The assumption is made that a maximum control current of $1\,\mathrm{A}$ is sufficient. **A** shows the maximum heat removed from the cold side for different currents at any given temperature difference. The green arrow indicates the expected heat removed until the temperature difference of $10\,^{\circ}\mathrm{C}$ is reached. It starts at $6.5\,\mathrm{W}$ heat transport and ends at $5.5\,\mathrm{W}$ heat transport. The heat transport drops to some steady state when the temperature difference is reached, indicated with the blue arrow. **B** shows the waste heat produced during this process, going from $11\,\mathrm{W}$ to $9\,\mathrm{W}$ during cooling, indicated with the green arrow, and then dropping to some steady state value indicated with the blue arrow. **C** gives the maximum required input voltage to be at $3.5\,\mathrm{V}$. The coefficient of performance (COP) starts at 2 and drops to 1.5 during cooling, then it follows the $\Delta T = 10$ curve until some steady state is reached. **D** the COP shows that a lower control current would reduce the excess heat generation more; however, this would result in a slower thermal response. A COP of 2-1.5 is acceptable for the purpose of this proof of acceptance.

The selected TEC is able to transport $6.5\,\mathrm{W}$ to $5.5\,\mathrm{W}$ of heat at a control current of $1\,\mathrm{A}$, generating $11\,\mathrm{W}$ to $9\,\mathrm{W}$ of excess heat. The waste heat production is well within the cooling capabilities of the designed waterblock. The size of the TEC is 12x25x3.8mm.

Note that to start calculations, some size and performance assumptions had to be made. Therefore, this type of part selection is an iterative process, and there is almost certainly a smaller configuration possible with similar performance. An optimization study of the grid holder, TEC, and waterblock combination could be used to further improve this system. However, it is not necessary for the design of a working proof of principle.

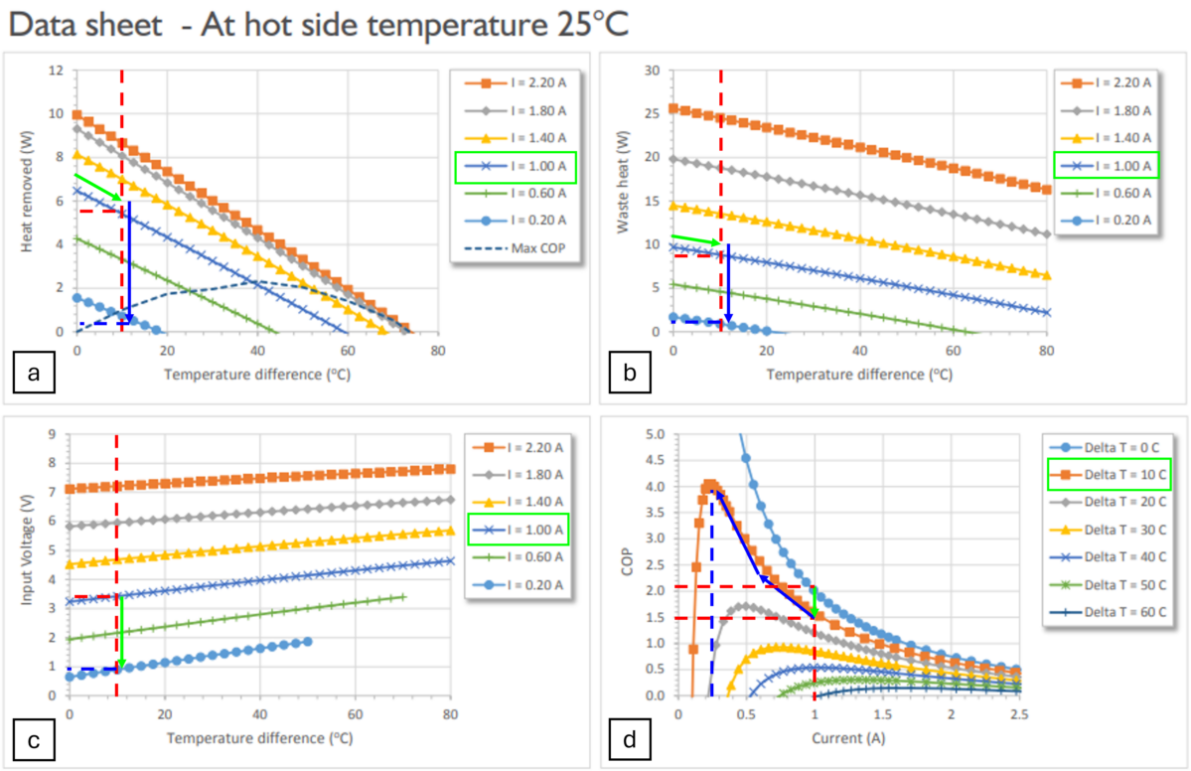

Figure 1.5: a. Heat removed at a temperature difference for a given current. **b.** Sum of generated heat and transported heat, indicated as waste heat at a temperature difference for different drive currents. **c.** Required input voltage at a temperature difference for different drive currents. **d.** Coefficient of performance at a drive current for different temperature offsets.

TEC Controller

A suitable TEC controller can be selected based on the specifications of the selected TEC. The maximum required voltage is $6.5\,\mathrm{V}$, and the maximum control current was assumed to be $1\,\mathrm{A}$. This value could change in the future, so the maximum allowed current of $2.2\,\mathrm{A}$ was used as a selection criterion. Other criteria were:

1. A working LabVIEW script from the manufacturer available to allow for future automation of the system.
2. PID control capabilities.
3. Data logging capabilities.
4. PID autotune functionality.
5. Heating and cooling capabilities.
6. USB connectivity for communication and data logging.

A controller from Meerstetter Engineering (TEC-1091) was selected that meets all requirements. Some specifications:

- DC Input Voltage: $5\,\mathrm{V} - 24\,\mathrm{V}$
- Output Voltage: 0 to $\pm 21\,\mathrm{V}$ (max. $0.9 \cdot U_{\mathrm{IN}}$)
- Output Current: 0 to $\pm 4\,\mathrm{A}$, <1% Ripple

Dew Point Sensor

Requirements:

1. The sensor must measure absolute humidity, relative humidity, and temperature
2. Calculate the dew point internally

3. USB connectivity for data logging
4. A working LabVIEW script from the manufacturer available to allow for future automation of the system

The selected sensor (SENSOR-TEC UFT75-ST2) calculates the dew point internally based on the measured temperature and humidity, it meets all requirements and is the same one as used by [1] in the Cryowriter system.

Temperature Sensors

The selected NTC sensors were chosen based on their size and fast thermal response time. One oversight was that the leads were uncoated, so installing them in a hole in a copper part is problematic. The solution for this problem was to coat the leads with liquid electrical tape from the company Plastidip. This dries into a rubber-like state and evenly coats the wire leads.

Detailed Design

Requirements:

1. Good thermal contact between gridholder and EM grid.
2. the grid holder needs to fitvbetween AFM and microscope objective.

Grid Holder

The grid holder needs to fit in the confined space, which defines the major outside dimensions. The EM grid is held in tweezers and needs to be placed flat on the surface of the grid holder. Therefore, some relieved space for the tweezer tip is needed. The grid holder may not obstruct the field of view of the microscope objective. There is a $2.5\,\mathrm{mm}$ hole below the EM grid that tapers at 45° to create clearance. The position of the temperature sensor was designed to be as close as reasonably possible to the edge of the EM grid. It is positioned at the middle of the grid measured from the TEC interface to take the center temperature of any temperature gradient that may occur in the EM grid due to the TEC placement on the side. The position of the grid location is not centered with the TEC interface; this is to allow enough space to mount the grid clip mechanism. See Figure 1.6.

Water Block

The water block design had to fulfill a couple of functions: it needs to provide sufficient cooling of the TEC hot side, create a rigid mounting for the TEC and grid holder, and have an interface to mount the entire DP stage assembly to the plunge freeze mechanism. The geometry of the cooling channel was shown to be not critical in the COMSOL simulations. The minimum size of the water block and cooling channels needed to effectively cool the theoretical steady-state heat load is much smaller than the final design presented here. The water block was dimensioned with fabrication techniques in mind; deep drilling of pure copper with drill diameters below $4\,\mathrm{mm}$ becomes significantly more difficult. Tapping threads below M2 in copper is also considered more difficult and should be avoided unless it is absolutely necessary. Therefore, the cooling capacity of the final design is much larger than needed, but it is easy to interface with the other components and not too difficult to manufacture. Mounting of the grid holder and TEC is done with three M2 screws that clamp the TEC between the grid holder and water block. The mounting face of the water block has some relief and constraining features to position the TEC. See Figure 1.6.

Grid Clip

The EM grid and grid holder need to make sufficient contact for thermal transfer. The grid itself is $0.01\,\mathrm{mm}$ thick and deforms easily through light disturbances. The tweezers holding down the grid at one point along the edge do not ensure that the entire circumference of the grid is touching the grid holder. A spring-like retaining clip was designed to provide more points of contact to press the grid against the grid holder. Figure 1.7 shows the functionality of the design. The grid clip has three fingers on its end that press down on the grid edge. The clip carrier is $0.1\,\mathrm{mm}$ higher than the grid holder surface to make sure the tips of the clip are the first parts that contact the grid and holder, see **d**. To further ensure this functionality and get enough preload, the clip is given a curvature during fabrication. The clip carrier has two functional positions: the open and closed positions. In the closed position, the clip has to be forced onto the grid. The actuation needed to induce this moment force is provided by a

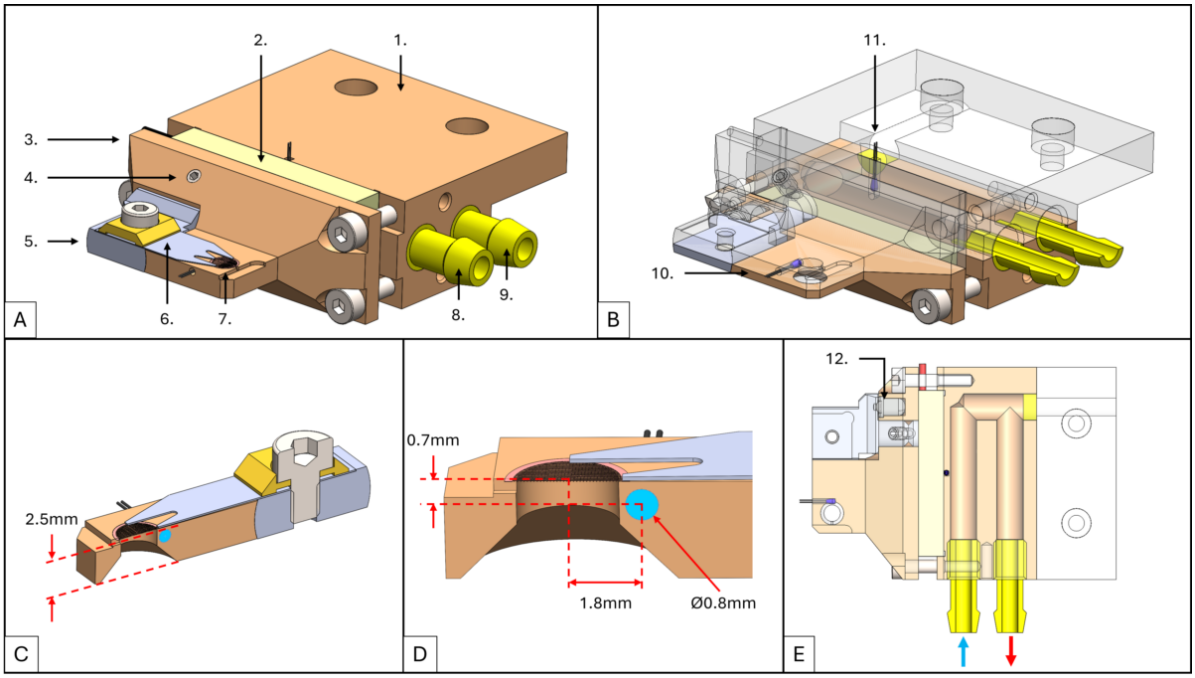

Figure 1.6: A: 1: Water block, 2: TEC, 3: Grid holder, 4: Lock screw, 5: Clip carrier, 6: Grid clip, 7: EM grid, 8: Water inlet, 9: Water outlet. **B:** 10: Grid temperature sensor, 11: Hot side temperature sensor. **C:** Section view through the middle of the EM grid. **D:** Zoom in of Section view C, relative position between temperature sensor and EM grid. **E:** Section view to show the flow path through the water block. 12: Ball detent that registers the clip carier.

ball detent insert next to the clip carrier rotation pin. The spring-loaded ball pushes against a $45°$ angled surface on the back face of the clip carrier. This applies a force at an angle indicated with the red arrow in **a**. The grid clip needs to rotate to an open position that is far enough to clear the path of the EM grid if it is loaded onto the grid holder from above. A $45°$ indent above the angled surface provides a registration point for the ball detent to push in and provide a well-defined and repeatable open position. The forces acting on the indent that register the clip carrier in the open position can be seen in **b**. The clip carrier is retained in the grid holder with an angled set screw that falls into an angled groove in the end of the carrier rotation pin, see **c**. This constrains the axial motion and allows only one rotational motion.

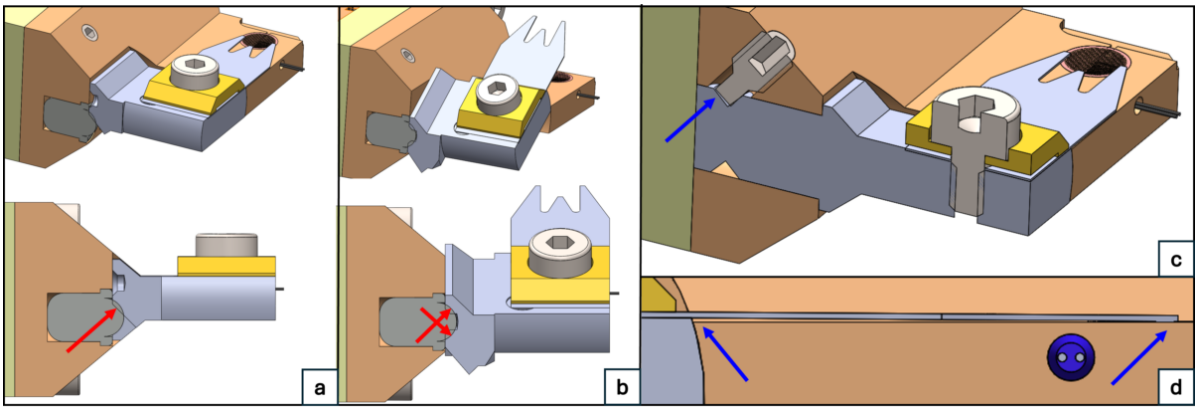

Figure 1.7: a. Section view of the ball detent and clip carrier in the closed position, with the ball pushing against a $45°$ angle to provide some holding torque on the grid clip. **b.** Section view of ball detent and clip carrier in the open position, with the ball registering in a $45°$ indentation. **c.** Section view of the clip carrier rotation pin, showing the set screw that constrains the clip carrier in place. **d.** Zoomed-in side view of the grid clip. The blue arrows indicate the clearance at the base of the clip and first contact at the tip when rotated to the closed position.

The entire DP stage needs to fit between the AFM and microscope objective. Figure 1.8 shows the

dimensioning in this space in the CAD design.

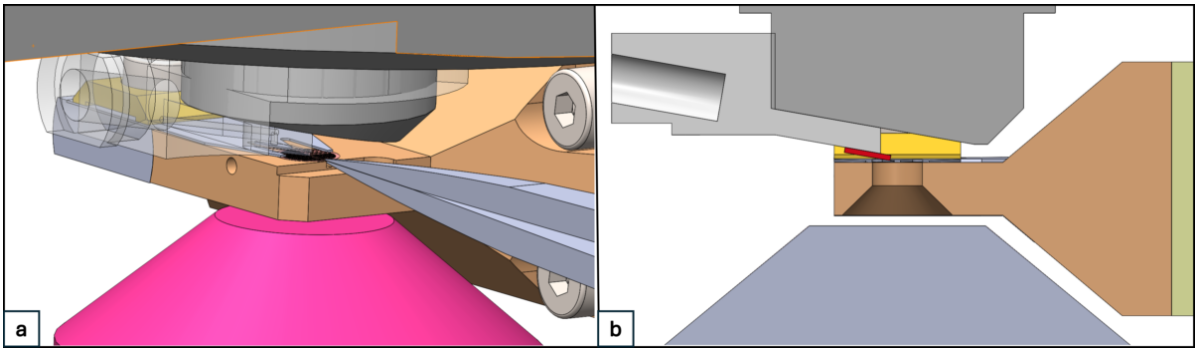

Figure 1.8: a. Isometric view of the grid holder between AFM and microscope objective. **b.** Section view of the grid holder between AFM and microscope objective to illustrate the clearance around the grid clip.

1.3. Fabrication and Assembly

DP Stage

All parts were made using conventional milling and lathing techniques.Some steps of the DP stage assembly can be seen in Figure 1.9.

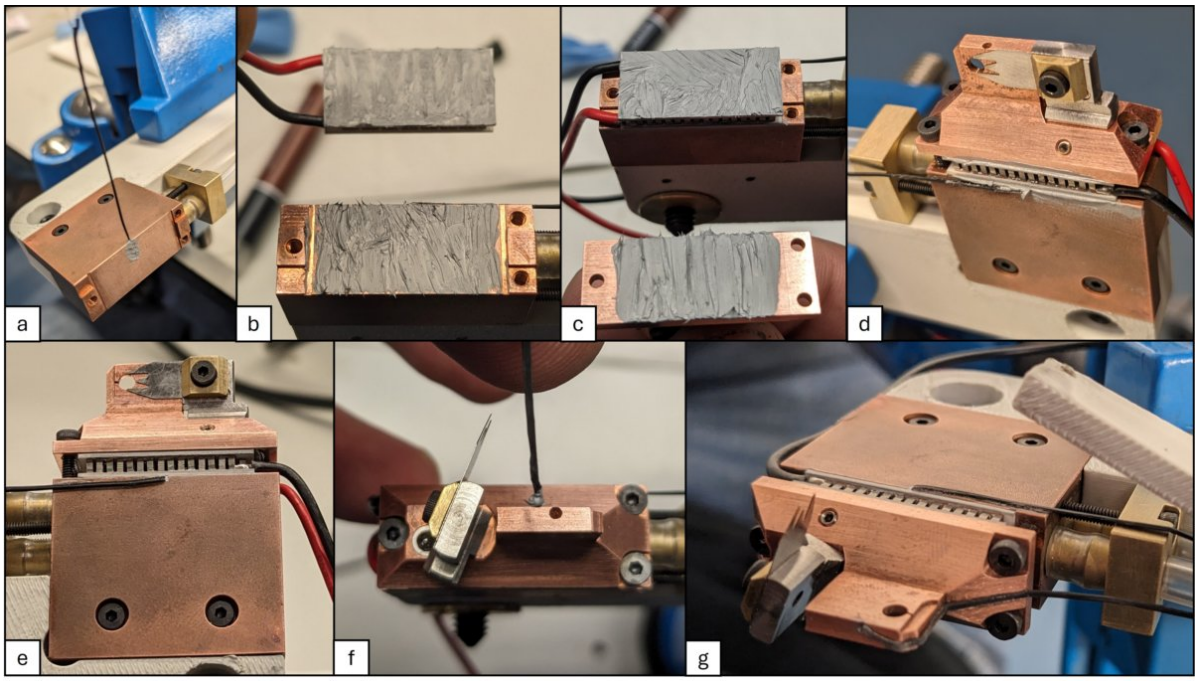

Figure 1.9: a. The water block is shown with the water lines already attached, the temperature sensor is mounted in its slot with thermal paste. **b.** The mating faces of the water block and TEC are coated with a thin layer of thermal paste before pressing them together. **c.** The mating surfaces of the TEC and grid holder are coated with a thin layer of thermal paste before being pressed together. **d.** The grid holder and water block are attached to each other with three M2x12 screws clamping down the TEC, excess thermal paste is squeezed out and wiped away. **e.** Top view of the DP stage, the temperature sensor leads are bent to the side and secured with super glue. **f.** The temperature sensor below the EM grid is mounted in a hole with thermal paste. **g.** The leads of the temperature sensor are bent to conform to the shape of the grid holder and secured in place with super glue.

DP Stage Control Box

The assembled electronics control box and water cooling components can be seen in Figure 1.10. The unit contains a $12\,\mathrm{V}$ power supply to drive the TEC controller, the water pump, and the cooling fan. The fan and pump both have a manual switch to turn them on and off.

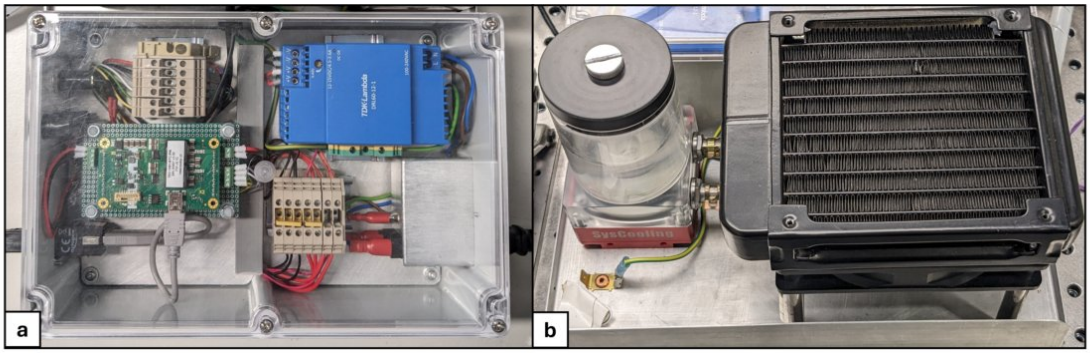

Figure 1.10: a. Electronics to control the DP stage. **b.** Water pump and fan/radiator.

1.4. Validation

The thermal response of the final system can be seen in Figure 1.11. It takes $15\,\mathrm{s}$ to drop the temperature of the grid holder from $20\,^{\circ}\mathrm{C}$ to $10\,^{\circ}\mathrm{C}$ with a current limit of $1\,\mathrm{A}$. This is a factor of 3 longer than the theoretical estimate. The steady-state current and voltage after the temperature drop is measured to be $0.25\,\mathrm{A}$ at $1.2\,\mathrm{V}$. Taking these values back to the graph in Figure 1.5, it can be seen that they roughly match the intended performance with a waste heat output of $0.3\,\mathrm{W}$. The functionality of the DP stage was further validated with the tests described in Supplementary 4 and 5 .

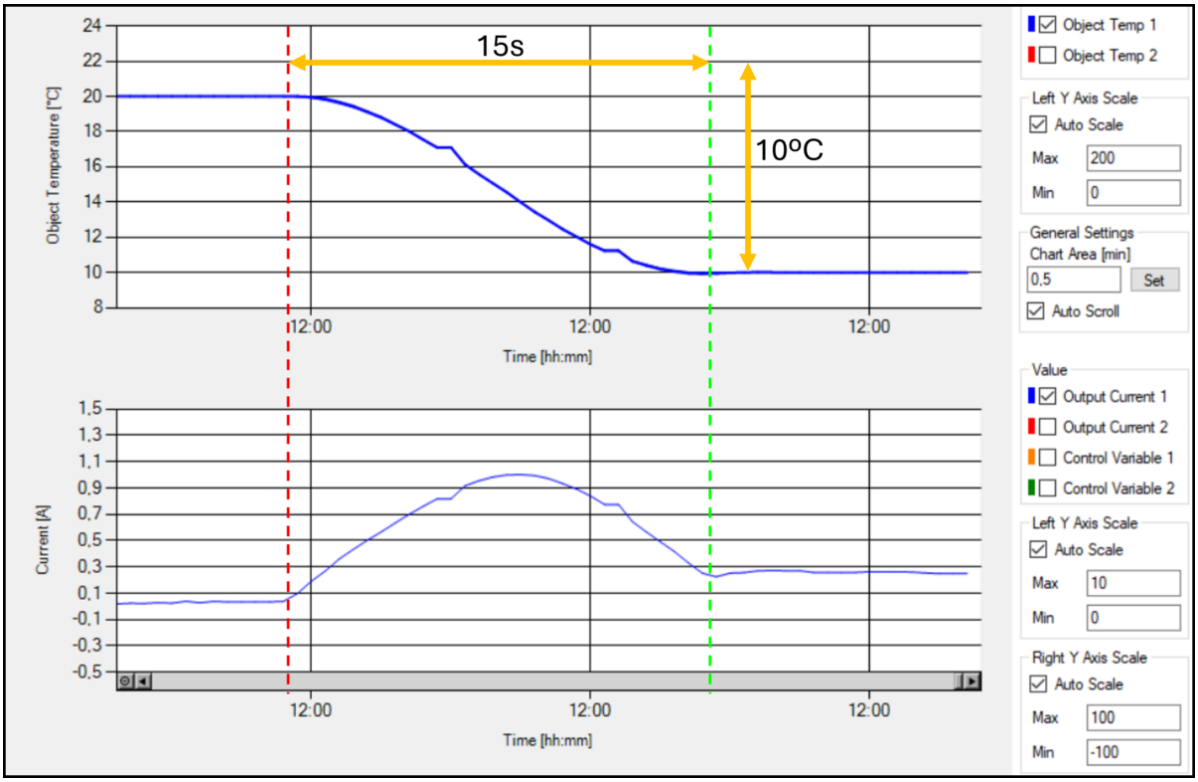

Figure 1.11: Screenshot of the TEC control software, showing the measured temperature and control current over time. The chart is set to a $30\,\mathrm{s}$ window.

The mechanism needs to fit between the AFM and microscope objective. This is not yet tested completely. Figure 1.12 shows the fit of the entire mechanism below the AFM. The microscope was not available at the time of testing.

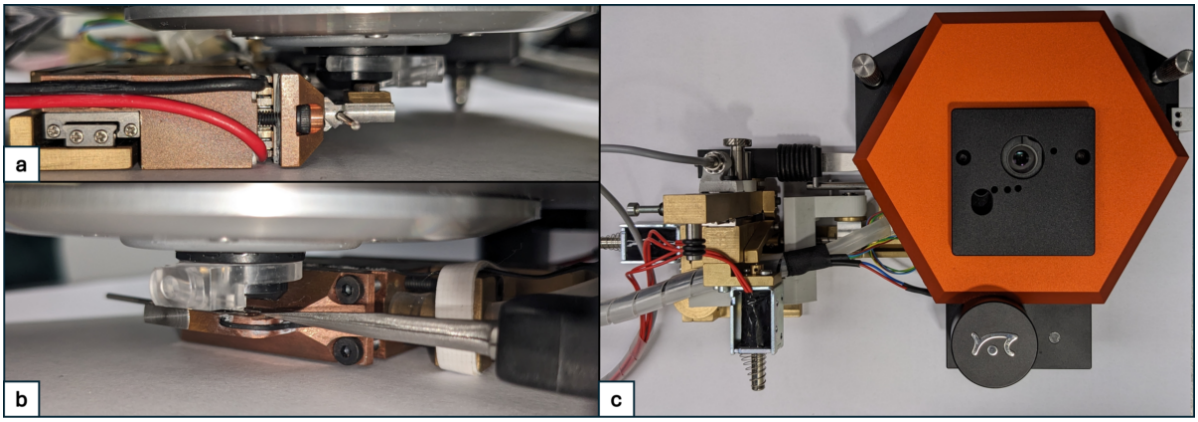

Figure 1.12: a. Side view of the DP stage below the AFM. **b.** Isometric view of the DP stage below the AFM, with grid and tweezers in position. **c.** Top view of the entire mechanism positioned below the AFM.

1.5. Recommendations

1. Automate the grid clip. this was an oversight in the design process, the assumption was made that the grid could be pulled out of the gridclip with the tweezers without opening the clip. the clip has more grip than expected and can pull the grid from the tweezers during the release action, the clip needs to be opened before the release action is triggered.
2. Do an optimization study on the combination of the grid holder, TEC, and water block; there is probably a much smaller configuration possible without compromising performance. A smaller TEC and grid holder would give a bit more room to move in the confined space.
3. Develop LabVIEW software to couple the dew point sensor and the TEC controller together. This would allow the user to input a temperature offset to the dew point and the system would automatically compensate for changes in the dew point. Some effort was put into this but it was too complex to get done within a reasonable time, and for the proof of principle, it was not strictly necessary.
4. Explore other orientations of the TEC. The TEC is oriented vertically in this design. It should be investigated if a design with a horizontal TEC is possible. This could result in a flatter design that is simpler to make.
5. Investigate if the shape of the grid holder affects evaporation due to passive convective cooling airflow. The Comsol simulations indicate some airflow over the EM grid surface due to passive convective cooling, the sideways piramid like shape of the gridholder may have an effect on the direction and magnitude of this airflow. investigate if the airflow has a positive or negative impact on the evaporation rate of the sample and optimize grid holder shape to either exploit this if the effect is possitive, or mitigate it if the effect is negative.

2. Design of Plunge Freeze Mechanism

This work describes the design process of the plunge mechanism. The same design methodology as explained in the DP stage design was applied.

2.1. Requirements

The following set of requirements describes the minimum functionality needed for a proof-of-principle test setup:

1. Less than $300\,\mathrm{ms}$ transition time from temperature-controlled grid holder to plunge freeze action.
2. Minimum $1.5\,\mathrm{m\,s^{-1}}$ plunging speed.
3. The entire mechanism fits between the AFM and microscope.

2.2. Design

Motion Sequence Scheme

The detailed explanation and reasoning behind the motion sequence scheme can be found in the system design section 2 of the thesis paper, the system analysis 5 in the literature study, the system configuration analysis in Appendix A, and the kinematic configuration analysis in Appendix B.

Detailed Design

The following additional functionalities are needed to make the system presented in the motion sequence scheme practically usable:

1. The grid needs to be loaded into the system. This has to be done using the tweezers to pick up the grid from its storage box. This is a delicate manual operation that requires complete freedom of motion of the tweezers. Therefore, the tweezers should be detachable from the plunger and need to be installed after placing and securing the EM grid in the tweezers.
2. The XY position of the EM grid needs to be adjustable when placing it on the grid holder. The position of the grid in the tweezers may vary due to the manual picking operation and the overall number of parts that define the relative position between the EM grid and tweezers. This makes it exceedingly difficult to design and produce the system with the placement defined only by the tolerance stack of all parts. Therefore, some adjustment freedom of the end position of the tweezers in X and Y is needed after installing them onto the system.
3. The Z height of the EM grid needs to be adjustable, for the same reasons stated for the XY directions. The grid should be at some distance above the grid holder after placing the tweezers into the system. Lowering the EM grid to its final position touching the grid holder should be an independent action from attaching the tweezers to the mechanism.
4. The Z position of the EM grid should be maintained during the release action of the EM grid by displacing the DP stage. The tweezers should start the rotation downwards only after the EM grid is completely cleared by the grid holder. This prevents folding damage to the EM grid.
5. Plunging should only be possible after the 90° rotation of the tweezers is completed. This could be done mechanically or in software.

The height of the mechanism that needs to fit under the AFM was chosen to be $12\,\mathrm{mm}$, the same height as the water block of the DP stage. The part of the mechanism that does not need to fit below the AFM has no height restrictions. The plunger travel was chosen to be $30\,\mathrm{mm}$.

Overview of Mechanism

The final design of the mechanism can be seen in Figure 2.1, with all relevant components labeled. A video animation of the mechanism movement can be found in Appendix C. The detailed design

was done with the available raw materials in mind, so all the parts were designed to fit within the raw materials that were in stock in the workshop.

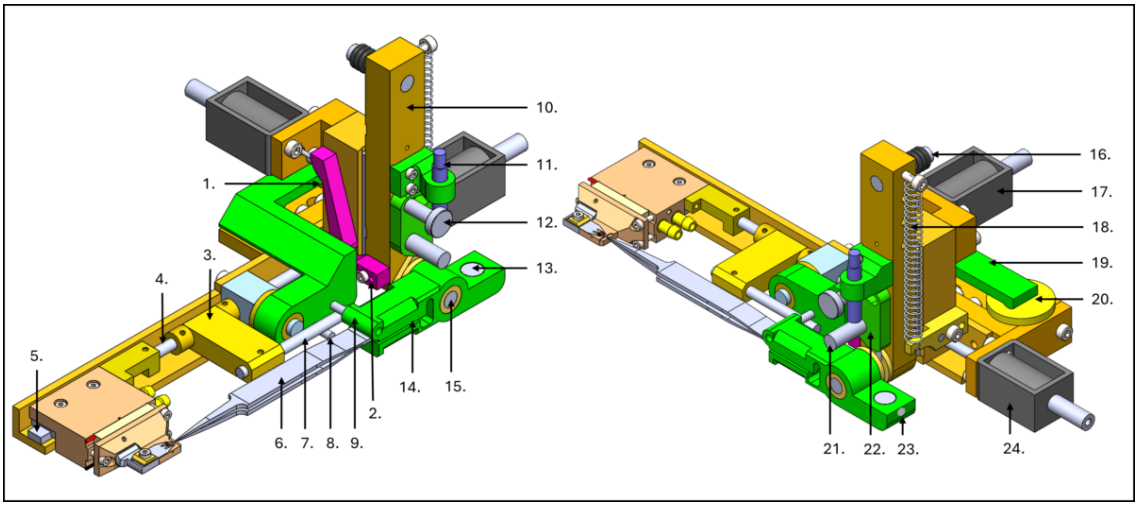

Figure 2.1: 1: Trigger lever. **2:** Trigger toe. **3:** Transfer lever. **4:** Control rod. **5:** Linear rails. **6:** Tweezers. **7:** Release pin. **8:** Height adjust pin. **9:** Pendulum support pin. **10:** Plunger. **11:** Inductive proximity sensor. **12:** Pendulum lock knob. **13:** Magnet. **14:** Pendulum base. **15:** Rotation pin. **16:** Plunge stop. **17:** Solenoid that actuates the plunger release. **18:** Spring. **19:** Height adjust arm. **20:** Height adjust knob. **21:** Stop pin. **22:** Pendulum lock lever. **23:** Set screw. **24:** Solenoid that actuates the grid holder release movement.

Tweezer Attachment and EM Grid XY Position

The rotation pin was chosen as the attachment/detachment point. A plain bearing arrangement was used, with the tweezers attached to the plain bearing with a compliant clamping mechanism. The XY position of the grid can be adjusted by changing the relative position between the tweezers and the plain bearing. The room for adjustment was built into the clamping mechanism, allowing some room for rotating the tweezers and sliding them in and out of the clamp. The tweezers are held in place by the friction of the two clamping surfaces.

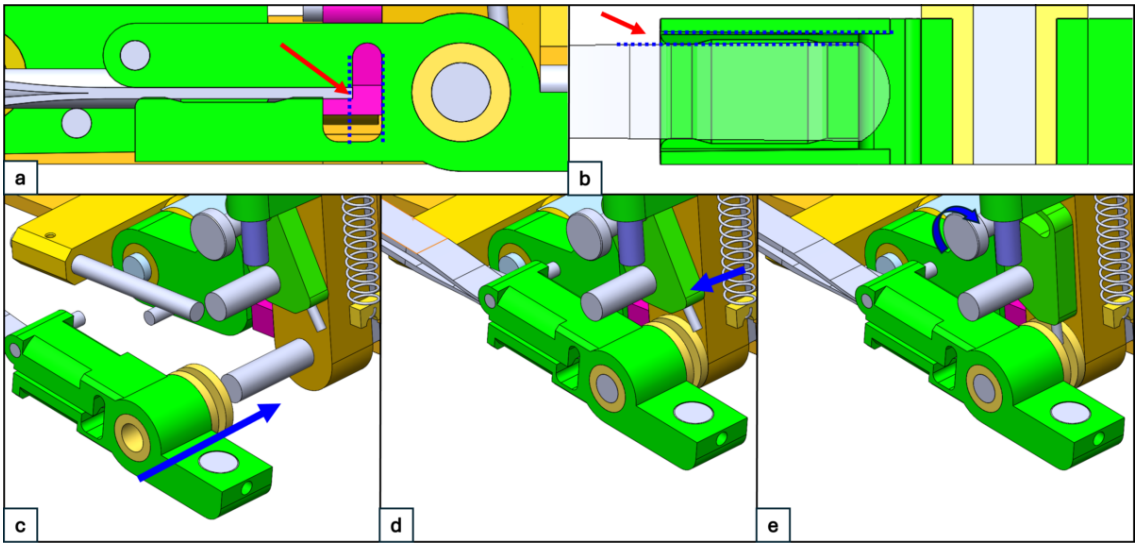

Figure 2.2: a. Sectioned side view of the pendulum base (14), showing the clearance in the clamp to adjust the tweezers (6) in and out for positioning. **b.** Sectioned top view of the pendulum base, showing the side-to-side clearance in the clamp to rotate the tweezers for positioning. **c.** Installing the tweezers onto the plunger (10) by sliding the pendulum base over the rotation pin (21). **d.** Locking the axial movement of the pendulum base by pushing the pendulum lock lever (22) into the groove. **e.** Tightening the pendulum lock knob to secure the pendulum lock lever.

EM Grid Z Positioning and Release

The Z position adjustment of the EM grid on the grid holder and the release of the grid and tweezers are two different functionalities that affect the Z placement constraint on the EM grid. The design challenge is to have both functions work independently and not influence the behavior of the other. Both motions are described in Figure 2.3. The two motions are decoupled with the transfer lever (3). It is mounted on the control rod (4) and is constrained axially with two shaft collars. This transfers the axial release motion to the release pin (7) while maintaining the freedom to transfer the Z height adjustment through the radial rotation freedom of the transfer lever.

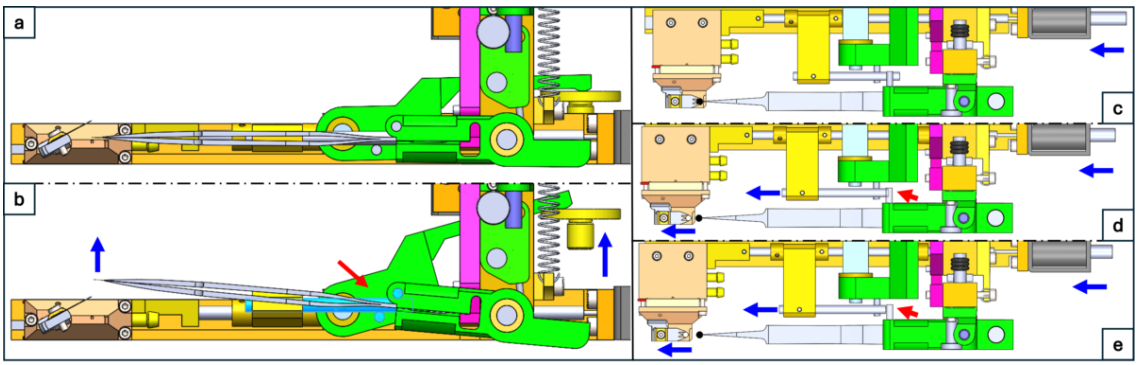

Figure 2.3: a. Front view to illustrate the correct position of the tweezers and EM grid on the grid holder after height adjustments. **b.** Exaggerated movement of the height adjust mechanism to show the working principle. The height adjust knob (20) is moved up out of its normal position in the base, tilting the height adjust lever (19) up. The height support pin (8), mounted in the height adjust lever, pushes the release pin (7) up. This movement rotates the pendulum support base and tweezers up through the pendulum support pin, which is supported by the release pin. **c.** Top view of the mechanism before the release motion is triggered. **d.** The solenoid (24) pushes against the control rod (4) to move the grid holder out from under the EM grid. The pendulum base is supported by the release pin (red arrow) until the EM grid clears the grid holder. **e.** The release pin is pulled out from under the pendulum support pin (red arrow). The timing of this motion can be adjusted by repositioning the release pin in the transfer lever (3).

Actuation

The release motion of the grid holder does not require positional accuracy; therefore, it is possible to actuate it with a solenoid with a sufficient stroke. A travel of at least $8\,\mathrm{mm}$ is needed to completely clear the grid after release. A solenoid with a travel of $12\,\mathrm{mm}$ was selected.

The plunger needs some form of actuation to reach a speed of $1.5\,\mathrm{m\,s^{-1}}$ in less than $30\,\mathrm{mm}$ of travel. Gravity would accelerate the plunger to this speed in roughly $120\,\mathrm{mm}$ of travel if frictional losses are neglected. There is no need for positional accuracy in the travel of the plunger; it can be stopped with a physical bump stop at the end of its travel. The actuation could be done with a solenoid or with some form of spring. Some effort was put into finding a standard solenoid with sufficient stroke length; the ones that were available had large overall dimensions and made it somewhat challenging to design a mechanism that fit within the available space. Due to this and time considerations, the relatively simple implementation of a spring and trigger mechanism was chosen. The same type of solenoid as in the DP stage release mechanism can be used to actuate the trigger mechanism.

Control System

The sequencing of the two solenoids is done with a microcontroller, programmed within the Arduino IDE. The code waits for a manual button to be pressed, which triggers the solenoid that pushes the grid holder away, causing the tweezers to start their rotation. The solenoid stays activated to keep the trigger safety mechanism disengaged. The code then waits for the proximity sensor to trigger the tweezer pendulum at the end of its rotation. This activates the solenoid that releases the plunger trigger. Both solenoids deactivate one second after plunging, and the code returns to its initial state.

Rotation and Plunging

Figure 2.4 explanes the trotation and plunging action. it also sohws the meachical safety feature that prevents accidental release of the plunger.

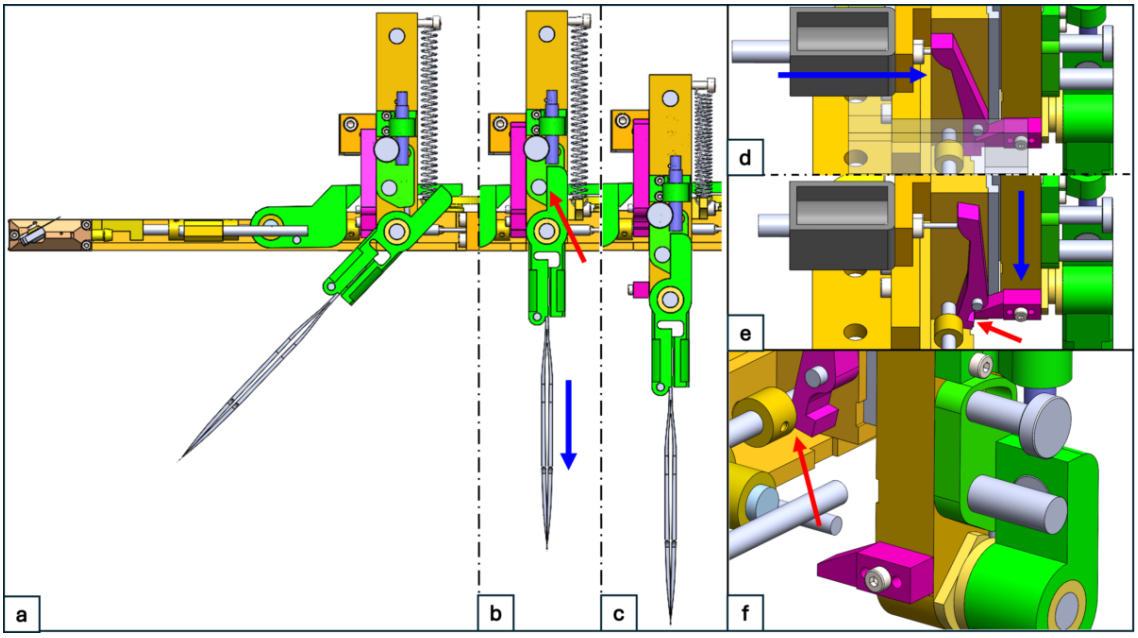

Figure 2.4: a. Side view of the tweezers during rotation. **b.** The pendulum base (14) hits the stop pin (21) at the end of rotation and sticks to it with a magnet (13). The set screw (23) is aligned with the proximity sensor (11), sending the trigger to the plunger release mechanism. **c.** Plunger after the plunging action. **d.** Close-up of the plunger release mechanism. The solenoid (17) pushes against the trigger lever (1) to rotate it. **e.** The trigger lever releases the trigger toe (2) (red arrow) mounted to the side of the plunger (10). **f.** Close-up of trigger mechanism after plunging. The red arrow shows a shaft collar mounted on the control rod (4). It can be seen that the trigger lever rests against the control rod in the open position. The shaft collar sits behind the trigger lever as a mechanical safety against accidental plunging. The shaft collar is pushed away during the release motion of the grid holder.

2.3. Validation

The mechanical movement of the mechanism was analyzed by tracking the position of the tweezer tip in a slow-motion video of the plunge action. Validation of the plunging speed is elaborated on in the results section 4 of the paper. Figure 2.5 shows the position and velocity of the tweezer tip in X and Z directions during the plunging action. The speed graph of the X position shows a large vibration after rotation, caused by the pendulum base (14) hitting the stop pin (21). This vibration causes a side-to-side motion of the EM grid during the plunge action that may result in the grid not entering the ethane completely horizontally. This may affect the cooling performance of the plunge freezing.

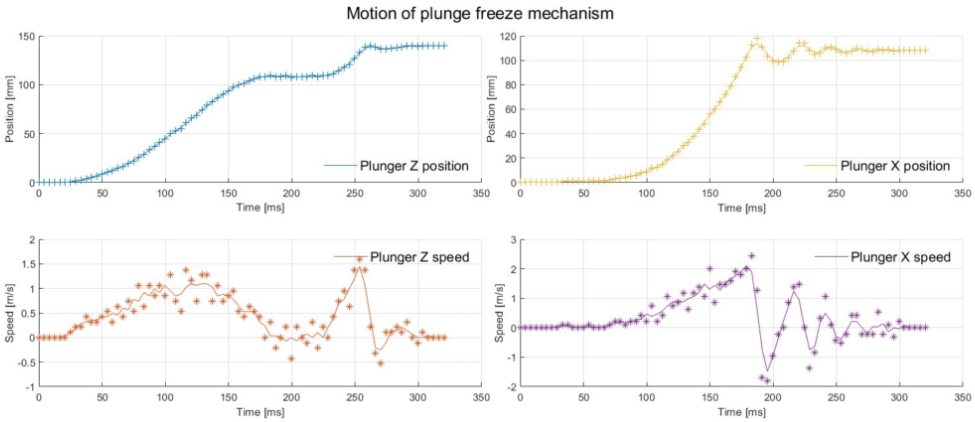

Figure 2.5

2.4. Recommendations

1. Redesign or replace the trigger release mechanism. The trigger release mechanism becomes less reliable when a stronger spring is installed to actuate the plunger. The plunger only just reaches the speed of $1.5\,\mathrm{m\,s^{-1}}$, and this is with the most pretension that can be applied before the trigger becomes less reliable. Alternatives to the plunger triggering and actuation should be considered if faster plunge speeds need to be achieved. A solenoid could be used for actuation, omitting the need for a trigger mechanism. The standard available solenoids with a travel of $30\,\mathrm{mm}$ are somewhat large and may be difficult to incorporate into a compact design. It could be worth considering a custom-designed solenoid, but only after a more exhaustive search of the available standard solenoids is done.
2. The undamped resonance of the tweezer pendulum and the linear motion of the plunger should both be mitigated. This could be done by adding mechanical damping in the form of rotary and linear viscous dampers. They are available in many different sizes and with a large variety of damping characteristics. Incorporating damping in the current mechanism may be difficult as the specification of the required dampers is completely dependent on the physical characteristics of the system. There may not be a suitable standard part with the right size and performance. A better option is to make the addition of viscous damping a core requirement when designing the next iteration of the system. Off-the-shelf linear and rotary viscous dampers can be selected if the need for viscous damping is considered from the start of the design process.
3. Use different solenoids or another actuator type. The solenoids used are specified for $12\,\mathrm{V}$. They are driven with $24\,\mathrm{V}$ to increase the pushing power. At $12\,\mathrm{V}$ they are unable to provide enough power to actuate the system. This works for the short actuation period without overheating; it is, however, not good practice. Therefore, the selection of actuators in the next iteration should be re-evaluated.
4. Consider other production methods during the design process of a future version. All parts were specifically designed to be easy to machine by hand with conventional milling and lathing techniques. The only reason for this is that it made it possible to build the system within a short time span with the available resources and minimal dependency on external production partners, eliminating lead times and the need for a flawless detailed design. However, this means that the design may not take advantage of the design possibilities associated with more modern production techniques. CNC machining, 3D printing, and sheet metal laser cutting and bending should be considered in the next iteration as primary production techniques. This would limit the need for knowledge about manual machining and would simplify the overall manufacturability of the system. It does require a more comprehensive detailed design process.
5. Change to a better version of the tweezers. There are very similar tweezers, from the same manufacturer, that are specifically designed for plunge freezing. They have a little black plastic sliding clip to close them. The tweezers used now are number 5 tweezers; the correct ones have the 5L designation. They have a thicker base that makes them easier to attach to.
6. Use a different method to attach the tweezers to the mechanism. The current mechanism uses a 3D-printed clamp that is held closed with rubber O-rings. The clamping relies purely on friction and does not prevent the tweezers from slipping slightly at the end of the plunging action. While this does not compromise the functionality, it does mean that the position of the tweezers has to be readjusted each time a new grid is placed in the system. A more secure way of interfacing with the tweezers is needed. One possibility is to adapt the attachment mechanism used in the Vitrobot. It clamps the tweezers with screws and has a dovetail clamping system to attach the tweezers to the plunger. This could be adapted so that the tweezers are installed with the dovetail slide instead of the current method of sliding the entire tweezer pendulum on the rotation pin. This could also make the incorporation of viscous damping and adjustment in the X and Y directions easier to implement because the attachment and rotation functionality are separated.
7. Automate opening the grid clip. It is important to first investigate if the spring clip is actually necessary. It needs to be tested if there is a significant difference in evaporation time of similar droplets and therefore thermal transfer with or without the grid clip used. It could be that the thermal contact can be made good enough with a better working and more repeatable alignment system for the EM grid on the grid holder. This would simplify the design of the grid holder.

3. Design of Manual nL Droplet Dispenser

3.1. Problem Description

To validate the performance of the DP stage, a test with manually dispensed droplets was done. This was initially done manually before building the more complex PL/FL dispensing hardware. The smallest pipette available could dispense $2\,\mu\mathrm{L}$ droplets. The problem with this size droplets is that the evaporation time is exceedingly long and not practical for complete evaporation tests. It is possible to dispense smaller volumes by hand with a syringe and a sufficiently small dispensing needle. The required force to overcome the capillary forces in the needle is quite large, which makes controlling the displacement of the syringe plunger by hand difficult and not repeatable. Hence, an adapter was designed to dispense sub-$100\,\mathrm{nL}$ droplets using a standard $1\,\mathrm{mL}$ syringe with a 32 gauge straight dispensing needle with Luer lock connection.

Practical requirements:

- Manufacturable with materials available.
- With manufacturing techniques available.

3.2. Design

The $1\,\mathrm{mL}$ syringe has a travel of $58\,\mathrm{mm}$ to dispense its entire volume. The goal is to dispense volumes around $100\,\mathrm{nL}$, which would require a syringe plunger displacement of $5.8\,\mu\mathrm{m}$. There are different mechanical principles that can be used to generate this motion. It can be done, for example, with a screw that is rotated to push on the plunger. If we use a metric fine thread with a pitch of $0.5\,\mathrm{mm}$, one rotation would displace a volume of $8.6\,\mu\mathrm{L}$. The rotation required to push in the plunger $5.8\,\mu\mathrm{m}$ to generate a $100\,\mathrm{nL}$ volume displacement would only be $4.2°$ and require 86 markings on the dial. For ease of use and less sensitivity to manual input accuracy, it would be beneficial to have a larger ratio between input motion and output motion. This can be achieved with a differential screw arrangement. This type of mechanism converts the input rotation into a translation that is the difference of two thread pitches. If a metric thread `M5x0.8` and a metric fine `MF10x0.75` are used, one full rotation would lead to a plunger displacement of $0.05\,\mathrm{mm}$ and an equivalent volume displacement of $860\,\mathrm{nL}$. The dial would need 8.6 markings to get even $100\,\mathrm{nL}$ divisions. This is, however, not practical in use, so an even number of divisions is preferred. Eight divisions give a volume displacement of $107.5\,\mathrm{nL}$, which is close enough for the intended purpose of this device. It is possible to deviate from standardized threads to get the exact difference needed, but this makes fabrication far more complicated and would have taken too much time.

Figure 3.1 shows a cross-section of the mechanism. If the differential nut rotates 1 revolution, it unscrews $0.75\,\mathrm{mm}$ from the body and also extends the plunger $0.8\,\mathrm{mm}$ into the body, resulting in a displacement inwards of $0.05\,\mathrm{mm}$.

3.3. Fabrication

Brass was chosen as the material because it was available in the correct sizes, is easy to machine, holds geometry well, and has good sliding properties against steel. The plunger is made of steel. See Figure 3.2.

3.4. Validation

The volume was measured using a USB microscope. The test setup can be seen in Figure 3.3. An image of the droplet on the end of the needle was captured with one mark of rotation, two marks of

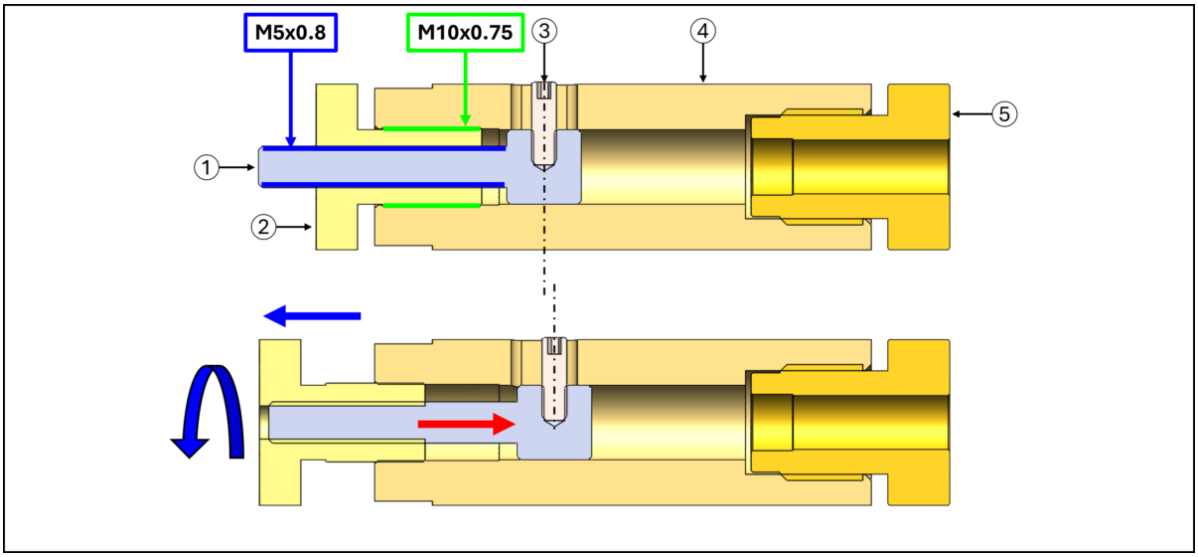

Figure 3.1: 1. Plunger with an `M5x0.8` thread. **2.** Differential nut with `M10x0.75` thread on the outside and `M5x0.8` thread on the inside, engraved with eight markings on the outside diameter. **3.** `M3xL10` setscrew, slides in a slot in the body to constrain rotational motion of the plunger. **4.** Body of the mechanism, with an `M10x0.75` thread on one side to accept the differential nut, an `M14x1.5` thread on the other side to accept the retaining nut, and a $3\,\mathrm{mm}$ x $8\,\mathrm{mm}$ slot on the side to house the sliding set screw. **5.** Retaining nut that holds the syringe in place and clamps it in position when tightened. Rotating the differential nut one revolution results in a linear motion of the differential nut of $0.75\,\mathrm{mm}$ in the direction of the blue arrow, and the plunger moves $0.8\,\mathrm{mm}$ in the direction of the red arrow, resulting in a $0.05\,\mathrm{mm}$ motion of the plunger into the body.

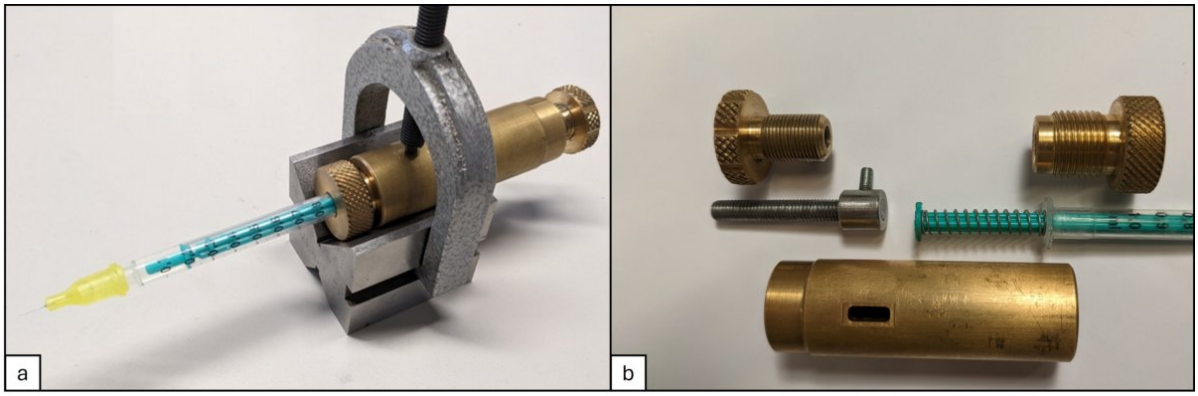

Figure 3.2: a. Assembled mechanism mounted in a toolmaker's V-block. **b.** All parts before assembly. Note that the syringe handles are clipped off to fit in the mechanism. There is also a spring installed around the syringe plunger to add a small preload in one direction to eliminate any play in the differential screw arrangement.

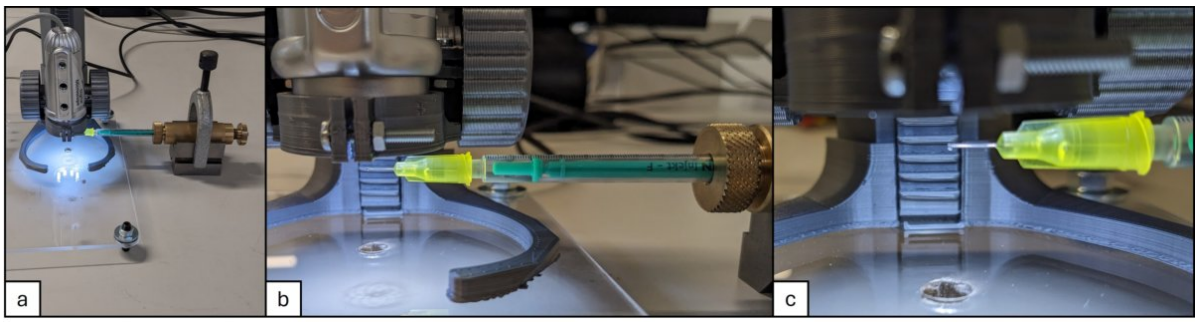

Figure 3.3: a. Overview of the test setup. A USB microscope in a stand with height adjustment to focus, the syringe was positioned below the microscope mounted in a toolmaker's V-block. **b.** Close-up of syringe position. **c.** Close-up of the needle with a droplet on the end.

rotation, and three marks of rotation, in succession. One such sequence can be seen in Figure 3.4. This was done 5 times to give a total of 15 images with 5 of each droplet size. Determining the diameter of the droplet was done by placing 3 points on the edge of the droplet and 2 on the edge of the needle in a MATLAB script. The diameter of the needle is known and used to calculate the pixel size needed to calculate the diameter of the droplet. This manual operation was done 5 times for each image giving a total of 75 data points. Figure 3.5 shows the results of these measurements. The linearized displaced volume is $19\,\%$ less than the theoretical designed displaced volume. The standard deviation shown is a combination of the variation in the size of the 5 droplets measured at each position and the manual error of measuring them 5 times each.

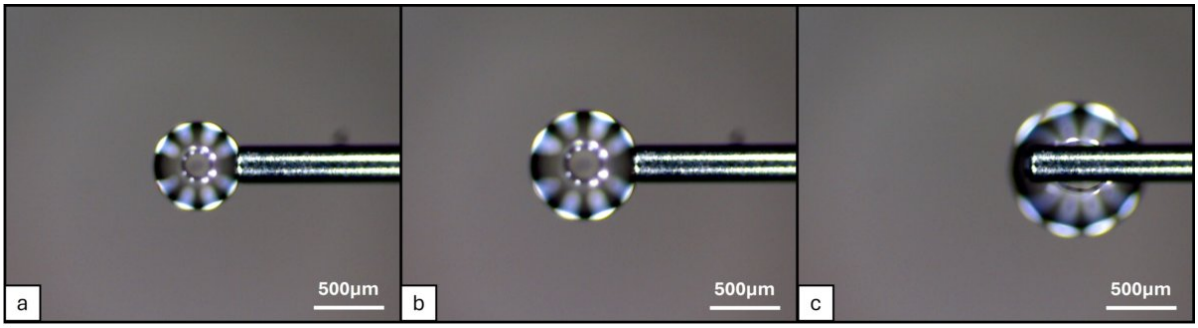

Figure 3.4: a. Droplet produced with one mark rotation, with a volume of approximately $90\,\mathrm{nL}$. **b.** Droplet produced with two marks of rotation, with a volume of approximately $180\,\mathrm{nL}$. **c.** Droplet produced with three marks of rotation, with a volume of approximately $285\,\mathrm{nL}$.

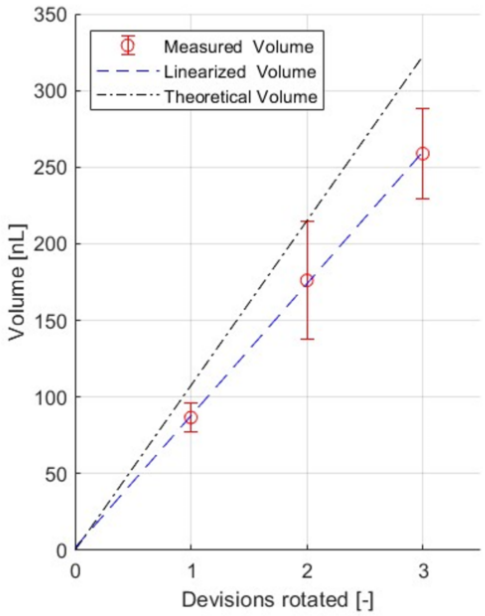

Figure 3.5: Result from dispensed volume tests.

3.5. Recommendations

Using a larger diameter fine thread instead of the `M5x0.8` on the plunger can reduce play in both linear and rotational directions without complicating manufacturing; it can still be done with a standard metric fine tap and die. Changing the pitch of the plunger and dial so that the plunger has the smaller pitch and the dial has the larger pitch results in a screw motion inwards to displace volume, which is a more intuitive use mode.

4. Test Report nL Experiments

4.1. Test Description

The DP stage was specifically designed and built to cool down the sample and reduce evaporation rate to extend process time. This functionality was tested before continuing with the development of the rest of the system. The goal of this test was to validate this principle without the need for a complicated dispensing method required to make pL or fL droplets. Instead, it was tested with the smallest volume droplets that could be dispensed by hand. For this purpose, a manually operated attachment for a $1\,\mathrm{mL}$ syringe was designed and fabricated, allowing for the controlled formation of $100\,\mathrm{nL}$ droplets at the tip of the dispensing needle. A detailed description of this mechanism can be found in Supplementary 3. During testing, droplets between $40\,\mathrm{nL}$ and $100\,\mathrm{nL}$ were dispensed. The droplets were dispensed on a treated glass surface with known surface hydrophilicity.

4.2. Test Setup

The volume of a spherical cap-shaped droplet can be calculated by measuring its radius and contact diameter in a side-view picture, assuming it is spherical and the contact diameter is round.

The test setup used for this experiment can be seen in Figure 4.1. Two USB microscopes were used to capture the top and side view data. The side view microscope was mounted on a Thorlabs XYZ stage for positioning, while the top view microscope was mounted on a single Z stage. The DP stage was mounted on a holder with three ballpoint feet that rest on a point-line-plane mounting surface to avoid overconstraining the position of the DP stage. The mounting surface was adjusted in X and Y and secured to position the DP stage in the middle of the field of view of the top view microscope. This kinematic mount allows for easy handling of the DP stage outside of the test setup and good repeatability of its position when placing it back, eliminating the need for an XY stage in either the DP stage positioning or the top view microscope.

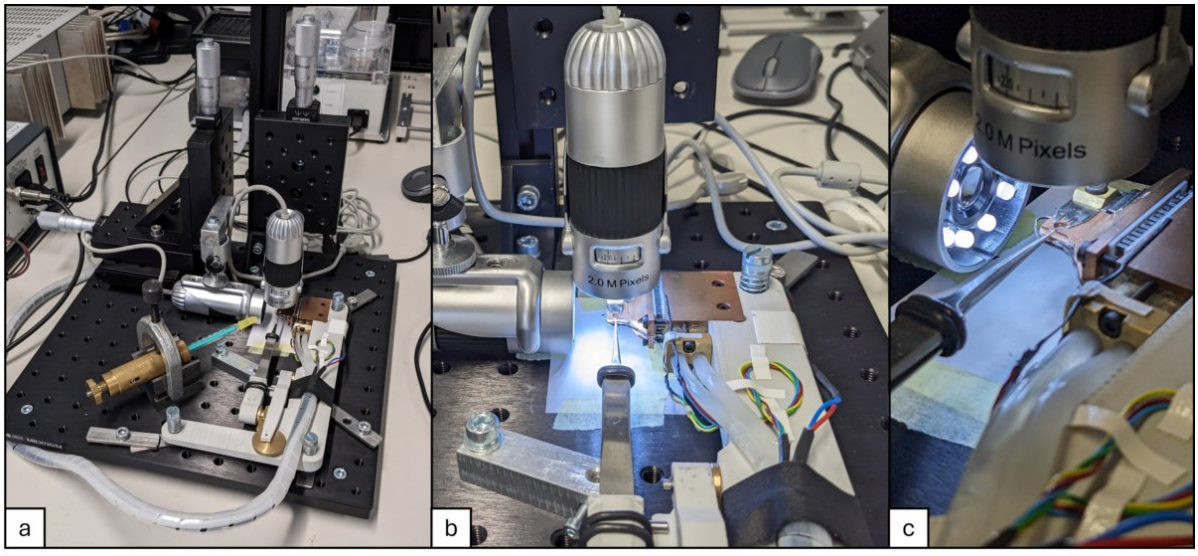

Figure 4.1: a. Overview of the test setup. **b.** Side view of the two cameras and DP stage during a measurement. **c.** Closeup showing a piece of glass, held by the tweezers and grid clip onto the grid holder.

The nL dispenser was mounted in a toolmaker's V block. There is an angled stop mounted to the table surface next to the tweezers. The V block is pushed against this stop, constraining its position in the XY plane. Then, to dispense, the V block with the nL dispenser is tilted forward to lower the needle to the glass surface and dispense a droplet. This method of positioning put the droplet in the same place

for every test with enough precision to avoid adjusting the position of the microscopes after dispensing.

A reference measurement is needed to determine the size of the pixels in the picture to convert the measurements from pixels to meters. For this purpose, a photo from the top is needed to determine the diameter of the droplet based on the size of the hole in the grid holder below the glass plate. The diameter measured in the top view is used to calculate the pixel size in the side view, as there are no other features to reference in the side view. See Figure 4.2 for the top and side view of one of the measured droplets.

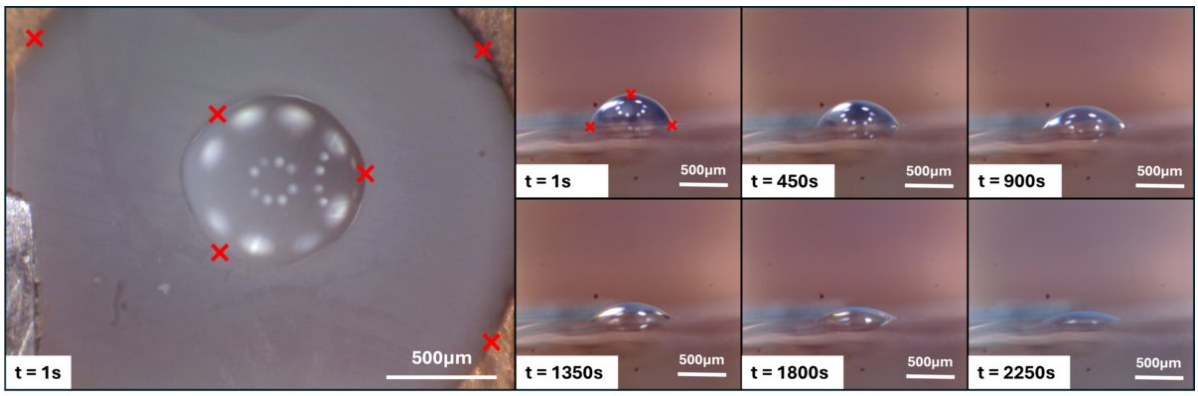

Figure 4.2: Photo series showing the evaporation of a droplet on a glass surface. The temperature of the grid holder was set to $0\,^{\circ}\mathrm{C}$ offset to the dew point. **t = 1 s**: The top view of the droplet just after dispensing is used to determine the size reference needed to analyze the side view data. Three points are placed on the circumference of the droplet, and three points are placed on the edge of the hole on the grid holder. The hole has a diameter of $2.5\,\mathrm{mm}$. This information is used to calculate the diameter of the droplet, which is then used to calculate the pixel size in the side view. This pixel size value is used to analyze all subsequent frames.

4.3. Results

Average Evaporation Rate

Figure 4.3 shows the volume of nine droplets over time at different temperature offsets. During these tests, the ambient temperature varied between $18.8\,^{\circ}\mathrm{C}$ and $19.1\,^{\circ}\mathrm{C}$, with relative humidity between $57\,\%$ and $60\,\%$. The setpoint temperature of the controller was manually adjusted before each test to account for changes in the measured dew point. The graph shows results from the point each droplet reached $35\,\mathrm{nL}$. The average evaporation rate measured is shown in the right graph. A test with a $9\,^{\circ}\mathrm{C}$ temperature offset equal to ambient temperature served as a baseline, showing an evaporation rate of $223.0 \pm 97.3\,\mathrm{pL\,s^{-1}}$. The evaporation rate at $0\,^{\circ}\mathrm{C}$ temperature offset was $29.5 \pm 55.8\,\mathrm{pL\,s^{-1}}$, with the standard deviation larger than the measured value, highlighting a limit of the data acquisition method. Some data points gave a negative evaporation rate due to manual errors in placing points, leading to inaccuracies.

Evaporation Behavior

The droplets showed two modes of evaporation. The droplet maintains a constant contact diameter during the first $75\,\%$ of the evaporation, with a reducing contact angle. The droplet evaporates with a reducing diameter and contact angle during the last $25\,\%$. This behavior was observed in all experiments, independent of the temperature offset to the dew point, start volume, and evaporation time. The data is plotted in Figure 4.4, normalized to display this behavior. The diameter on the Y-axis is normalized to the start diameter at the beginning of each experiment. For the first two graphs, the time on the X-axis is normalized to the total evaporation time of each experiment. The diameter is split into two graphs to highlight behavior that was observed in four out of the nine experiments. The diameter appears to reduce suddenly around $60\,\%$ of the evaporation time and then continues to be constant after the jump. The split in the contact angle measurements shows that the jump appears to have a small effect on the constant reduction of the contact angle.

The data presented so far suggest that the evaporation rate stays somewhat constant regardless of the droplet's evaporation mode. Evaporation happens at the air-liquid boundary, so it would be reasonable

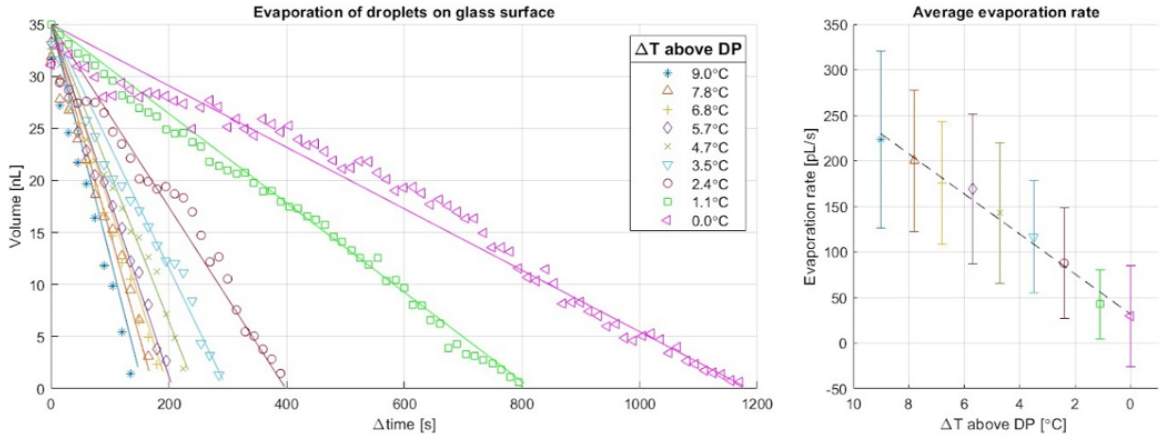

Figure 4.3: Results from nine evaporation tests on a glass surface at different temperature offsets to the measured dew point.

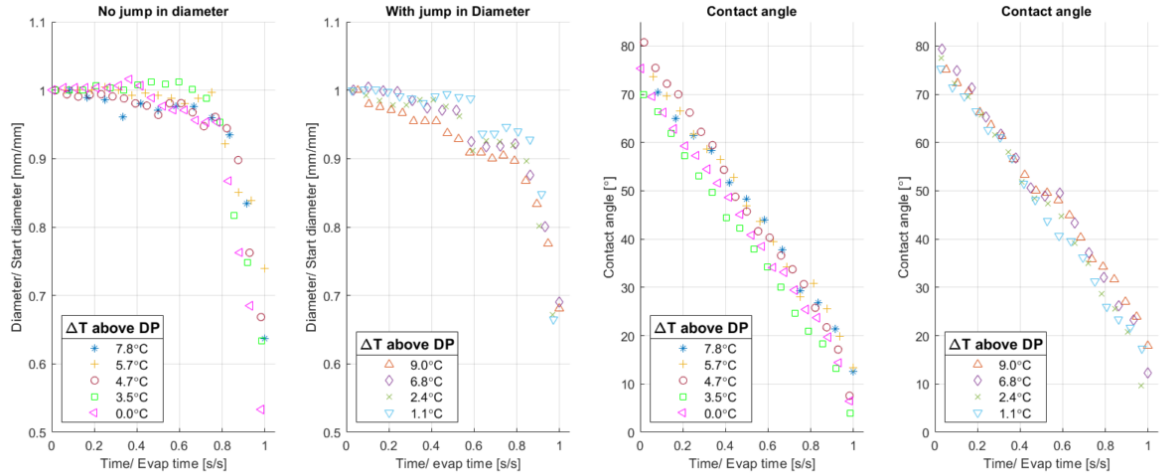

Figure 4.4: Normalized diameter and contact angle data from the Nine evaporation tests, all data is represented on a normalized time axis.

to assume that the surface area of the droplet has some effect on the evaporation rate. The normalized diameter, surface area, and volume were taken from the combined data of the nine experiments. The normalized evaporation rate was calculated from this volume, and with this dvdt and the surface area, the behavior of the mass flux during evaporation can be estimated. The described data is plotted in Figure 4.5. The expected evaporation behavior would be that the rate of evaporation per surface area, or the actual mass flux, stays somewhat constant for a given temperature offset. However, this is not the observed behavior. The evaporation rate appears to stay constant and is not influenced by the surface area. The mass flux therefore increases in the second mode of evaporation.

This repeatable behavior implies that, at least at the $100\,\mathrm{nL}$ scale, the rate of evaporation is mostly determined by the temperature offset and unaffected by droplet shape. The evaporation time is mostly determined by the starting volume. The transition between evaporation modes is likely caused by the interaction between the water surface tension and adhesion to the substrate.

This behavior has no major effect on the intended use case. The best-case scenario would be to have a large starting diameter and no reduction in diameter during evaporation to get the largest possible measurement area for a given start volume. The behavior implies that the evaporation time only depends on the start volume and not the starting contact angle and diameter. This could mean that the evaporation time for a given volume is independent of the hydrophilicity of the substrate it is located on.

Dispensing on a more hydrophilic surface to start with a large diameter and lower contact angle would be preferable and could be done without a major increase in the evaporation rate due to the relatively large surface area. This will result in a later transition between modes or even only evaporation in mode one. This would give the largest usable area to measure for a given starting volume. One important note is that this may only apply to droplets in the nL range; the change of scale to the pL and fL range may change the observed behavior significantly.

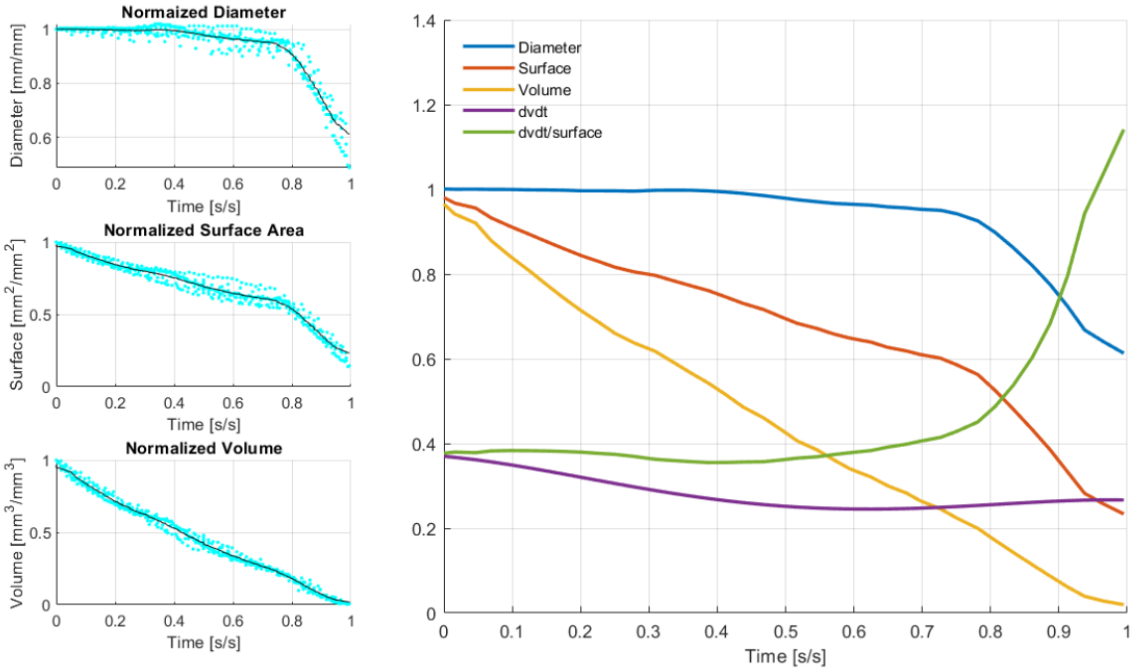

Figure 4.5: Average evaporation behavior of the nine tests combined.

Contact Angle on EM Grid

A contact angle measurement of an nL droplet on a hydrophobic EM grid was needed to analyze data from the experiments described in Supplementary 5. The goal of this test was to obtain the start angle of the droplet. The same methods as described before were used to obtain the data. See Figure 4.6. The measured start angle was $70°$. The evaporation behavior observed in the diameter and volume data is similar to the data obtained in the previous experiment.

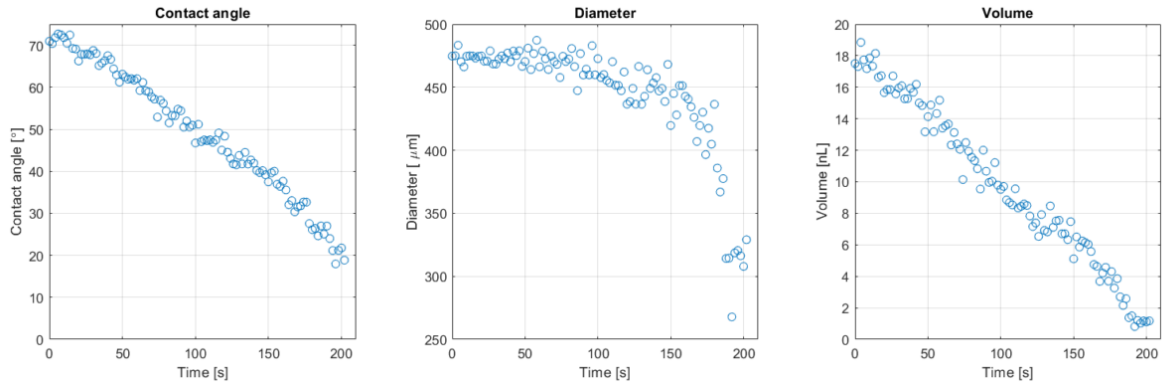

Figure 4.6: Data form an droplet Evaporating from an Hydrophobic EM grid.

4.4. Recommendations

1. Repeat the DP offset experiments more than once per temperature offset to get a more reliable data set.
2. Repeat the DP offset experiments on surfaces with different hydrophilicity to see if the evaporation rate is actually not dependent on this variable.
3. Repeat the DP offset experiments on an EM grid with and without plasma cleaning to see if the change of substrate has a significant effect on the evaporation behavior.
4. Automate the data acquisition from the droplet side view. All frames (1000+) were processed by hand, which limited the amount of tests that could be done in the available time.
5. Find a way to record both top and side view throughout the experiment. This would give a better estimate of the diameter. Only the first top image was used in the presented experiments due to the inability of the capture software to record two microscope inputs at the same time on one computer.

5. Test Report pL Experiments

5.1. Test Description

The goal of this test is to repeat the experiments that measure the evaporation rate of nL droplets but now on pL droplets, to compare the evaporation behavior at these different size scales. The measurement method used for the nL experiments, the side view microscope, does not have enough resolution and zoom to obtain usable measurements for pL droplets. Therefore, the interferometer setup is used to measure the shape of the dispensed droplets. Dispensing pL-sized droplets is not practically doable with a manual syringe; hence, the microfluidic cantilever was used. The experiment described here is partly for practice and preparation for the partial integration test, to gain a better understanding of the dispensing and measurement steps before integrating the plunge freezing into the process.

5.2. Test Setup

The test setup used for this experiment is the same as that used for the partial integration testing described in Supplementary 6. The plunging mechanism was not used in this test. The droplets were dispensed on an untreated EM grid. The user manual in Appendix D describes this procedure.

5.3. Results

Dispensing pL Droplets

It was possible to dispense droplets on the carbon film in the middle of a grid square without touching the grid bars. Figure 5.1 shows five droplets just after dispensing.

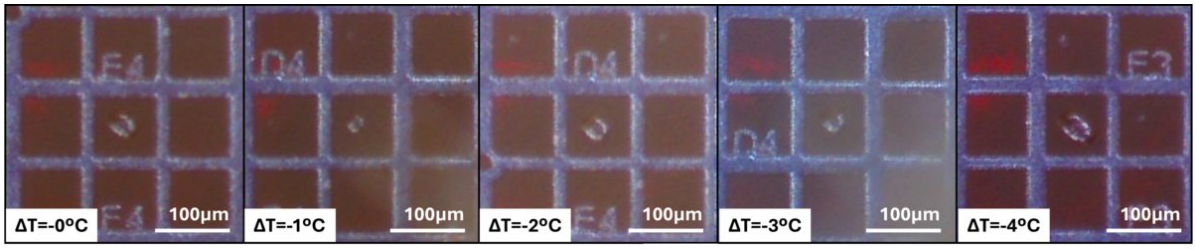

Figure 5.1: Droplets on an EM grid just after dispensing.

Real-Time Thickness Measurement

The intention was to measure the shape of the droplet during evaporation. This was not done successfully. The measurement method does not work on droplets with a large contact angle, and it only produced usable thickness data at the end of the tests. The raw fringe pattern data was used to measure the droplet diameter during evaporation. Figure 5.2 shows some fringe pattern data recorded with the interferometer at different time intervals from the delta $T = -3\,^{\circ}\mathrm{C}$ droplet test. Note that the observable change in diameter is small between the $55.1\,\mathrm{s}$ and $87.2\,\mathrm{s}$ frames. The end of the evaporation time was determined by manually reviewing the data and finding the point from which this somewhat constant diameter was observed.

Average Evaporation Rate of pL Droplets

The diameter of the droplet just after dispensing was measured in the footage from the USB microscope, using the size of the grid squares as a size reference. The starting contact angle was assumed to be 70°, based on a nL experiment on an EM grid. The measurement method and the mentioned nL experiment are described in Supplementary 4. See Figure 5.3 for the diameter data. The data is shifted on the X-axis to align the linear fit of each measurement to a starting diameter of $45\,\mu\mathrm{m}$. This was done to better illustrate the effect of temperature on the slope of each fit. Note that all droplets started smaller than

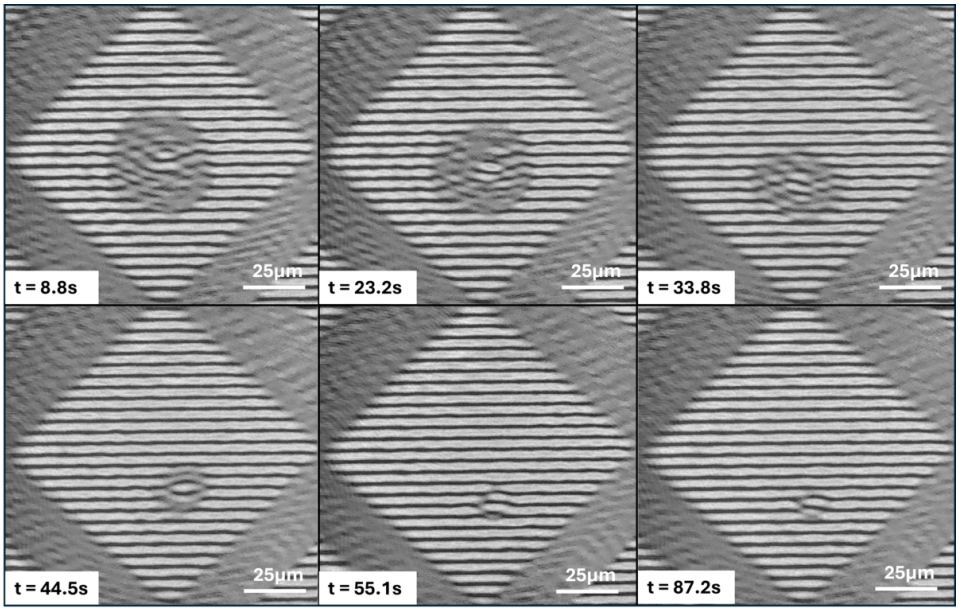

Figure 5.2: Sequence of fringe pattern data from the delta $T = -3\,^{\circ}\mathrm{C}$ measurement.

$45\,\mu\mathrm{m}$. The final diameter of the droplet that remains was estimated by taking the average of the last 10 measurements. This value is indicated with the horizontal fitted lines at the end of each measurement. This diameter and the last measured thickness with the interferometer were used to calculate the final volume of the remaining droplets.

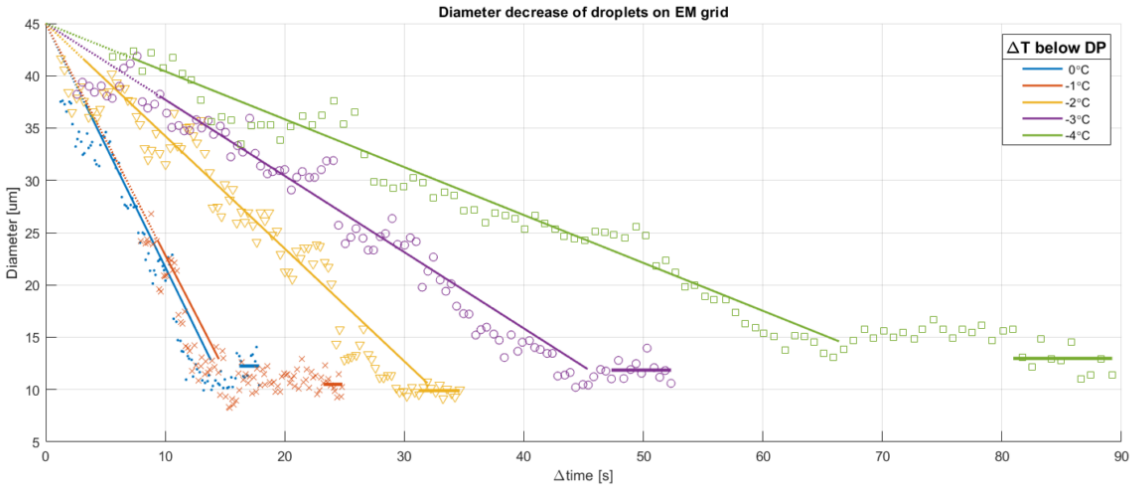

Figure 5.3

The average evaporation rate was estimated based on the volume reduction and total evaporation time, shown in Figure 5.4. The error bars show the standard deviation of the data acquisition method used, not the deviation between multiple experiments.

ΔT below DP temp.	Start Diameter (µm)	Start Volume (pL)	End Diameter (µm)	End Volume (fL)	Time (s)	Average Evaporation Rate (fL/s)
-0°C	35.26 ± 1.65	7.06 ± 0.97	12.26 ± 1.18	4.81 ± 1.06	20.7s	340.63 ± 44.80
-1°C	25.70 ± 1.50	2.74 ± 0.46	10.50 ± 0.90	3.33 ± 0.58	15.1s	181.28 ± 29.02
-2°C	33.27 ± 1.07	5.91 ± 0.55	9.91 ± 0.49	6.11 ± 1.00	38.7s	152.45 ± 13.61
-3°C	28.51 ± 0.95	3.72 ± 0.37	11.86 ± 0.96	8.17 ± 1.46	50.7s	73.16 ± 6.93
-4°C	41.04 ± 3.14	11.23 ± 2.48	12.99 ± 1.53	6.09 ± 1.63	134.6s	83.40 ± 17.54

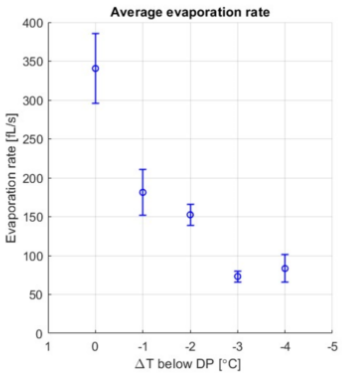

Figure 5.4: Results from measuring the average evaporation rate of five droplets on a hydrophobic EM grid at different temperature offsets below the measured dew point.

5.4. Recommendations

1. Repeat the experiment on plasma-treated EM grids.
2. Improve the dispensing process to be able to dispense droplets on the plasma-treated grid without touching the grid bars.
3. Conduct more than one measurement for each temperature offset to get a more reliable data set.
4. Automate the transfer from dispensing to measuring. The time between dispensing and starting a measurement was reduced to less than $5\,\mathrm{s}$ through a lot of practice, but this is not a viable testing method for droplets smaller than $1\,\mathrm{pL}$ due to the shorter evaporation times.

6. Test Report Integration Experiments

6.1. Test Description

The test integrates manual dispensing with a microfluidic cantilever on an EM grid, real-time thickness measurement with a Mach-Zehnder interferometer, and a plunge freezing procedure. The test has two main goals: to validate the performance of the new DP stage and plunge freezing mechanism, and to validate the thickness measurement method by comparing the measured thickness just before plunge freezing with the measurements from CryoEM. This test report supplements the test procedure described in the main paper in **Part I** of this work. Any additional information is provided here.

6.2. Test Setup

The test setup is described in the Materials and Methods section 3 of the paper.

6.3. Test Procedure

The EM grids received plasma treatment to make the surface more hydrophilic. Liquid ethane is prepared in a Vitrobot ethane cup after the startup sequence of the test setup is completed. The complete test procedure can be found in the user manual in Appendix D.

6.4. Measurement Principle

The following explanation of the measurement principle used is taken directly from the work by [2] that explains its development. No changes were made to the fundamental working principle of the technique when implementing it into the test procedure.

An interference fringe pattern is the intensity distribution recorded by the CCD detector. This can be formulated mathematically as follows:

$$i(x,y) = a(x,y) + b(x,y) \cdot \cos\left(\Delta\phi(x,y)\right) \tag{6.1}$$

Here, $i(x,y)$ represents the interference pattern as an intensity distribution over the CCD. It is represented as a function of x and y, which is the distance of a pixel from the origin. For a pixel in the jth column and ith row, starting from the origin:

$$x = j \cdot \delta \qquad\qquad y = i \cdot \delta$$

where δ is the size of a single pixel. $a(x,y)$ and $b(x,y)$ represent the DC component and modulation amplitude of the interference pattern. The term $\Delta\phi(x,y)$ is the Optical Phase Difference (OPD). The OPD is the resultant phase field obtained by adding the signal $\phi_s(x,y)$ and carrier waves $\phi_c(x,y)$. The signal wave contains the desired height information $h(x,y)$:

$$\Delta\phi(x,y) = \phi_s(x,y) + \phi_c(x,y) \qquad \phi_s(x,y) = \frac{h(x,y) \cdot 2\pi(n-1)}{\lambda} \qquad \phi_c(x,y) = 2\pi f_x \cdot x + 2\pi f_y \cdot y$$

where n is the refractive index of the test sample (droplet) and λ is the wavelength of the light used. The carrier wave is characterized by the carrier frequencies f_x and f_y in the x and y directions, respectively.

These are spatial frequencies which are related to the fringe spacing as:

$$f_x = \frac{1}{\Delta x \cdot \delta}$$

$$f_y = \frac{1}{\Delta y \cdot \delta}$$

Δx and Δy are the fringe spacings, in pixels, observed in the interference fringe pattern. The carrier frequencies, therefore, have the units m^{-1} in SI standards.

Equation 6.1 can be expressed in complex notation as follows:

$$i(x,y) = a(x,y) + \frac{1}{2} \cdot b(x,y) \cdot \left(e^{-i\Delta\phi(x,y)} + e^{i\Delta\phi(x,y)}\right) \tag{6.2}$$

which can be simplified as:

$$i(x,y) = a(x,y) + \left(0.5 \cdot b(x,y) \cdot e^{-i\phi_s(x,y)}\right) \cdot e^{-i\phi_c(x,y)} + \left(0.5 \cdot b(x,y) \cdot e^{i\phi_s(x,y)}\right) \cdot e^{i\phi_c(x,y)}$$

$$i(x,y) = a(x,y) + c(x,y) \cdot e^{-i\phi_c(x,y)} + c^*(x,y) \cdot e^{i\phi_c(x,y)} \tag{6.3}$$

where

$$c(x,y) = \left(0.5 \cdot b(x,y) \cdot e^{-i\phi_s(x,y)}\right) \tag{6.4}$$

and $*$ denotes complex conjugates.

Taking the Fourier transform of Equation 6.3, we get:

$$I(u,v) = A(u,v) + C(u - f_x, v - f_y) + C^*(u + f_x, v + f_y) \tag{6.5}$$

where u and v are the coordinates in frequency space. Equation 6.5 represents three distinct peaks in the Fourier space. This is because the terms $a(x,y)$, $b(x,y)$, and $c(x,y)$ are all slowly varying compared to the carrier frequency. The three peaks are centered at locations $(-f_x, -f_y)$, $(0,0)$, and (f_x, f_y).

Multiplying the $I(u,v)$ with a filter to extract only one peak, we get:

$$C(u - f_x, v - f_y) = I(u,v) \cdot F(u,v)$$

Translating this peak to the center by shifting the image by an amount f_x and f_y in x and y directions, we get $C(u,v)$. $C(u,v)$ is equal to the Fourier transform of Equation 6.4. Therefore, taking the inverse Fourier transform we get:

$$c(x,y) = F^{-1}(C(u,v))$$

The real part and the imaginary part of this can be used to demodulate the phase using:

$$\phi_w(x,y) = \tan^{-1}\left(\frac{\mathsf{imag}[c(x,y)]}{\mathsf{real}[c(x,y)]}\right)$$

The term $\phi_w(x,y)$ is wrapped between $-\frac{\pi}{2}$ to $\frac{\pi}{2}$. Thus, it needs to be unwrapped using a suitable algorithm. Once it is unwrapped, the signal phase field $\phi_s(x,y)$ is obtained. The height profile can be obtained using the formula:

$$h(x,y) = \frac{\phi_s(x,y) \cdot \lambda}{2\pi(n-1)}$$

Practical Use of Height Measurements

The height profile is analyzed, and the maximum and minimum values are extracted from each measurement. The calculations are influenced by the orientation of the fringe pattern and the direction the fringes curve toward through the droplet. This sometimes results in a fringe pattern interpretation that gives a negative height pattern instead of a positive one. The value to use during the experiment was based on the shape of the height profile presented to the operator in a 3D plot during the experiment, which gave a clear indication if the fringe pattern was interpreted positively or negatively.

Measurement Software Alterations

Some minimal changes were made to the measurement algorithm provided by [2]. Functionality was added to capture, rotate, and crop a reference image at the start of a new measurement cycle. The calculations done on the reference image were performed every measurement cycle in the original program. Since this calculation only needs to happen once, it was taken out of the measurement loop and calculated only once after capturing the reference image, making the measurement loop roughly twice as fast, with around six measurements per second. The display of the measurement data to the operator was changed to include the fringe pattern and a height map of the calculated data. The height data displayed was passed through a moving average filter to give the average of the last five measurements, filtering out some of the high-frequency noise in the measurements to make it easier to interpret the data during the experiment. The unfiltered raw image and calculated height were stored for further analysis. The raw data storage method was altered from storing each measurement in a separate .csv file to storing all data in a cell array in RAM. This was done to enable real-time data display during the measurement, as the generation of separate .csv files took too much processing time. The measurement data in this cell array is stored in one .mat file at the end of the experiment. A cancel button was added to stop the measurement program. This button breaks the measurement loop and initiates data storage, preventing improper shutdown of the background processes that handle the USB microscope input. MATLAB had to be shut down after every measurement to reset the system.

6.5. Results

The results of two separate tests are presented and discussed. The first test shows a successful thickness measurement, but the activation of the plunging sequence took too long, causing the droplet to completely evaporate before plunge freezing. This was confirmed with CryoEM. The second test resulted in a successful validation of the thickness measurement with CryoEM. This test is discussed in detail in the results section 4 of the paper.

The droplet was dispensed on a plasma-cleaned EM grid, with a temperature offset of $-3\,^{\circ}\mathrm{C}$ to the measured dew point. The shape of the dispensed volume is elongated in the direction of the microfluidic cantilever during dispensing, as seen in Figure 6.1 **a**. This caused the droplet to cross the grid bars and not be fully inside the field of view during measurement. The fringe pattern was too distorted up until $31.5\,\mathrm{s}$ into the experiment (see **c**). After that, a linear decay in thickness was observed. An important note is that the droplet appears to retract from the field of view when looking at **c, d, e** in sequence.

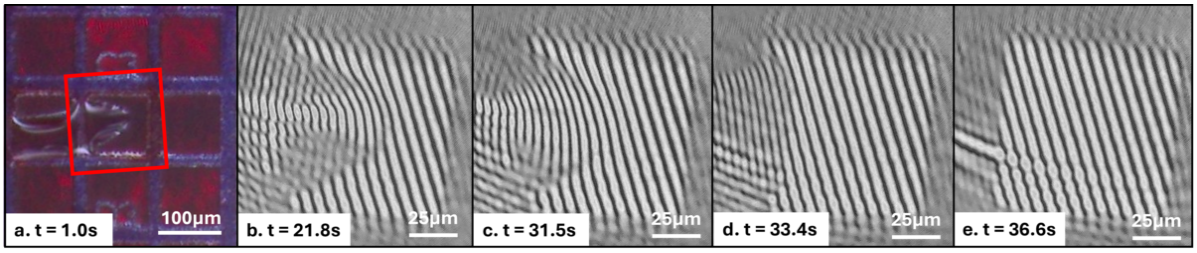

Figure 6.1: a. Image of droplet just after dispensing. **b, c, d, e** Sequence of fringe pattern measurements during the evaporation of the droplet.

The plunge sequence was started based on the speed at which the thickness appeared to approach the $500\,\mathrm{nm}$ threshold (see Figure 6.2). Releasing the grid clip took just under two seconds, combined with the second it takes to activate the plunge action by hand, resulting in the droplet being fully retracted from the field of view before plunge freezing. This was confirmed with CryoEM, as seen in Figure 6.3. There is some ice left in the grid square on the left of the measured grid, confirming that the droplet retracted and reduced its overall size in addition to its thickness during evaporation. This highlights the importance of dispensing the entire volume within the field of view.

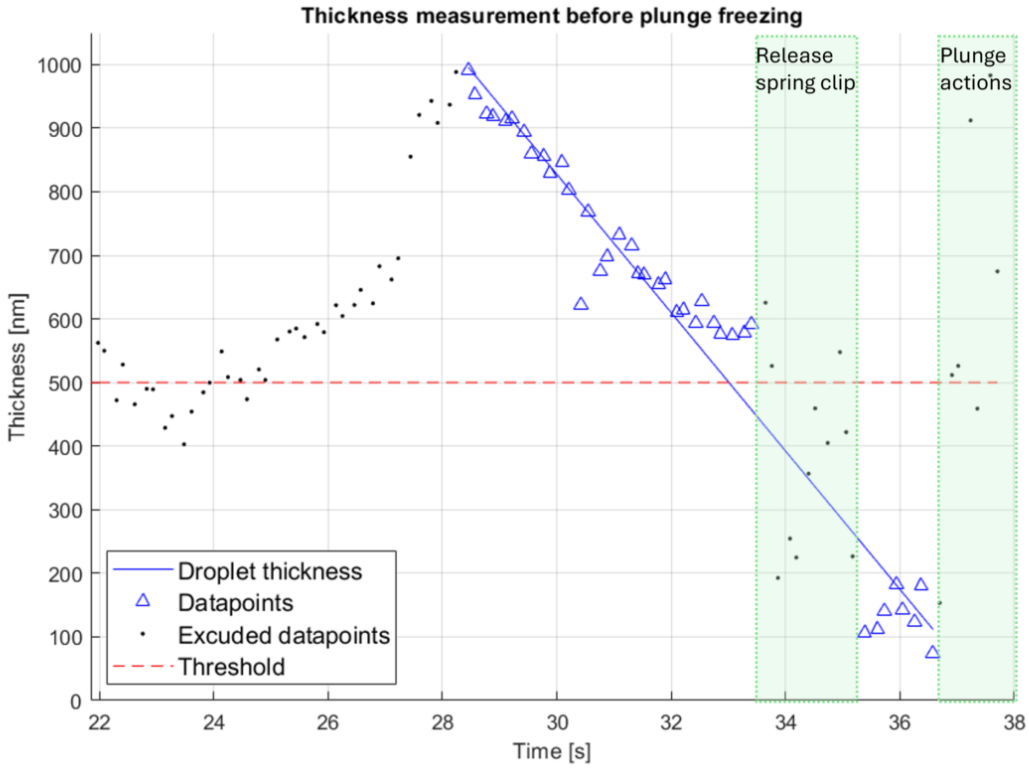

Figure 6.2: Last $16\,\mathrm{s}$ of height data from a thickness measurement just before plunge freezing.

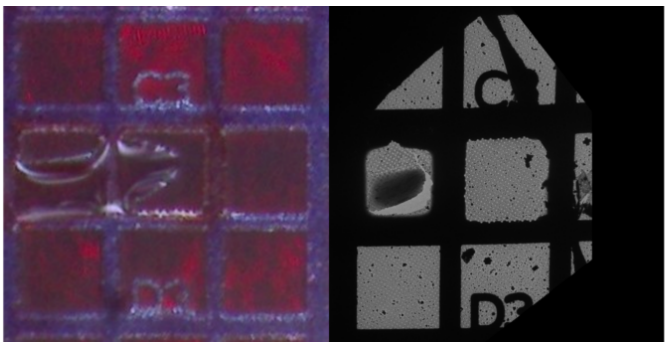

Figure 6.3: Side-to-side comparison of the droplet just after dispensing and the image taken with CryoEM at the same location.

6.6. Recommendations

1. Use a smaller aperture microfluidic cantilever, to have more control over the dispensed volume and location.
2. Implement a pressure controller with the ability to trigger a predetermined dispense time. The manual on-and-off operation is not accurate and is another extra variable during the test procedure.
3. Use the correct tweezers. The type used for Vitrobot and Leica differ slightly from the ones used now; they are specifically designed for plunge freezing and should have been used from the start. they have a mechanism build in specifically to keep the tweezers closed.
4. Add some vibration isolation between the interferometer and the ethane cup. The boiling of liquid nitrogen caused vibrations in the thickness measurement.
5. Eliminate the need for a reference frame. All the actions and motions made between taking the

reference image and starting the actual measurement contribute to a misalignment between the reference frame and the actual measured frame.

6. Use a CCD with higher resolution. This would allow for measuring with finer fringe spacing, potentially enabling measurements of thicknesses multiple times greater than the wavelength of the laser. It would also allow for the field of view to cover more than on grid square.
7. Use a CCD without automatic brightness adjustment. This feature changes the overall brightness of the measured frames during the experiment, making it difficult to perform preprocessing of the data such as stabilization or fringe alignment.
8. Improve the measurement algorithm to make it possible to measure droplets that cover more than one grid square. This would make the process control needed for dispensing not that critical.
9. Find the actual low contact angle limit of the measurement method. This would help to improve process control and give a better estimate of the potential capabilities of the system.
10. Calibrate the thickness measurement method with solid transparent reference droplets. This would be a valuable tool to debug and improve the interferometer measurement. It remove the time component due to evaporation as a test variable.
11. Calibrate the DP stage temperature measurement with a known good temperature reference. This would identify any static temperature offsets in the measurements. This was not absolutely needed to evaluate the potential of the system; it is necessary to improve data quality and make it possible to compare data to other publicised work.
12. Long-term: Implement active temperature control of the liquid ethane, similar to how it is implemented in the Leica preparation system. This system keeps the ethane $1\,^{\circ}\mathrm{C}$ above its freezing point.

Part III

Literature Study

1. Cryo-Electron Microscopy

This chapter will describe the working principle of transmission electron microscopy and give some example imaging results that can be obtained and generated to study biological material. Before imaging, there are certain conditions and requirements that the biological sample must meet. These are described in the last section.

1.1. Transmission electron microscopy

The working principle of transmission electron microscopy (TEM) can be compared to that of an optical microscope. The main differences are the illumination source from light to electrons, the development of electromagnetic lenses instead of glass lenses, and the operation of TEM in a high vacuum. The main components of a TEM are shown in Figure 1.1a. The last aspect is crucial when operating the TEM because the image resolution is affected by the scattering of electrons that collide with a residual gas molecule. The highest vacuum within the microscope is as low as $10^{-10}\,\mathrm{mbar}$. The magnification achieved by the TEM is $10\,000$ times higher than that of optical microscopes. 1.1b shows this resolution differences. This is a result of the wavelength of the electrons being significantly smaller than that of light.

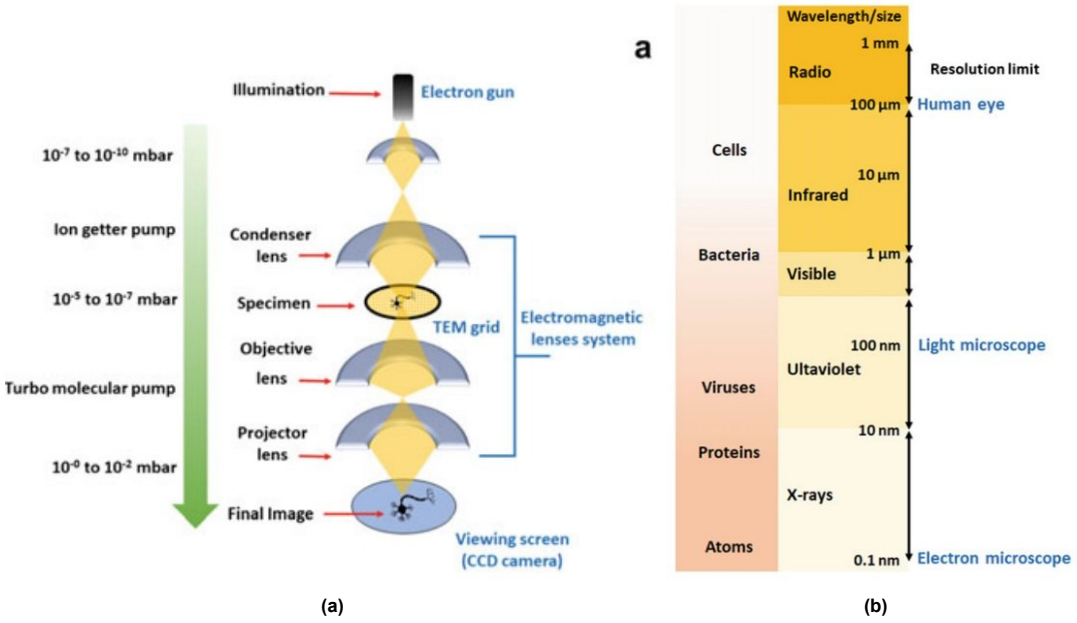

Figure 1.1: a. Main components of a transmission electron microscope **b.** Resolution limit of different imaging techniques [10]

1.2. Biological samples

The advancements in Structure determination by single-particle analysis (SPA) enable the full reconstruction of high-resolution 3D structures of macromolecules. Figure 1.2 shows the TEM micrographs and the corresponding 3D reconstructions of four standard proteins used to validate the TEM imaging techniques. These images were obtained with a $0.3\,\mathrm{nm}$ resolution. The 3D reconstruction with SPA used between $10\,000$ and $47\,000$ particles to create 3D images. The improved image resolution and novel imaging techniques used in cryo-electron microscopy push further development in structural biology.

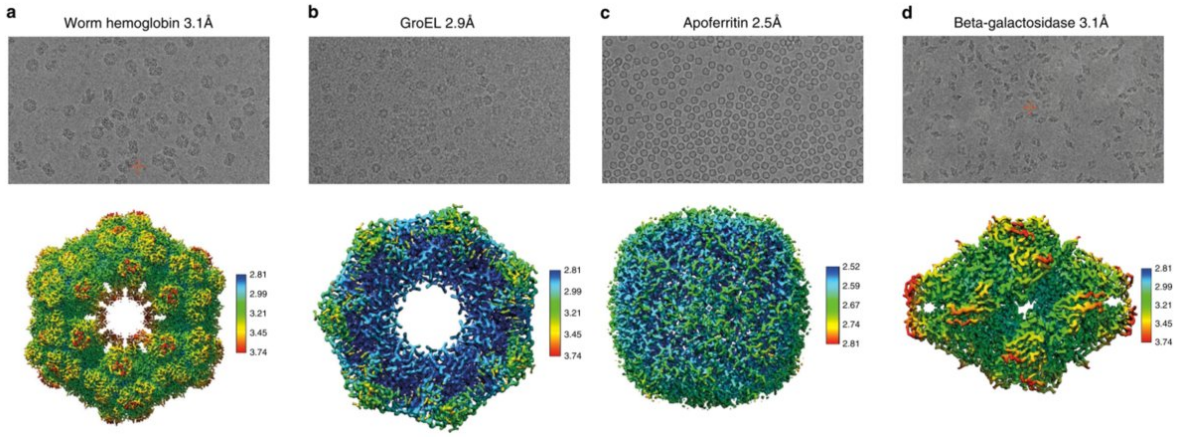

Figure 1.2: Micrographs (top) and reconstructions (bottom) of the proteins worm hemoglobin, GroEL, apoferritin, and beta-galactosidase respectively. The size of each protein in the Micrographs is given after its name in angstroms [13]

1.3. Sample requirements

A Transmission Electron Microscope (TEM) maintains a vacuum during imaging, this means that the biological sample is exposed to this vacuum. The sample would completely denature and evaporate if the sample was put into the TEM in a liquid state. Evaporation contaminates the vacuum chamber of the TEM, and biological material loses its original form when it denatures. A new sample preparation technique was developed by Dubochet et al. in the 1980s [4] to solve these two problems and enable the use of electron microscopes to study biological material in its native state [11]. The new technique solves the denaturing problem by rapidly freezing the sample material with a cooling rate of $10^5\,\mathrm{K/s}$ or higher. Water will freeze in an amorphous state without the formation of ice crystals when the cooling rate is high enough. This process vitrifies the biological sample material in its native state without distorting the shape through the formation of a crystal structure. The vitrification process is done by rapidly plunging a EM grid containing a water layer with biological material in it into a bath of liquid ethane. The desired cooling rate is reached when the plunging speed exceeds $1.5\,\mathrm{m/s}$. The EM grid is a $300\,\mathrm{mm}$ diameter copper disc with a mesh grid structure. A carbon layer of $10\,\mathrm{nm}$ thick is present on this copper mesh. The carbon grid contains holes of roughly $1\,\mu\mathrm{m}$ in, see Figure 1.3. When a sample is present on the sample grid, the TEM looks through the $1\,\mu\mathrm{m}$ holes to form images.

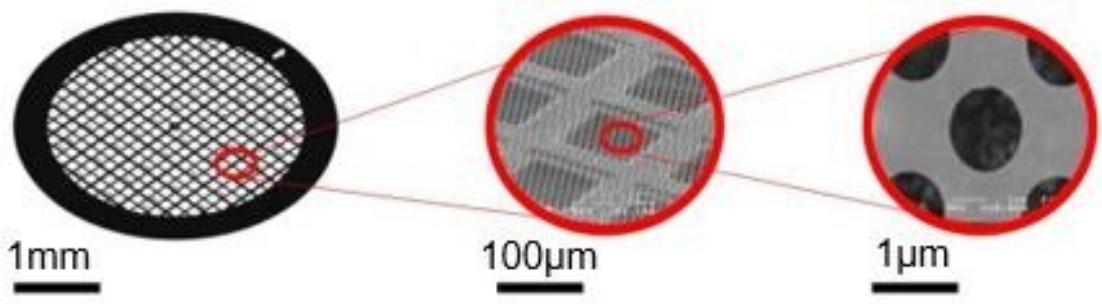

Figure 1.3: Zoom-in on an EM grid to show the grid squares and holes in the carbon nanofilm

Keeping the EM grid and sample at cryogenic temperatures inside the TEM also prevents the outgassing of the ice. The maximum water layer thickness the TEM can image through is around $300\,\mathrm{nm}$. Thicker layers give poorer contrast and even can become opaque to the electron beam. Figure 1.4 illustrates an side-view of a ice layer on an EM grid covering two grid squares.

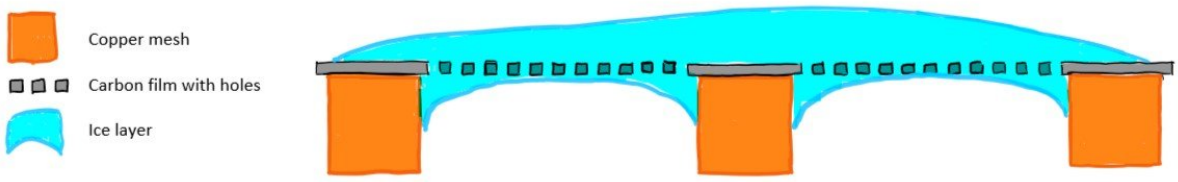

Figure 1.4: Side view illustration of an ice layer covering two grid squares of an EM grid.

A TEM can accept sample carriers in the form of an autogrid, which consist of a small copper ring that can retain a copper EM grid with a spring clip. The EM grid is placed in the autogrid clip after vitrification under cryogenic conditions. Figure 1.5 shows the parts of an autogrid and an EM grid clipped into the autogrid.

Figure 1.5: Autogrid clip and ring, clipped autogrid containing a EM grid from the front and back

2. Sample preparation systems

The preceding chapter describes in what form the TEM accepts samples and in what state the sample material needs to be in order to obtain good images. This chapter will begin with describing all the major steps necessary in the sample preparation process for cryo-EM. After that, the state-of-the-art development of the sample preparation process will be presented and evaluated. Six different sample preparation systems from the literature will be evaluated and compared.

2.1. Process overview

A complete overview of all the major steps in the sample preparation process for Cryo-EM can be seen in Figure 2.1. The whole process can be divided into four sub-processes. The first step is the creation of the buffered sample material that is to be dispensed on the EM grid; the second step is the preparation of the EM grid to accept the sample; the third part is dispensing the sample on the EM grid, controlling the water layer thickness and vitrifying the sample; the fourth and last step is preparing the vitrified sample to be accepted by the TEM and storing it until it is used. Each step will be discussed below.

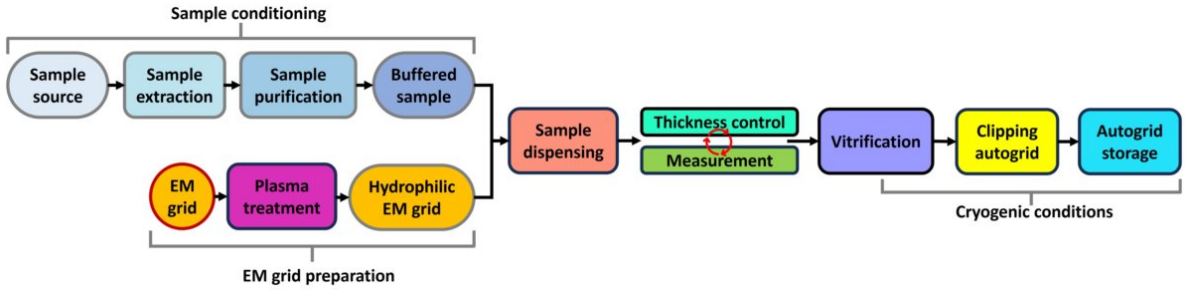

Figure 2.1: Schematic overview of the steps involving sample preparation for Cryo electron microscopy.

Sample conditioning

The sample conditioning part is shown with an input form the sample source, this is the place where the initial sample material is collected, the sample extraction is the process step of acquiring enough of the specific biological material that is to be studied from the source. The sample purification step contains the processing of the sample material to the desired purity and quality. The outcome of the sample conditioning is a buffered sample solution with enough volume to be dispensed on an EM grid.

EM grid preparation

The surface of an EM grid is most often too hydrophobic to obtain good spreading of the sample material after dispensing. To improve this control, a low-energy plasma treatment is used. Plasma generates ions and radicals that interact with the surface of the grid to remove organic contamination and has a physical and electrostatic interaction with the surface to make it more hydrophilic [11].

Dispensing, Thickness control and Vitrification

First, the sample material is dispensed on the plasma-treated EM grid, after which some form of layer thickness control is implemented to create a thin enough layer for the TEM to see the trough. Ideally, this thickness would be measured before vitrification; however, this is often not the case. After thickness control, the EM grid with the sample is frozen/vitrified by rapid immersion in liquid ethane. These three process steps are time critical because, after dispensing, the sample is subjected to environmental conditions, and the sample starts to evaporate. Figure 2.2 shows the breakdown of all relevant processes and positions. There are four positions defined; these are positions where an EM grid with

a sample needs to go during the process, and at these positions, the different process steps are performed. transport of the EM grid may occur in between the defined process positions. There are four process times associated with the process steps $t_{dispense}$, $t_{measure}$, t_{plunge}, and t_{DPC} . These are the time it takes to dispense the sample, to measure the thickness of the sample, the time it takes to plunge freeze the sample, and the total time the EM grid is mounted in the dew point controller, respectively. The time the EM grid is exposed to ambient conditions and does not have direct temperature control is indicated with $t_{abmient}$. There are two transport times; the dispensing position to measurement position time $t_{disp2meas}$ and the measurement position to plunge position time $t_{meas2plunge}$.

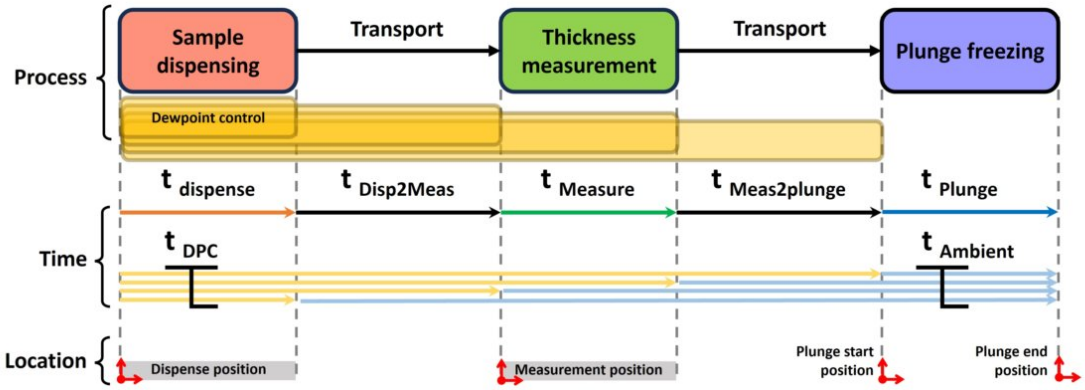

Figure 2.2: Process description that shows the process steps at the top, the associated process times in the middle, and the location of each process in the bottom. The top row shows the order of process steps, note that the dew point control is depicted with four different length blocks to indicate that it can be applied in four different ways parallel to the main process order at the top. The four different arrows indicating t_{DPC} and $t_{abmient}$ show these possible time lengths. The locations indicate name of the physical place of each process

Grid clipping and storage

The EM grid with the vitrified sample should be transferred from the liquid ethane to a container with liquid nitrogen. The EM grid can be clipped into an autogrid in this container. After that, the grid is stored in the container and can be transported with the container to the TEM.

2.2. Vitrobot

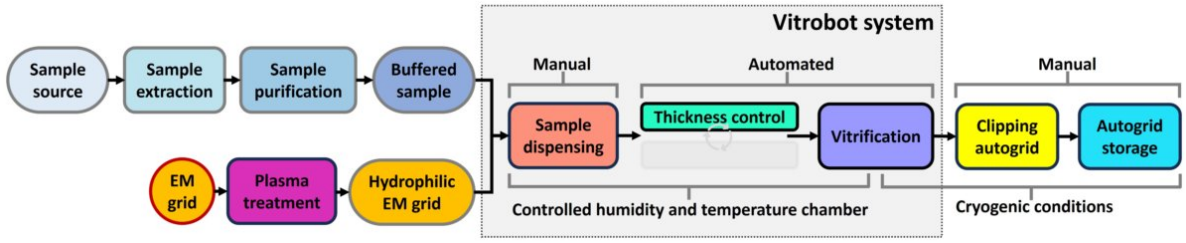

Figure 2.3: Sample preparation process with the Vitrobot system boundary.

The first sample preparation system that is reviewed here is a commercially available system that can be considered the standard way sample preparation has been done since its inception. The Vitrobot, commercially available from Thermofischer [14], integrates the thickness control and vitrification process steps into one automated system. Dispensing is done manually with a pipette and requires about $3\,\mu\mathrm{L}$ of sample material. The thickness control is done by blotting away excess sample material to obtain the desired thickness of the water layer. This method uses pieces of filter paper to absorb the sample material off the EM grid by touching the EM grid for a predefined Blotting time. Blotting time is one of the process parameters that is changed to alter the thickness of the final water layer. The vitrification of the sample is done by plunge freezing, the process of dipping the sample grid into a bath of liquid ethane at a speed of at least $1.5\,\mathrm{m/s}$ to achieve the desired cooling rate. Sample dispensing

and blotting are performed in a temperature and humidity controlled process chamber. The plunger exits the bottom process chamber during the plunging operation. The Vitrobot system boundary within the entire sample preparation process can be seen in Figure 2.3.

Kinematic configuration

The kinematic configuration of Vitrobot is shown in Figure 2.4. The EM grid, held in tweezers, is placed inside the process chamber and directly connected to the plunge mechanism. The dispense position, thickness control position and plunge start position are all at the same location. The sample is dispensed using a manual pipette through an opening in the process chamber (a). After dispensing two disks of blotting paper, approach the EM grid and pinch it for a predetermined time (b). The tweezers and EM grid are rapidly actuated downwards, and stop at the plunge end position inside the container of liquid ethane(c). The entire process consists of only two motions and two positions and eliminates both transport times with this kinematic configuration.

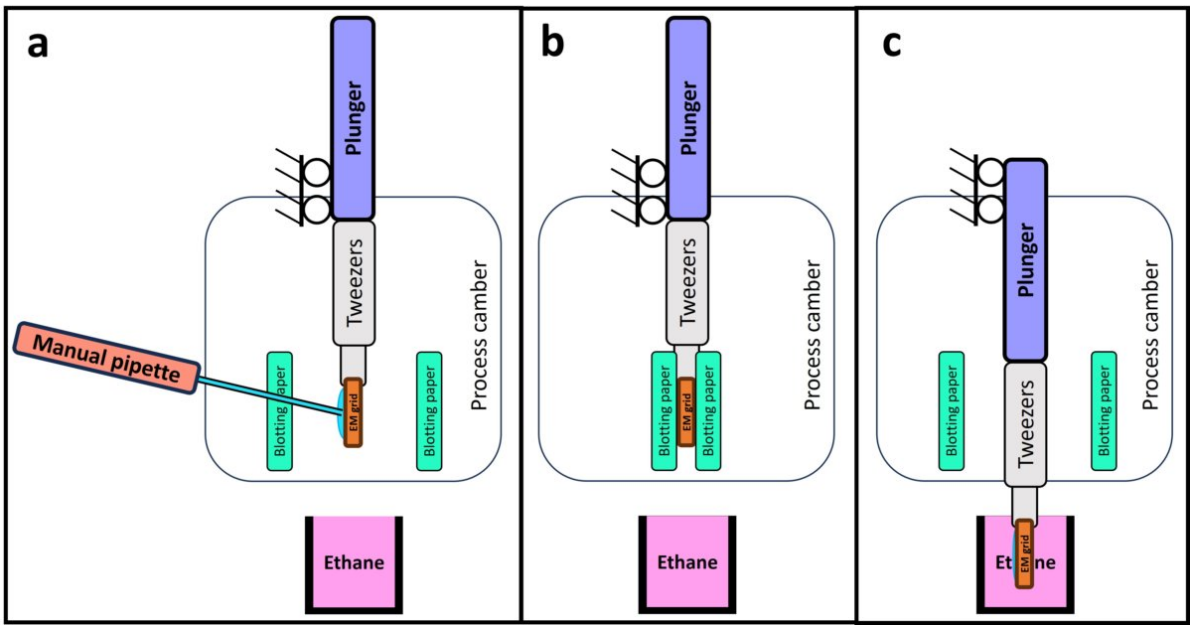

Figure 2.4: Vitrobot process description. **a:** sample is dispensed with a manual pipette.**b:** Sample thickness is reduced by blotting.**c:** Sample vitrification by plunge freezing the EM grid in liquid ethane.

2.3. Spotiton

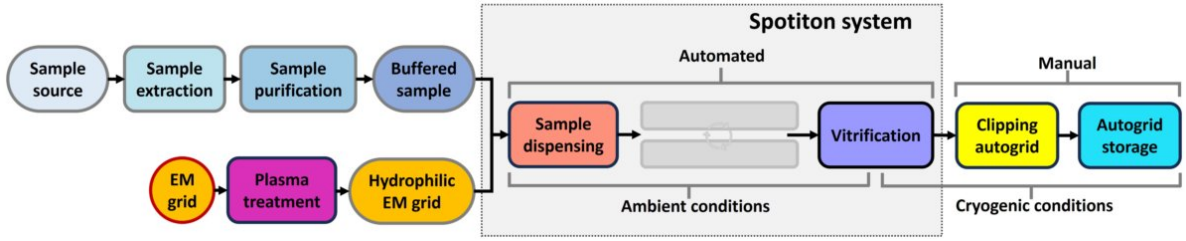

Figure 2.5: Sample preparation process with the spotiton system boundary.

The spotiton system was developed in 2012 at the Scripps Research Institute in the United States [8]. The boundary of the system is the same as the standard method (Vitrobot) 2.5. The three different process methods used are the dispensing method, the absence of a temperature and humidity controlled process chamber, and no active thickness control mechanism. dispensing is done with a piezoelectric inkjet nozzle. Each droplet has a volume of $32\,\mathrm{pL}$ and multiple droplets can be dispensed in rapid suc-

cession to increase the volume of a single sample droplet or to print a pattern of multiple dispensed samples. There is no active mechanism to control the thickness of the sample after dispensing.The thickness is controlled by altering the amount of material that is dispensed, this is an iterative process. vitrification is done by plunge freezing.

Kinematic configuration

A notable difference from the standard method is the absence of any humidity or temperature control chamber, which is possible due to the specific order of operations that the ink jet dispensing process allows. The order of operations can be seen in figure 2.6. The inkjet dispensing occurs after the plunge action is initiated; the ink-jet nozzle prints automatically on the EM grid when it passes the print head during the plunging operation (b). The time between dispensing and vitrification is reduced to the millisecond range by integrating the dispensing step into the plunging operation. The whole process can be performed under ambient conditions due to this process time reduction.

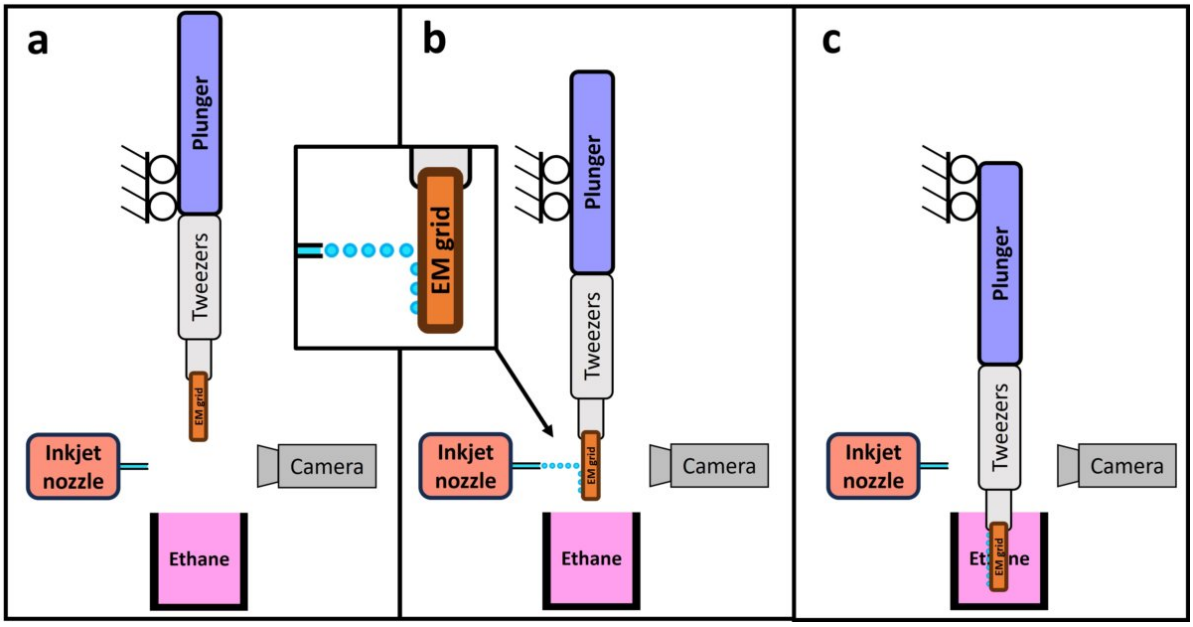

Figure 2.6: Spotiton system process description.**a:** initial state of the system.**b:** the plunge mechanism is activated. The ink-jet nozzle dispenses sample droplets on the EM grid during the plunging action.**c:** plunge motion stops with the EM grid inside the liquid ethane container.

2.4. Cryowriter

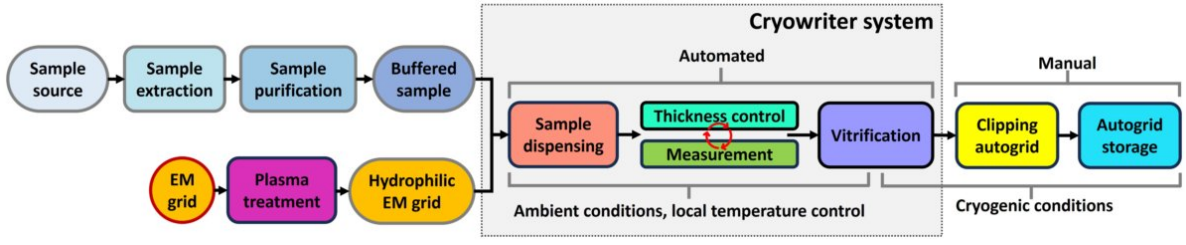

Figure 2.7: Sample preparation process with the Cryowriter system boundary.

The Cryowriter system was developed in 2016 at the University of Basel, Switzerland [1]. It has the same system boundary as the standard method, as can be seen in Figure 2.7. The differences in the process methods used are the dispensing method, dispensing orientation, absence of a process chamber, use of local temperature control, and active thickness measurement after dispensing. The

dispensing is done automated with a micro capillary, and the grid moves in a sinusoidal or circular pattern to distribute the liquid during dispensing. There is no humidity and temperature controlled chamber; instead, the EM grid is temperature controlled using an active temperature control stage called a dew point stage or DP stage and a temperature-controlled mounting mechanism for the tweezers that hold the EM grid. The temperature is set to keep the EM grid and the sample at a temperature close to the dew point temperature of the room to prevent evaporation; this will be explained in more detail in Chapter 4. The DP stage acts also as a thickness control method; By increasing the temperature of the EM grid a few degrees above the dew point, the evaporation rate is increased, and the thinning of the water layer is done through evaporation. The second method of thickness control is by re-aspiration with the microcapillary after dispensing and spreading. The layer thickness is monitored in real time with a laser transmission intensity measurement. This measurement method is explained in more detail in Chapter 3. The plunge-freeze mechanism is activated when a thickness threshold is reached during measurement.

Kinematic configuration

the system does not need a controlled environment to function in. This is possible due to the local temperature control with the DP stages and because of its specific kinematic configuration that minimizes transport times. The plunge freezer used in these systems differs from the standard method. The dispensing and measurement steps are done on a horizontally oriented EM grid, so after the measurement step, the EM grid needs to rotate $90°$ before it can be plunged. The rotation and plunging motion are performed in rapid succession. The motions are shown in Figure 2.8. First, the mounting mechanism that holds the tweezers moves closer to the plunger and releases it, for a brief moment, the tweezers and EM grid are completely detached from the rest of the system and in free fall (c). A magnet is mounted at the end of the tweezers; this magnet attracts the tweezers to the end of the plunger and attaches it to the plunger. a hinge inside plunger that can rotate $90°$ is released due to the added moment force generated by the weight of the tweezers. This flips the tweezers and EM grid $90°$ and places them colinear with the plunge axis (d). An electronic contact on the hinge is closed that triggers the plunge action (e). The entire motion of rotation and plunging reduces the sample exposure to ambient conditions to below $300\,\mathrm{ms}$.

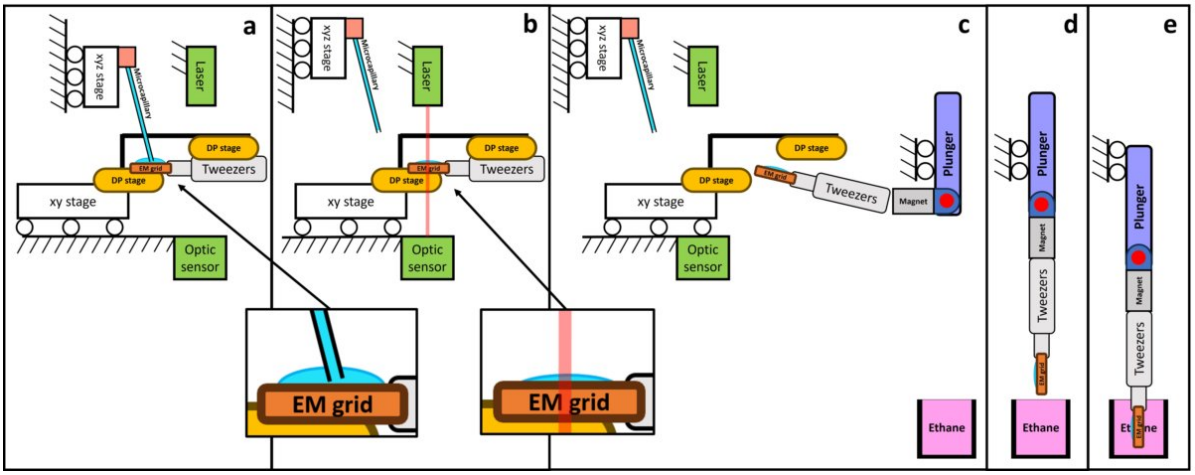

Figure 2.8: Cryowriter process description.**a:** The sample is dispensed from a microcapilary and the xy stage is used to move the EM grid while dispensing, this is done to improve the spreading of the sample. The EM grid is positioned in a Dew point stage. **b:** The microcapilary is moved up, the xy stage positions the sample into the laser beam and a real time thickness measurement is started. **c:** When the correct thickness is reached , the xy stage moves toward the plunge mechanism and the tweezers are released, for a brief moment the tweezers and EM grid are in complete free fall and are attracted to the magnet on the plunge arm. When the tweezers attach to the magnet, the hinge is released due to the added weight of the tweezers.**d:** The tweezers rotate around a hinge in the plunge arm. An electrical contact is triggered at the end of the rotation to initiate the plunge motion. **e:** The plunge mechanism made with a solenoid vitrifies the sample.

2.5. Vitrojet

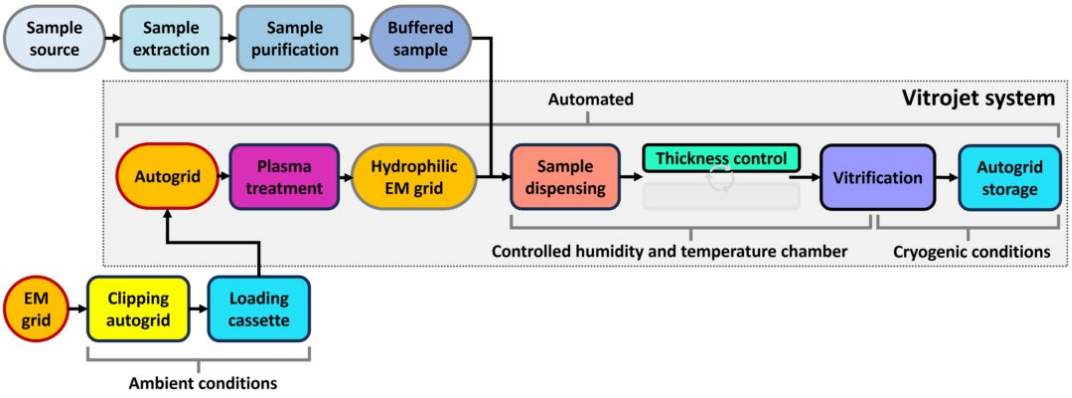

Figure 2.9: Sample preparation process with the Vitrojet system boundary.

The Vitrojet system was developed in 2020 at Maastricht University in the Netherlands [13], and is developed into a commercial product by the company Cryosol [3]. The system incorporates more process steps than the standard method. The order of operations has also been altered. The process steps that have been added are plasma treatment and autogrid storage at the end of the process. The differences in the process methods used are the dispensing method and the vitrification method. A new way of dispensing sample material on EM grids was developed. A flat-tip metal pin is dipped in a drop of sample liquid at the end of a pipette. A couple of nL of sample is transferred to the tip of the metal pin, the pin is brought in close proximity to the EM grid, and the liquid is spread on its surface. The distance between the pin and the grid, the speed of movement, and the pattern are parameters that are used to control the thickness of the sample layer. In addition, a new method of vitrification was developed. The EM grid is placed between two jets that spray it with liquid ethane; this way, the EM grid is cooled from the center to the outside rather than from the edge in traditional plunge freezing. After jet vitrification, there is a plunge freeze step to cool the rim of the autogrid. This innovation enables a direct change in the order of the process. The EM grids can be pre-clipped into autogrids before the process begins. Jet vitrification reaches a cooling rating high enough because it cools the autogrid from the middle to the edge, so the added thermal mass of the autogrid does not influence the cooling rate of the sample layer. A cassette filled with autogrids is inserted into the system before the process starts. This also simplifies the handling of the EM grid within the system. The rim of the EM grid is easier to hold and less fragile.

Kinematic configuration

All process steps are stacked on top of each other. After each step, the plunge mechanism moves down one station, and the following process is performed. This aligns all critical transport steps and reduces each of them to one motion in the downward z direction. The kinematic configuration enables a tight integration of all process steps into a compact system. The complete sequence of events is described in Figure 2.10.

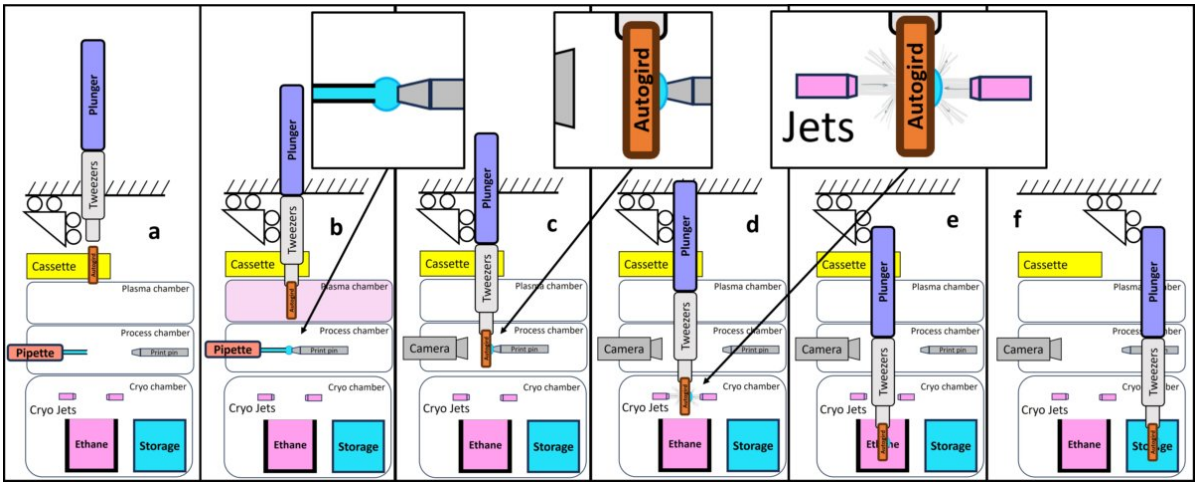

Figure 2.10: Vitrojet process description.**a:** start position of the system. The tweezers are located directly above the autgrid cassette. **b:** The tweezers move down to pick up an autogrid from the cassette; after that it moves down into the plasma treatment chamber below. The autogrid receives plasma treatment. A print pin is dipped into a droplet of sample presented to it by a pipette to transfer a few nanoliters of sample material to the tip. In the process chamber below the plasma chamber **c:** The autogrid is moved to the humidity and temperature controlled process chamber. The print pin is used to print the sample material onto the EM grid. The process is monitored with a camera. The pin moves in a spiral motion during printing to improve the spread of the sample. **d:** Directly after pin printing, the autogrid is transferred to the cryogenic chamber below the process chamber. The autogrid is placed between two cryogenic jets that spray the sample with liquid ethane to cool the grid from the middle first. **e:** After jet vitrification the grid is rapidly plunged into a container of liquid ethane to cool in the outer rim of the autogrid. **f:** After vitrification the autogrid is moved to an autogrid storage cassette inside a container filled with liquid nitrogen.

2.6. Linkham plunger

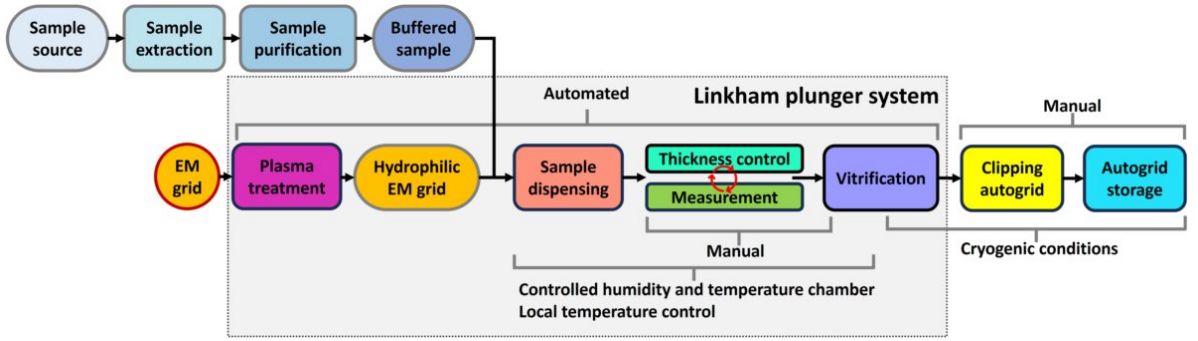

Figure 2.11: Sample preparation process with the Linkham plunger system boundary.

The linkham plunger system was developed in 2022 at Leiden University in the Netherlands [9]. The system boundary incorporates more process steps compared to the standard method. The plasma treatment step and automated grid handling before dispensing and after vitrification are added to the standard functionality. The differences in configuration are the dispensing method and the thickness control method and the addition of a thickness measurement method. The application of the sample to the EM grid is carried out by completely immersing it in a container filled with the sample material (d). see Figure 2.12 for process-step illustrations. Part of the thickness control method is to slowly retract the EM grid from the sample container to drain some of the excess liquid (e). The thickness control and measurement are done at the same time. Two suction tubes are placed against the edge of the em grid to suck away excess liquid. The thickness of the water layer is monitored with a light microscope by the system operator. The thickness measurement method will be discussed in more detail in Chapter 3. vitrification is done by plunge freezing.

Kinematic configuration

The linkham plunger system has all the process steps arranged in one line. The plunger is mounted on an xz stage and can move up and down and sideways to access the different process steps. The alignment of each process step in the y direction is done manually before the process begins. There is no particular benefit to this arrangement with regard to transport time minimisation; the main benefit is the ease of automation and linking the process steps together. The entire sequence of events is explained in more detail in the description of Figure 2.12.

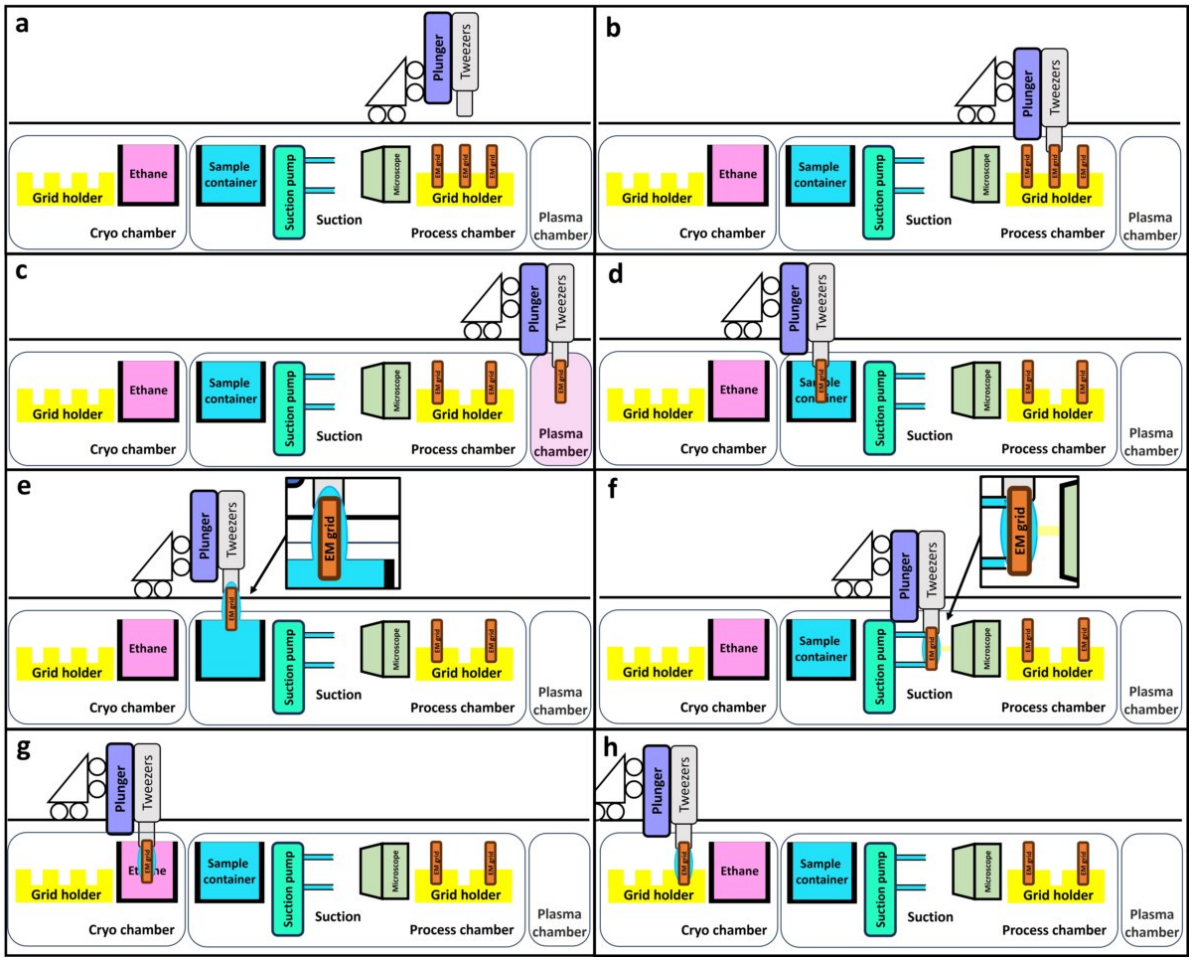

Figure 2.12: Linkham plunger process description. **a:** The plunger is moved with an xz stage and is placed above an EM grid storage rack. **b:** One of the EM grids is retrieved from the grid rack. The plunger moves up and sideways towards the plasma treatment chamber. **c:** The plunger moves down and places the EM grid inside the plasma chamber,. The tweezers are removed from the chamber during plasma treatment. The tweezers pick up the EM grid again after plasma treatment. The plunger moves sideways towards the sample container. **d:** The EM grid is fully submerged in the sample solution.**e:** The EM grid is slowly retracted from the sample solution to drain most of the liquid. The plunger moves to the suction and measurement position. **f:** the sample is positioned in front of a light microscope and two suction nozzles are pressed against the edge of the EM grid. The sample thinning is done through controlled suction. The thickness is visually monitored by the operator.**g:** The operator activates the plunge sequence when the correct thickness is observed. The plunger moves up from the suction position, sideways to the plunge start position above the container of liquid ethane, and the sample is vitrified with plunge freezing. **h:** The EM grid is stored in a rack submerged in liquid nitrogen after vitrification.

2.7. AFM4CryoEM

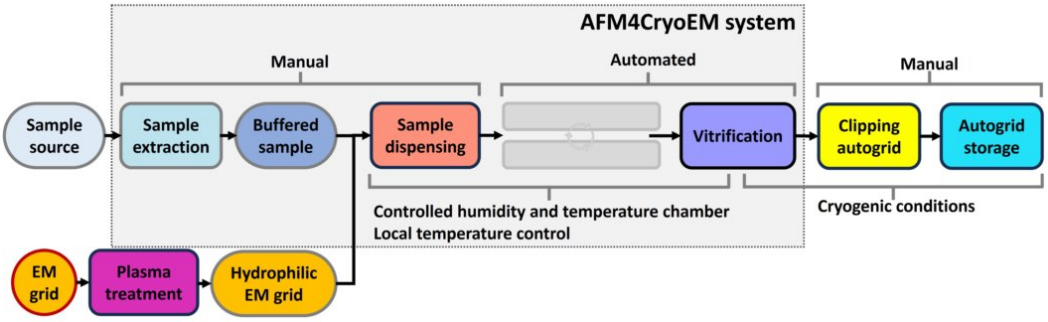

Figure 2.13: Sample preparation process with the AFM4CryoEM system boundary.

The AFM4CryoEM system was developed in 2018 at the University of Delft in The Netherlands [12]. The system incorporates an additional step into its process and omits one step entirely. The sample dispensing method is different from the standard method. The system boundary can be seen in Figure 2.13. The added sample extraction step and the dispensing step are both done with A Microfluidic Atomic Force Microscope (AFM) cantilever. The cantilever is used to aspirate subcellular material from a single living cell [5], this material is directly dispensed on the EM grid with the hollow cantilever, omitting the complete purification step of the sample preparation process. Vitrification is done by plunge freezing.

Kinematic configuration

The AFM and the plunge mechanism are placed next to each other with a xy stage that transports the EM grid between them. Figure 2.14 shows the movements made by the system. The xy stage transports the EM grid to the plunge mechanism after dispensing with the AFM (b,c). The DP stage rotates $90°$ to align the EM grid with the tweezers at the end of the plunge arm (c). The tweezers move down and pick up the EM grid from the DP stage and move up again (d). The DP stage rotates down, and the xy stage moves to the side to clear the plunge path (e). After this, the plunge mechanism is activated to vitrify the sample (f). A global humidity and temperature chamber is used to limit the evaporation rate during transport from the DP stage to the beginning of the plunging. The kinematic configuration is not specifically designed to minimise transport times, but to connect and automate two existing processes.

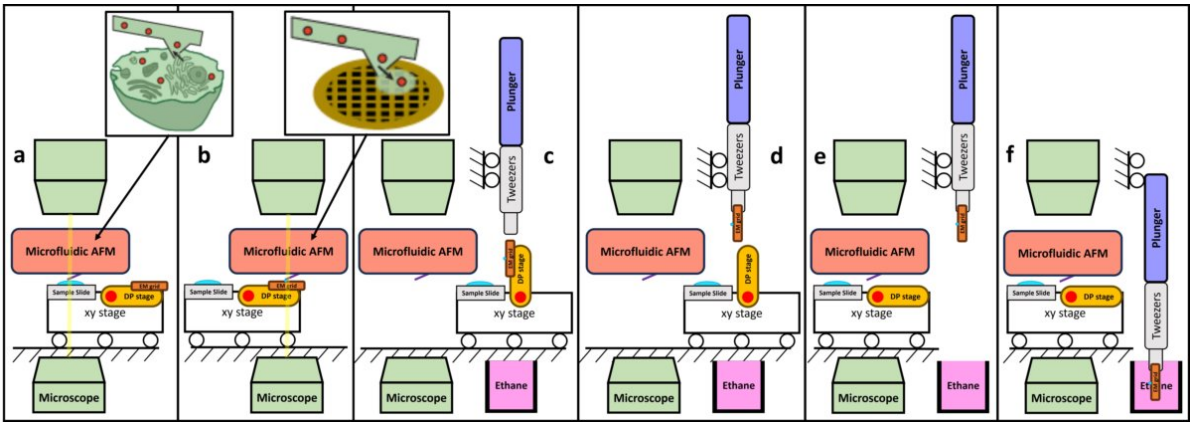

Figure 2.14: AFM4CryoEM process description. **a:** The microfoluidic AFM is positioned manually to aspirate subcellular material from a single cell. The AFM is moved up and the xy stage positions the EM grid in a DP stage under the AFM. **b:** the EM grid is positioned manually, the AFM dispenses the collected sample material onto the EM grid. **c:** The xy stage transports the EM grid with the sample to the plunge mechanism. The DP stage rotates to a vertical position to align the EM grid with the tweezers attached to the plunge mechanism **d:** The tweezers move down and pick up the em grid from the DP stage, the DP stage rotates back down and the xy stage moves sideways to clear the plunge path. **e: f:** The plunge mechanism rapidly plunges the EM grid into a container of liquid ethane to vitrify the sample

2.8. Discussion

Six different preparation methods from the literature have been presented, each of them tries to improve the same process in different ways; in this section, the solutions used to solve the same process steps will be compared and discussed. An overview of the relevant characteristics of each system can be found in Table 2.15. The system boundary's show the amount of process steps incorporated in the system, even the systems with the same boundary have different methods to perform the same process steps. Figure 2.16 shows all system boundaries in one figure to show the differences. Some specific methods for dispensing and plunge freezing enabled the order of operations to be altered in the sample preparation process or the complete omission of a process step. The kinematic configuration for most of the systems was used to minimise transport times and with that limit the evaporation of the sample material. Other methods to limit evaporation relied on local and global control of temperature and humidity. The degree of automation varies between systems, but each reviewed system added more automation to the process compared to the standard method (Vitrobot).

Dispensing orientation

Four of the systems use dispensing methods that can be used on a vertical EM grid. The supply of sample material to the dispensing hardware does not have a predetermined orientation due to gravity effects. This holds for the manual pipette, inkjet nozzle, and pin printing. Grid immersion is an exception in that it cannot be done easily with a horizontal EM grid because the sample container relies on gravity to keep the sample contained. The Cryowriter and AFM4CryoEM systems both dispense on a horizontal EM grid, the dispensing cannot easily be done on a vertical EM grid due to two reasons. First, both systems aspirate from a volume of sample material on a glass slide or Petri dish. They have a horizontal configuration and are dependent on gravity and surface tension to hold the material on them. The second reason that applies only to the AFM4CryoEM system is that the normal working orientation of the AFM is horizontal and it is not able to operate in a vertical orientation. The cryowriter could, in theory, rotate the micro-capillary and dispense on a vertical EM grid. However, this would complicate the positioning of the sample in the measurement position and the release motion of the DP stage from the EM grid, which is tightly integrated with the rotating motion in the current system.

Thickness measurement and control:

Two systems control thickness during the dispensing process. The specific dispensing mechanism used allows them to alter the thickness of the dispensing sample layer. vitrojet does this through tight control of pin print parameters, and spotiton does it by altering the amount of droplets it dispenses in one place. Two systems control the thickness after the dispensing step. vitrobot uses the blotting technique to absorb most of the sample material. The cryowriter uses a temperature offset at the dew point stage to thin the sample through controlled evaporation. Two systems implemented some form of thickness measurement and both systems have active thickness control during measurement. The cryowriter measures the transmission intensity of a laser through the sample layer, while thinning is done through controlled evaporation. The linkham plunger controls the thickness through suction during fringe pattern observation. Two thickness measurement systems have been shown, which only one actually measures the thickness (cryowriter), the other relies on fringe pattern recognition and relating that to a certain thickness (linkham plunger). Both of these methods require a layer of sample material to be present on the EM grid, to determine its thickness.

EM grid handling

Three of the systems have tweezers attached to the EM grid at all times, vitrobot spotiton and cryowriter. Notable is that Cryowriter is the only one that does a transfer of the tweezers to the plunge mechanism instead of an EM grid transfer to the plunge mechanism, as the following three systems do; they have a pick-up procedure at some point in the process. Vitrojet and Linkham plunger use it to prepare multiple sample grids by having grid storage at the beginning and the end of the process. The payoff of the added complexity of automated tweezers is that it enables the automation of more process steps. The AFM4CryoEM system also has automatic tweezers and pick-up, but does not yet use these to expand its system boundary.

Transport time minimisation

Vitrobot and spotiton perform both the dispensing and thickness control steps at the plunge start position and therefore eliminating transport between them. Vitrojet cannot perform plasma treatment and dispensing at the same location because of the environmental requirements of these two process steps, and therefore stacks the two process chambers on top of each other to minimise the travel distance and exposure to other environmental conditions. This is a completely different integration approach than used for the linkham plunger; they place both process chambers next to each other and access them form above. This gives three transport motions to perform in two different directions for the linkham plunger and only one transport motion for the vitrojet. The same holds for the transfer from the dispensing/thickness control to vitrification. transport motion of both the Cryowriter and AFM4CryoEM system must include a rotation due to the orientation constraints of their dispensing and vitrification methods. The cryowriter minimises transport time by integrating the DP stage release, rotation, and plunge action into one passively controlled sequence of mechanical motions that take less than $300\,\mathrm{ms}$. The AFM4CryoEM system does not utilise a specific kinematic configuration to minimise transport time. The time between DP stage release and the onset of the plunging motion is 8 seconds and is performed by three position-controlled actuation axes. The system relies on global humidity and temperature control to minimise evaporation during these 8 seconds. Chapter 5 explains this process in more detail.

Vitrification method:

five of the six systems use the same vitrification method, namely plunge freezing. Vitrojet innovates in this step of the process with jet vitrification. This improvement enables the use off autogrids from the start of the process and with that simplifies grid handling and process automation. The system could potentially be used in a horizontal orientation to vitrify samples that are dispensed by the horizontal dispensing methods and with that eliminating the need for a rotation in the transport motion between dispensing and vitrification.

	Vitrobot	Spotiton	Vitrojet	Cryowriter	Linkham plunger	AFM4cryoEM
Dispensing method	Manual with pipette	Inkjet printing	Pin printing	Microcapillary	Grid dipping	Microfluidic AFM with hollow cantilever
Dispensing orientation	Vertical	Vertical	Vertical	Horizontal	Vertical	Horizontal
Minimum required sample volume	3µL For one grid	5µL For multiple gids	0.5µL For multiple grids	3nl ~ 20nL For one grid	10µL For multiple grids	100fL ~ 1pL For one grid
Sample form	Purified protein	Purified protein	Purified protein	Purified protein Or a single Cell	Purified protein	Sub cellular material from a single cell
Thickness control method	Blotting	Microwire wicking	Varying pin printing parameters	Re-aspiration and evaporation	Slow retraction and suction	N/A
Thickness measuring method	N/A	N/A	N/A	Laser transmission intensity	Visual inspection of fringe patterns	N/A
Measurement orientation	N/A	N/A	N/A	Horizontal	Vertical	N/A
Global environmental control	Humidity and temperature-controlled process chamber	None	Humidity and temperature-controlled process chamber	None	Temperature-controlled process chamber	Humidity and temperature-controlled process chamber
local environmental control	None	None	Temperature controlled EM grid and print pin	Temperature controlled EM grid and Tweezers	Temperature controlled EM grid and Tweezers	Temperature controlled EM grid
Integrated plasma treatment	No	No	Yes	No	Yes	No
Sample carrier	EM grid	EM grid	Pre-clipped autogrid	EM grid	EM grid	EM grid
Freezing method	Plunge freezing	Plunge freezing	Jet vitrification	Plunge freezing	Plunge freezing	Plunge freezing

Figure 2.15: Comparison table of all reviewed systems.

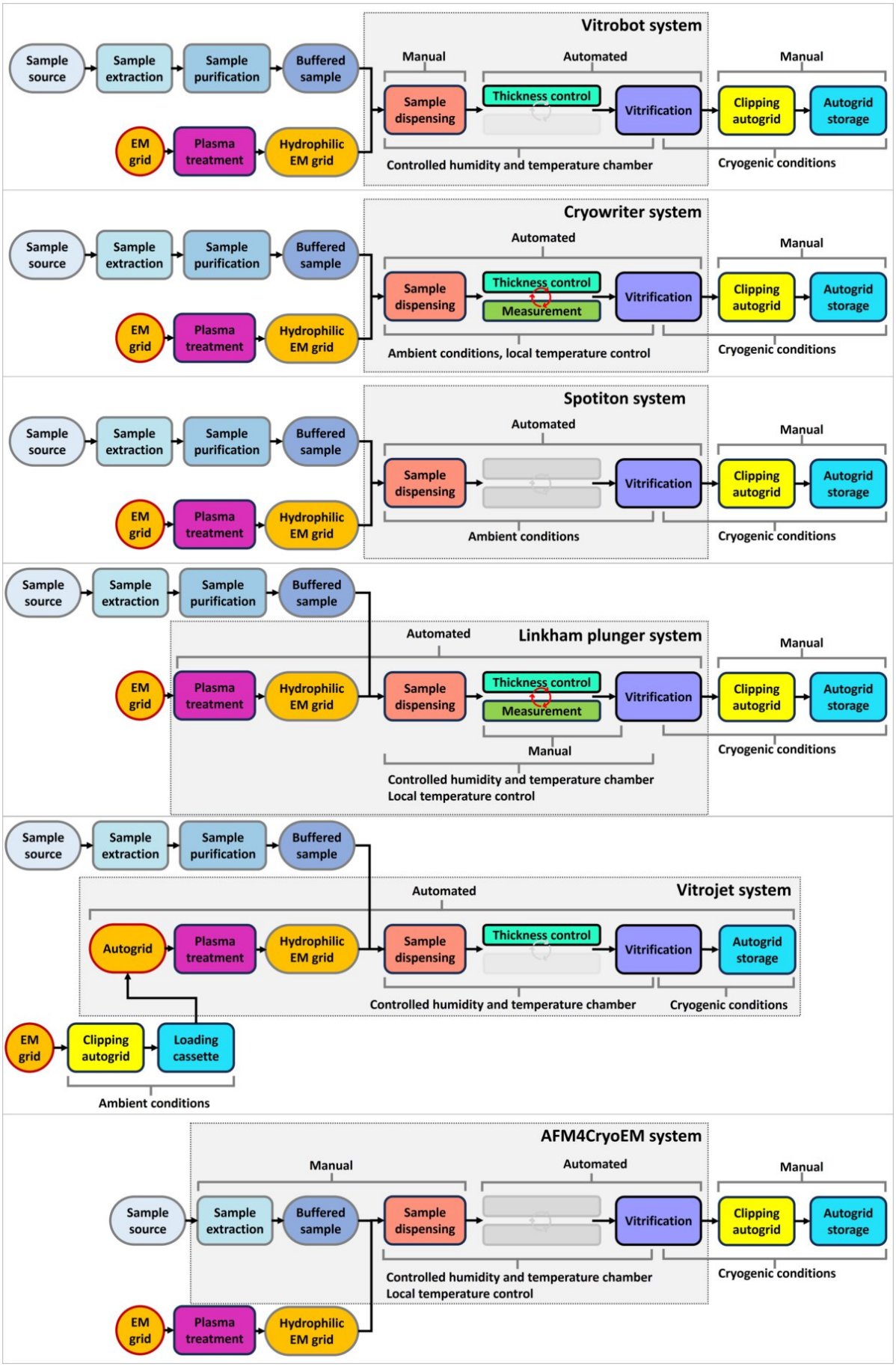

Figure 2.16: Overview of all discussed sample preparation systems. This figure illustrates The differences in process order and amount of process steps incorporated into each system boundary.

3. Thickness measurement methods

Two thickness measurement methods are discussed in the previous chapter. To evaluate whether these measurement methods could be implemented in the AFM4CryoEM sample preparation system. A measurement method developed for the AFM4CryoEM system as a master thesis by Alok Bharadwaj in 2019 using a Mach-zehnder interferometer to measure sample thickness is also discussed. The measurement procedure for the AFM4CryoEM system is intended to be automated.

3.1. Fringe pattern recognition

The measurement method used by the Linkham plunger uses a microscope to view the water layer on the EM grid during the thinning process. The operator of the system has a table with reference pictures that depict the fringe pattern of a water-layer at differing thicknesses. This table can be seen in figure 3.1is used as a comparative reference to determine the thickness of the water layer. This system can be used when multiple grid squares start out completely filled with liquid. A meniscus is formed at the edges of the grid squares when the water volume is reduced. The specific change in the shape of this meniscus is what generates the varying fringe pattern that can be observed.

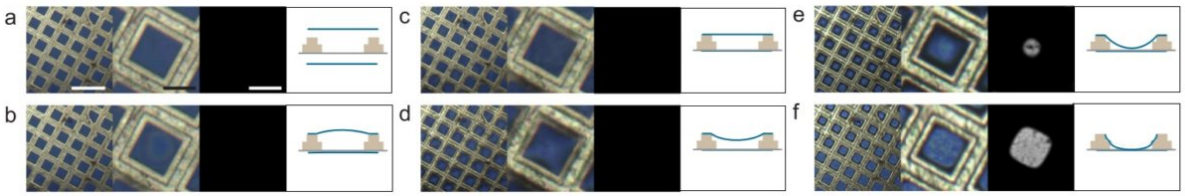

Figure 3.1: reference chart for comparing fringe patterns. [9]

The AFM4CryoEM system uses a microfluidic AFM to disperse samples with a small volume in the femtoliter to picoliter range. The smaller sized samples in this range do not have enough volume to fill one grid square, so the thickness of the waterlayer cannot be determined with the fringe pattern inspection.

3.2. Transmission intensity

The measurement method used by the Cryowriter system uses transmission spectroscopy to monitor the thickness of the water layer. The transmission intensity of a laser through the water layer is measured, and when the thickness changes, the transmission intensity also changes. Internal reflections in the water layer cause an alternating pattern in the measured intensity as a result of constructive and destructive interference. The change in intensity with changing water layer thickness can be seen in Figure 3.2. The method was tested with two different wavelengths to verify the working principle of the measurement.

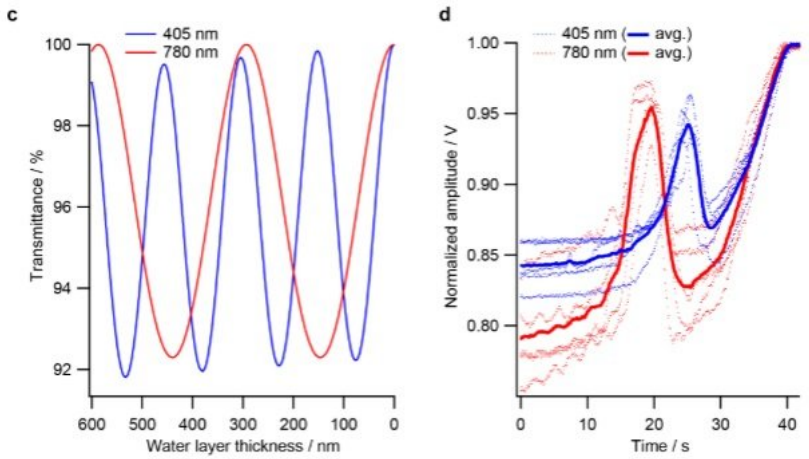

Figure 3.2: Transmission intensity vs water layer thickness for two different wavelengths of light. Transmission intensity measured through a evaporation water layer on an EM grid over time for two different wavelengths of light. [1]

The method assumes that the thickness of the water layer is somewhat constant over the entire area covered by the laser beam. This assumption does not hold if a water droplet with a diameter smaller than that of the laser beam were measured. The transmittance pattern would depend on the diameter of the droplet as a result of the reduced surface area that is measured. Some information about the diameter of a droplet is needed to measure the thickness with this method. The measurement method in its current form does not provide this information. This method cannot be used in its current form in the AFM4CryoEM system.

3.3. Mach-Zenhder interferometry

A measurement system was developed specifically for the waterdroplet size range that can be dispensed with the AFM in the AFM4CryoEM system. A Mach-Zenhder interferometer is used to obtain the shape of the droplet on an EM grid.

Thickness measurement

Alok Bharadwaj developed a measurement method in his master's thesis using a Mach-Zehnder interferometer and was able to measure the height profile of a glycerol droplet on a glass slide [2]. The optical setup used for his study can be seen in Figure 3.3. The measurement method uses the phase shift generated by the droplet in the interference pattern between the two light paths to measure the shape profile of the dorplet. The height can be obtained from this measurement by assuming that the shape of the droplets is a spherical cap. The measured interference pattern and the processed result showing the droplet height can be seen in Figure 3.4. Note that this measurement method relies on the shape of the droplet and shows the difference in height between the center of the droplet and its edge; therefore, the entire droplet or most of it needs to be present in the field of view to obtain a successful height measurement.

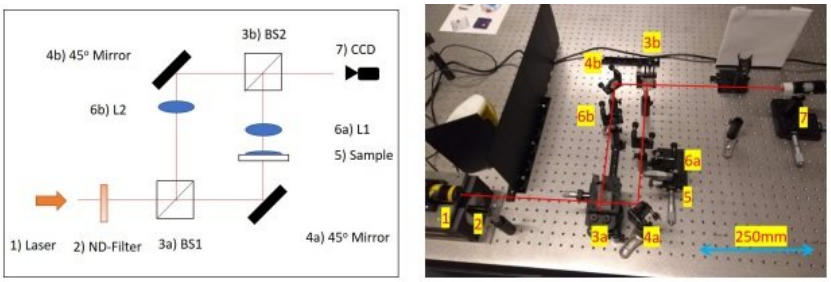

Figure 3.3: Schematic representation of the optical path and elements used in the test system. picture of the test system.

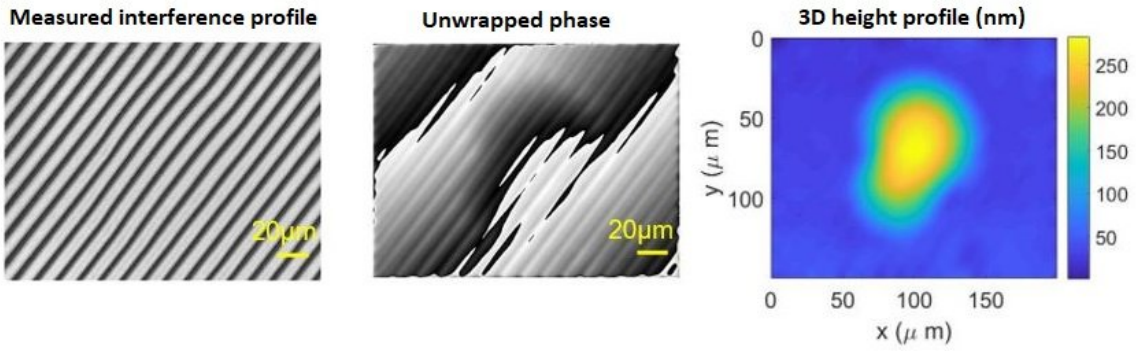

Figure 3.4: The measurement data at different post processing steps.

Measuring on an EM grid

Mariana Silva dos Santos Cos used the method developed by Alok in her Master's thesis to measure the height profile of a glycerol droplet dispensed on an EM grid and plunge freeze it after thickness measurement in real time. The thickness measurement was validated with TEM imaging. Figure 3.5 shows three height profile measurements of an evaporating glycerol droplet on an EM grid. A plunge-freeze mechanism was incorporated into the interferometer system, and the sample droplets were vitrified after reaching a height threshold.

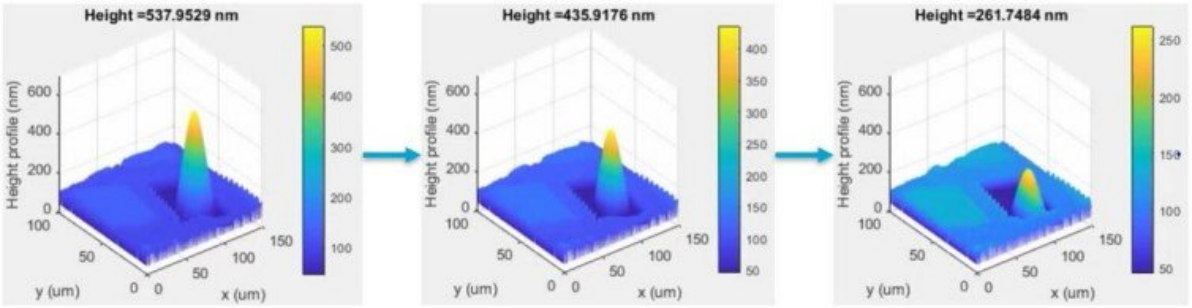

Figure 3.5: Measured height profile of droplet inside a grid square, at three different times during evaporation.

Note that the test was performed on droplets smaller than the grids of the EM grid. The measurement method has not yet been validated on droplets that are partially covered or intersected by one or more grid bars, and the upper limit of droplet sizes that can be measured could be limited by the size of the EM grid squares if it can be measured on partial droplet shapes. Figure 3.6 shows several different droplet sizes within grid squares.

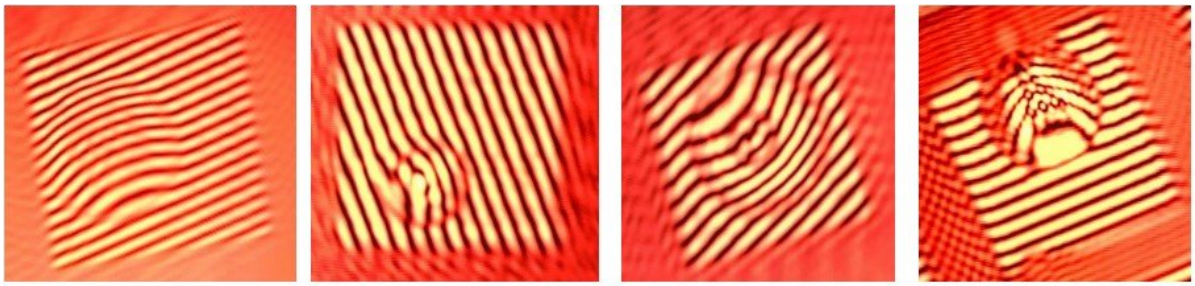

Figure 3.6: Four different droplet sizes inside grid squares. dispensed with modified ink-jet printer

4. Evaporation of micro water droplets

One of the features most reviewed systems have in common is that they minimised the time between the thickness control/measurement step and the plunge freezing; This is done to limit the exposure time to ambient conditions and minimise the decrease in layer thickness due to evaporation. How fast each process step needs to be is determined by the evaporation rate of the sample. The evaporation behaviour of water droplets and the influence of environmental conditions on this behaviour will be discussed in this chapter.

4.1. Dew point

The dew point describes the temperature at which the rate of evaporation and the rate of condensation would be equal in a volume of air with a certain humidity content. If the volume of air is cooled down from ambient temperature to the dew point, the volume of air becomes saturated and dew will form. Condensation will form on an object that is cooled down to or below the dew-point temperature inside the volume of air. The dew point depends on relative humidity RH and air temperature T. The temperature of the dew point T_{DP} is the same as the temperature of the air when the relative humidity is 100%. Absolute humidity is the amount of water mass per unit volume of air. Relative humidity is the ratio between the partial vapour pressure of the air and the saturated vapour pressure of the water at the same temperature. This is the ratio between how much water is present and the maximum amount that could be present. The dew point can be expressed in terms of relative humidity and air temperature using the equation 4.1 [7]. There are sets of constants A and B for different temperature ranges.

$$T_{\mathrm{DP}}(T, \mathrm{RH}) = \frac{A\left(\log(\mathrm{RH}) + \frac{BT}{A+T}\right)}{B - \log(\mathrm{RH}) - \frac{BT}{A+T}} \tag{4.1}$$

The sample droplet evaporation rate can be significantly reduced if the EM grid temperature is kept close to the dew point. Precise temperature control of the EM grid would enable direct control over the thinning process of the sample during thickness measurement.

4.2. Evaporation Modes

The shape of the droplet is not influenced by gravity if the diameter is less than $2\,\mathrm{mm}$ The dominant force that influences the shape of the droplet is the surface tension. The mean surface curvature is thus constant throughout the droplet and the shape can be approximated as a spherical cap[6]. There are two evaporation modes during the droplet evaporation: it starts with evaporation in constant contact radius mode and later the radius decreases linearly with time, results of a measurement of a droplet on a silicon surface illustrate this behaviour as can be seen in figure 4.1 [6]. The reduction in the contact angle remains constant during both evaporation modes. Because evaporation happens in two different modes, the method of measurement of the droplet height cannot assume a constant contact radius and, therefore, the measurement method should not depend only on the radius or contact angle.

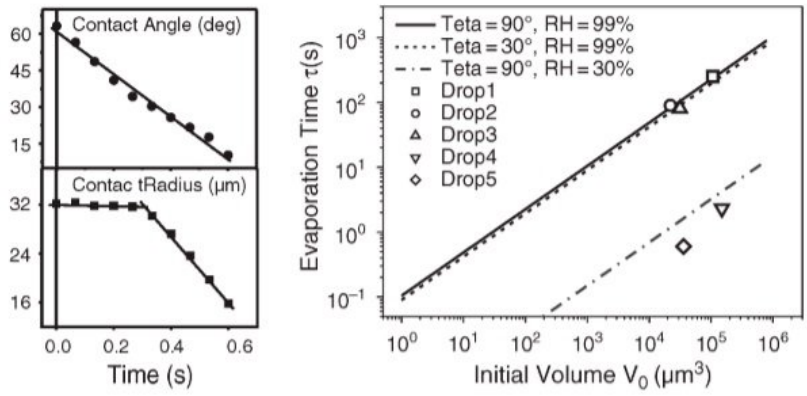

Figure 4.1: Evaporation of a water droplet of $32\,\mu\mathrm{m}$ radius on a silicon surface with time at $25\,^{\circ}\mathrm{C}$,$30\,\%$ RH, contact angle of 63° and surface tension of $7\,\mathrm{mN/m}$, the contact angle is in the top panel and the contact radius is in the bottom; (b) Evaporation time with initial volume for different contact angles and RH [6]

4.3. Evaporation rate in current setup

Experiments have been conducted in previous work [12] to determine the evaporation rate of water-droplets in the AFM4CryoEM system and evaluate the performance of its stage of dew. For these experiments, $0.5\,\mu\mathrm{L}$ MiliQ water was dispensed on an EM grid, placed on a temperature controlled dew point stage. The environmental conditions where $70\,\%$ relative humidity and $37\,^{\circ}\mathrm{C}$ air temperature. The temperature controller in the grid holder tries to keep the grid temperature at the dew-point temperature. The lifetime of the $0.5\,\mu\mathrm{L}$ droplet was $8.8\,\mathrm{min}$. The same-sized droplet evaporates in $2.5\,\mathrm{min}$ under normal ambient conditions. This corresponds to evaporation rates of $0.95\,\mathrm{nL/s}$ and $3.3\,\mathrm{nL/s}$, respectively. The DP stage of the system reduces evaporation by a factor of 3.5. The contact radius of the water droplets in these experiments was approximately $1\,\mathrm{mm}$, as can be seen in Figure 4.2, this contact radius remains the same throughout most of the experiment. This would correspond to constant contact-radius evaporation. More experimental data are needed to characterise the evaporation behaviour of waterdroplets in the picoliter range on an EM grid. A dew point stage that can reduce the evaporation rate even further needs to be developed to conduct these experiments.

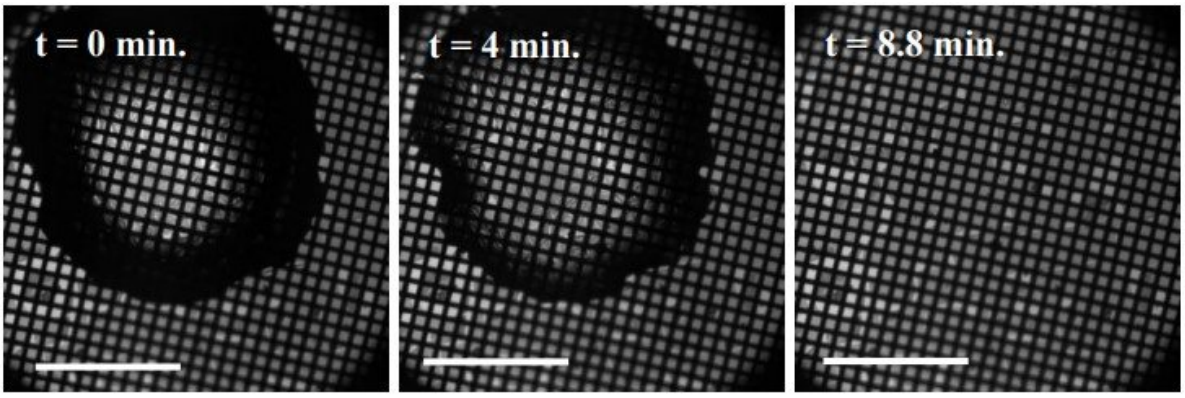

Figure 4.2: Evaporation of MiliQ in a humidity-controlled environment. A carbon coated EM-grid was loaded on the temperature controlled gridholder and $0.5\,\mu\mathrm{L}$ of MiliQ water was pipetted on the EM-grid. The humidity was measured to be $60\,\%$, while the local temperature was kept at the dewpoint ($37\,^{\circ}\mathrm{C}$). At t= $4\,\mathrm{min}$. some evaporation is noticeable, and the sample was evaporated completely at t= $8.8\,\mathrm{min}$. At ambient temperature and humidity the same volume was evaporated after $2.5\,\mathrm{min}$. Scale bar is $1\,\mathrm{mm}$ [12]

5. System analysis

The possibilities of incorporation of thickness measurement with the interferometer into the existing AFM4CryoEM system are evaluated. The process configuration of the process steps of the current system is just one of many ways the system can be built. all the other possible ways of arranging the process steps for this system are evaluated in a systematic analysis of all system configurations. The advantages and benefits of different configuration options will be stated and used to find the system with the lowest mechanical and control complexity. A kinematic configuration analysis shows the different possible ways to build the found system.

5.1. Thickness measurement in AFM4CryoEM system

Implementing a thickness measurement into the existing system can be done in two locations. After rotating the DP stage on a vertical Em grid or before rotation on a horizontal EM grid. Both possibilities are shown in figure 5.1. The benefits and challenges of horizontal versus vertical measurement are discussed in more detail in the next section. Note that measurement after the release of the EM grid from the DP stage in position(C) is not considered. This would require a humidity close to $100\,\%$ and does not give the possibility to manipulate the evaporation rate during the thickness measurement.

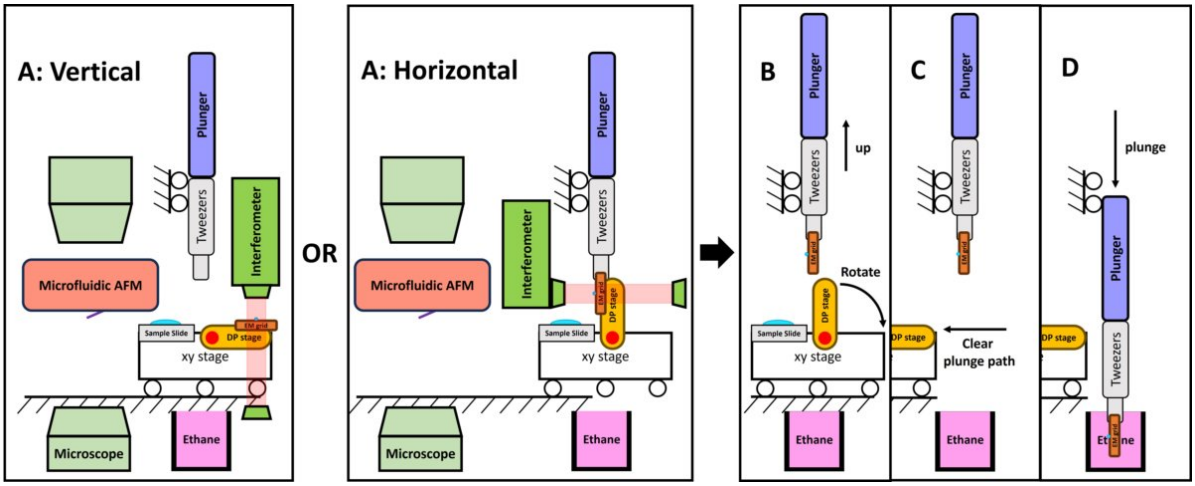

Figure 5.1: A:vertical, The interferometer is vertical aligned and measures on a horizontal EM grid.**B:Horizontal**, The interferometer is horizontal aligned and measures on a vertical EM grid. The tweezers have started the pickup of the EM grid but did not lift it out of the DP stage yet. **B:** The plunge mechanism moves up to release the EM grid from the DP stage. The DP stage rotates back down. **C:** The xy stage moves sideways to clear the plunge path. **D:** The plunger moves down rapidly to vitrify the sample.

There are a couple of challenges with implementing a measurement method in the current AFM4CryoEM system. The time between the EM grid pickup (A) and the finished plunge freeze (D) is about 8 seconds. ~1 second for the rotation of the DP stage (A) and ~7 seconds to clear the xy stage from the plunge path (C). The plunge time is ~60 milliseconds. The main limitation is the actuator type used for the xy stage. The xy stage uses piezoelectric linear actuators. They have a sub-micrometer step size that is great for positioning the sample carrier and EM grid under the AFM but the maximum travel speed is very low. The clearing step (c) has to be done due to the current Kinematic configuration of the system. The 8 second process time between theoretical measurement position and plunge-freezing action needs to be reduced to several hundred milliseconds before a measurement method can be implemented. One option is to modify the existing system and keep the same kinematic configuration. The second option is to investigate other possible kinematic configurations for the AFM4CryoEM sample preparation process. The next two sections will look at different possibilities in system and kinematic configurations

and propose a alternative kinematic configuration for the AFM4CryoEM system.

5.2. Possible system configurations

The six analysed systems in chapter 2 have shown that the same process can be performed in many different ways, in this section the outcome of a systematic system configuration comparison is presented with some of the key design considerations discussed in more detail. The complete system analysis can be found in Appendix A.

Design considerations

The first configuration option to evaluate is in what orientation thickness measurement is performed. Dispensing must take place on a horizontal EM grid and plunge freezing with a vertical EM grid. Somewhere in between, the grid needs to rotate, and the sample thickness has to be measured. So the measurement can be done on a horizontal or vertical EM grid. The main benefit of measuring on a vertical EM grid is that the rotation does not have to happen after the measurement and that the grid already has the correct orientation for plunge freezing. A challenge is to locate the sample on the EM grid to align it with the field of view of the interferometer. This challenge illustrates the biggest advantage of measuring on a horizontal EM grid, the dispensing and measurement step both happen in the same coordinate system, therefore, the location of the sample is known and the alignment of the sample with the measurement beam can be done without any additional optics or motion stages. The second configuration option to evaluate is the dew point stage implementation. One requirement is that the temperature of the EM grid can be adjusted to affect the evaporation rate of the sample during thickness measurement. This means that the EM grid is attached to the DP stage during the measurement step. From there the EM grid can be released from the DP stage at the measurement position, somewhere during transport to the plunge start position or at the plunge start position. The more important question that has an impact on the design complexity of the DP stage is whether the release occurs before or after rotation of the EM grid. The DP stage needs the ability to rotate if the release occurs after rotation. This increases the complexity of the mechanical design, given the tight space constraints between the AFM and microscope objective. The system with the lowest complexity shown in figure 5.2 measures the sample thickness and removes the DP stage before rotating the EM grid. The full argumentation can be found in Appendix A. Note that this is the same system configuration as used in the Cryowriter system.

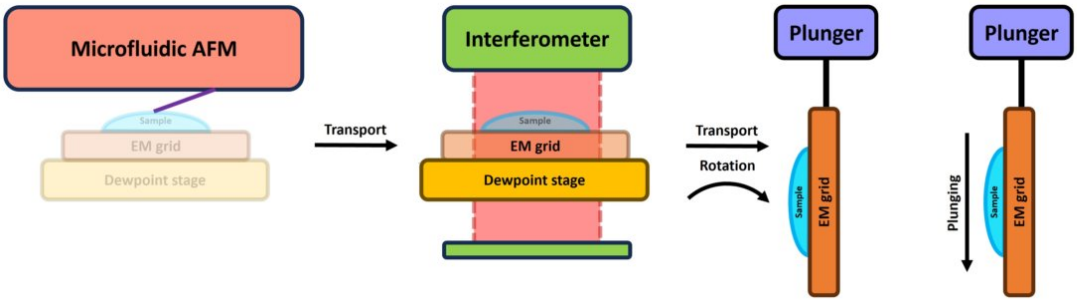

Figure 5.2: Variation 3.4

5.3. Proposed new kinematic configuration

The system configuration proposed in the previous section can be implemented in several different ways. One of them is the kinematic configuration used in the Cryowriter system. Applying an additional set of constraints, requirements, and assumptions results in four possible kinematic configurations. The entire analysis of the kinematic configuration can be found inB. There are four design options that need to be considered; the first two are about the transfer of the EM grid to the tweezers and the transfer of the tweezers to the plunge mechanism. If the tweezers need to pick up the EM grid at some point in the process, it requires additional automation and mechanical complexity. The same is true for the transfer of the tweezers to the plunge mechanism. Automating one or both transfers would eventually

help incorporate more process steps into the system for further automation, but at this point in the development the system with the least complexity needed to perform the process is considered. This is a system with the EM grid attached to the tweezers during the entire process and the tweezers attached to the plunge mechanism during the entire process. The next two design options are about the placement of the rotation point and the release motion of the DP stage. The rotation point can be implemented in two different ways, with a hinge in the plunge arm like the Cryowriter system or by rotating the entire assembly of the EM grid tweezers and plunge mechanism. The specific motion of releasing the EM grid from the DP stage can be done in two ways, either by moving the EM grid or by moving the DP stage. This results in four different kinematic configurations. Each of them is explained in more detail in Appendix B. The mechanical complexity of each of the models is comparable. Choosing one of them has to be done based on further definitions of the space constraints and other considerations and requirements that need to be found in preparation for the detailed design of the system. One of the kinematic configurations shown in Figure 5.3 to show what an alternative system configuration could look like.

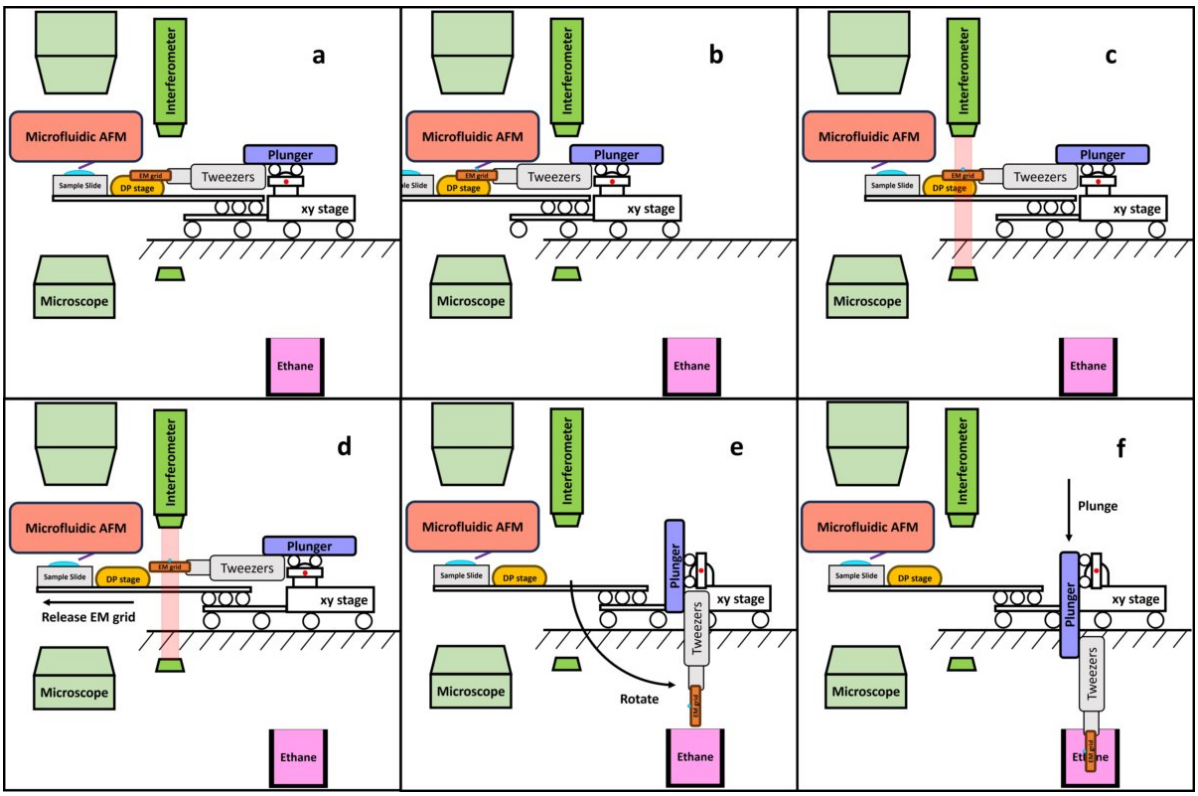

Figure 5.3: a: A sample is aspirated from a single cell with the microfluidic AFM. The xy stage moves to the left to position the EM grid and the DP stage under the AFM. **b:** The AFM dispenses a sample droplet on the EM grid. The xy stage is used to precisely align the AFM cantilever with the EM grid.**c:** The xy stage positions the sample droplet in the field of view of the interferometer. Real-time thickness measurement is started. **d:** a predefined thickness threshold is measured and the release of the EM grid from the DP stage is activated. The DP stage moves to the left to release the EM grid. **e:** The EM grid, tweezers, and plunge mechanism rotate from the measurement position to the plunge start position around a hinge point located between the plunge mechanism and the xy stage. **f:** The plunge mechanism is activated and the sample is vitrified.

The hinge point is located between the plunge mechanism and xy stage, this rotates the entire plunge mechanism. The DP stage moves away to release the EM grid. The EM grid is released at the measurement location and rotates down to the plunge start position. The plunger is already aligned with the cryogenic container during the measurement step, and no additional movements of the xy stage are needed to position the plunger after rotation. This configuration does not require an extremely fast xy stage, because it does not need to perform any time-critical motions after measurement. The xy stage in the current AFM4CryoEM kinematic configurations would need to be extremely fast to clear the way before plunge freezing (step **C** in figure 5.1).

The proposed new kinematic configurations have a lower mechanical and control complexity compared to the current AFM4CryoEM system and can be considered as an alternate route to modification of the existing system to incorporate the thickness measurement step.

6. Research objective

The AFM4CryoEM system has no thickness control and measurement system build in, as can be seen in the evaluation of the six different systems. The goal is to add these to functionalities and create a system that uses microfluidic AFM dispensing, an interferometer to measure the thickness of the sample, a dew-point stage to have controlled thinning of the sample through evaporation, and uses plunge freezing as a vitrification method. Others have shown in previous work in the AFM4CryoEM project that dispensing, measuring, and vitrification methods work individually.

The gap that is identified in the current research and literature is the identification and precise control of the microdroplet evaporation behaviour of an EM grid. The dew-point stage needs to be further developed to determine the relevant evaporation rates of sample droplets in the femtoliter to picoliter range and reduce the evaporation rate enough to allow for realistic process times. With this data, the time-dependent requirements of the system that are needed for the detailed design of a fully integrated system with automated thickness control and measurement can be determined.

This leads to the **research objective:** To obtain vitrified sample thicknesses between 50 nm and 300 nm with a reliable and reproducible process. The focus of this research will be to develop a dew point stage to gain robust control over the evaporation rate of a sample droplet dispensed on an EM grid.

Research question

How to keep a femtolitre volume sample dispensed on an EM grid by microfluidic AFM cantilever without evaporation and measure its thickness just before vitrification?

Subquestions

- What is the evaporation rate of micro droplets in ambient conditions?
- What is the lowest evaporation rate achievable with a dew point stage without global humidity and temperature control?
- What Kinematic configuration minimises transport time and system complexity?
- What is the shortest transport time achievable between EM grid release from the DP stage and vitrification?

Milestones

- Gain robust control of the evaporation rate of micro water droplets from an EM grid.
- Validate the sample thickness measured just before vitrification with Cryo-TEM.

References

[1] Stefan A. Arnold et al. “Blotting-free and lossless cryo-electron microscopy grid preparation from nanoliter-sized protein samples and single-cell extracts”. In: *Journal of Structural Biology* 197 (3 Mar. 2017), pp. 220–226. ISSN: 10478477. DOI: 10.1016/j.jsb.2016.11.002. URL: https://linkinghub.elsevier.com/retrieve/pii/S104784771630243X.

[2] Alok Bharadwaj. “Measurement of Low Contact Angle Droplet Topography Using Optical Interferometry | TU Delft Repositories — resolver.tudelft.nl”. In: (2019). [Accessed 19-10-2023].

[3] Cryosol-World. *Technology - cryosol-world*. 2023. URL: https://cryosol-world.com/vitrojet-solutions/technology/.

[4] Jacques Dubochet et al. “Cryo-electron microscopy of vitrified specimens”. en. In: *Q. Rev. Biophys.* 21.2 (May 1988), pp. 129–228.

[5] Murali Krishna Ghatkesar, Hector Hugo Perez Garza, and Urs Staufer. “Hollow AFM cantilever pipette”. In: *Microelectronic Engineering* 124 (July 2014), pp. 22–25. ISSN: 01679317. DOI: 10.1016/j.mee.2014.04.019.

[6] Murali Krishna Ghatkesar et al. “Scanning probe microscope-based fluid dispensing”. In: *Micromachines* 5 (4 2014), pp. 954–1001. ISSN: 2072666X. DOI: 10.3390/mi5040954.

[7] Krzysztof Górnicki et al. “Evaluation of models for the dew point temperature determination”. In: *Technical Sciences* 20 (Dec. 2017), pp. 241–257. DOI: 10.31648/ts.5425.

[8] Tilak Jain et al. “Spotiton: A prototype for an integrated inkjet dispense and vitrification system for cryo-TEM”. In: *Journal of Structural Biology* 179 (1 July 2012), pp. 68–75. ISSN: 10478477. DOI: 10.1016/j.jsb.2012.04.020.

[9] Roman I. Koning et al. “Automated vitrification of cryo-EM samples with controllable sample thickness using suction and real-time optical inspection”. In: *Nature Communications* 13 (1 Dec. 2022). ISSN: 20411723. DOI: 10.1038/s41467-022-30562-7.

[10] Euth Ortiz Ortega et al. *Characterization Techniques for Morphology Analysis*. Vol. 19. Springer, 2022, pp. 1–45. DOI: 10.1007/978-981-16-9569-8_1.

[11] L. A. Passmore and C. J. Russo. *Specimen Preparation for High-Resolution Cryo-EM*. Vol. 579. Academic Press Inc., Jan. 2016, pp. 51–86. ISBN: 9780128053829. DOI: 10.1016/bs.mie.2016.04.011.

[12] J W Pronk. “Aquaporin-2 trafficking: Studying cellular mechanisms with subcellular aspiration and cryo-electron microscopy”. In: (2018). DOI: 10.4233/uuid:b6c599e8-077c-44f1-bb71-e731bcc7d81f.

[13] Raimond B. G. Ravelli et al. “Cryo-EM structures from sub-nl volumes using pin-printing and jet vitrification”. In: *Nature Communications* 11 (1 May 2020), p. 2563. ISSN: 2041-1723. DOI: 10.1038/s41467-020-16392-5. URL: https://www.nature.com/articles/s41467-020-16392-5.

[14] thermofisher.com. *Vitrobot Mark IV System*. 2023. URL: https://www.thermofisher.com/nl/en/home/electron-microscopy/products/sample-preparation-equipment-em/vitrobot/instruments/vitrobot-mark-iv.html (visited on 10/09/2023).

A. System configurations

In this analysis of the system, the constraints and requirements of the dispensing process, the measurement process, and the plunging process are identified. A total of 18 different system variants were evaluated. This evaluation produces eight viable system configurations, two of which have the lowest system complexity. The analysis starts with three system-level requirements.

Requirements:

REQ-SY-01 The dispensing step has to be done with a Microfluidic AFM.

REQ-SY-02 The thickness measurement step must be done with a Mach-zehnder interferometer.

REQ-SY-03 The vitrification step must be done by plunge freezing.

A.1. Process steps

The sample preparation process consists of three main steps. Dispensing the sample on an EM grid, measuring the thickness of the sample, and plunge freezing the sample. The EM grid containing the sample needs to be transported in some way between the process steps. Each process step and transport have an associated process time and process location. Figure 2.2 shows the process timeline with these variables. The presence of active temperature control of the EM grid is depicted with the block labelled Dew point control. At what step the EM grid separates from the Dew point control is a free design variable and not yet known.

Each of the process steps has a set of constraints and requirements, the connection between dispensing and measurement and the connection between measurement and plunge freezing have to accept the output condition of one step and present the sample to the next step according to the expected input condition.

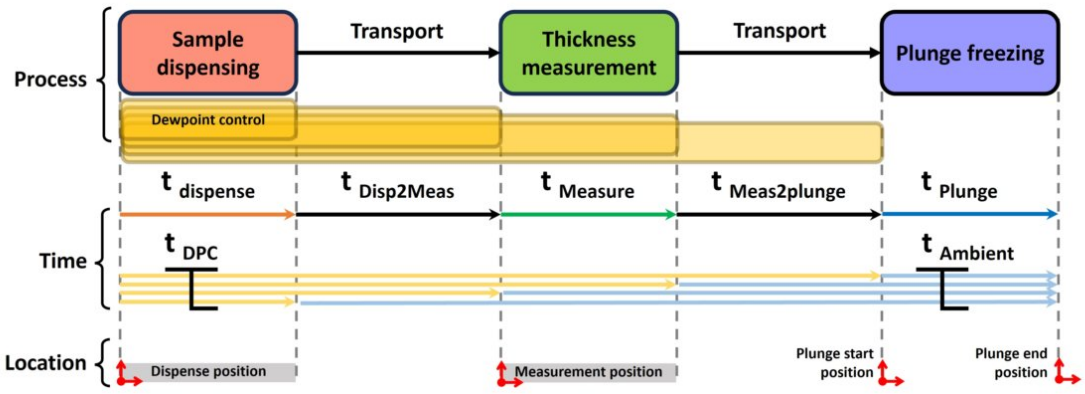

Figure A.1: Process, time and location description

Microfluidic AFM sample dispensing

The dispensing step is done in three stages; first, a sample is aspirated from a cell located in a sample holder. Second, the sample holder and the EM grid move to remove the sample holder and place the EM grid under the AFM, and third the sample is dispensed on the EM grid. The following list of constraints and requirements is used to see if there are different ways to perform this process.

Constraints:

CON-SD-01 The AFM is stationary, with manual adjustment of its location.in x and y direction.

CON-SD-02 The AFM and sample holder can be in the same location.

CON-SD-03 The EM grid and the AFM can be in the same location

CON-SD-04 The sample holder and the EM grid cannot be in the same location.

CON-SD-05 The internal Z motion of the AFM is used to approach the sample holder and the EM grid during aspiration and dispensing.

CON-SD-06 Dispensing is done on a horizontal EM grid.

CON-SD-07 The AFM can operate in an environment with a maximum relative humidity off 70%.

Requirements:

REQ-SD-01 The sample holder needs to be positioned with respect to the AFM with a accuracy of +- 0.002mm in x and y direction

REQ-SD-02 The EM grid should be positioned with respect to the AFM with an accuracy of +- 0.002mm. in the x and y directions.

Possible configurations:
With the above-mentioned constraints and requirements, there are two possible process configurations. First, the sample holder and the positioning of the EM grid are done with two separate xy stages. Second, since the sample holder and the EM grid have the same positional accuracy requirements and cannot be in the same place, it is possible to move them both with the same xy stage at a fixed distance from each other. The first option adds complexity without a clear benefit and, therefore, the second option is used. Figure A.2 depicts the process referred to as Sample dispensing for the rest of this chapter.

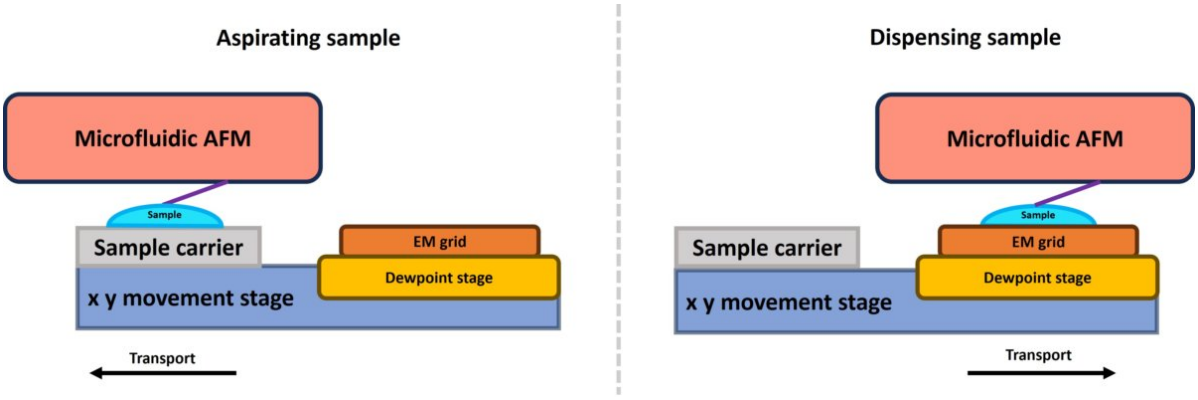

Figure A.2: Process description microfuidic AFM

Thickness measurement

The thickness measurement is performed with a mach-Zehnder interferometer. The functionality of this system is explained in chapter 3. The use of this measurement method brings its own set of constraints and requirements.

Constraints:

CON-TM-01 The measurement position cannot be the same as the dispensing position.

CON-TM-02 Measurement position is stationary.

CON-TM-03 Measurement position and plunge start position can be the same.

CON-TM-04 The field of view is 150μm by 200μm.

CON-TM-05 The maximum sample droplet that can be measured has a diameter of 100μ m.

CON-TM-06 The measurement beam can be horizontal or vertical.

Requirements:

REQ-TM-01 The whole sample droplet needs to be inside the field of view.

REQ-TM-02 The sample droplet should be positioned within the field of view with an accuracy of +-0.015mm in the x and y direction.

Plunge freezing

Plunge freezing an EM grid with a sample on it is the last step in the process. The following constraints and requirements are associated with this process step.

Constraints:

CON-PL-01 Plunge freezing is done with a vertically oriented EM rid, plunging in the negative z direction.

CON-PL-02 The plunger may move and rotate. as long as it ends up in a vertical orientation at the plunge freeze start position.

CON-PL-03 The plunge freeze start position is stationary.

CON-PL-04 The plunge end position is stationary and equal to the position of the cryogenic container.

CON-PL-05 The plunger needs at least a defined start position and a defined end position, no accurate position control is needed in between.

Requirements:

REQ-PL-01 The plunger and EM grid need to reach a speed of at least 1.5m/s before entering the cryogenic liquid.

REQ-PL-02 The plunger needs to stop in the plunge-stop position.

REQ-PL-03 Plunging needs to happen automated.(resetting may be done manually)

Transport

There are two different transport steps, moving the EM grid from the dispensing position to the measurement position and moving the EM grid from the Measurement position to the plunge start position.

Based on constraints CON-SD-06 and CON-PL-01, it is clear that the EM grid needs to rotate 90 degrees in one of these transport steps. Where in the process the rotation is placed is a free design variable.

The movement from the dispensing position to the measurement position must be done by moving the EM grid, because both the dispensing position and the measurement position are stationary and cannot be in the same place.

Movement from the measurement position to the plunge start position can be done in two ways,if the measurement position is not the same as the plunge start position the EM grid needs make this movement. If the measurement position and the plunge start position are the same, no movement is needed for transport.

Requirements:

REQ-TR-01 the transport time $t_{disp2meas}$ needs to be short enough to transport the sample droplet without Major sample volume loss due to evaporation.

REQ-TR-02 the transport time $t_{meas2plunge}$ must be short enough to transport the sample droplet without major loss of sample volume due to evaporation.

The specific value for these time requirements depends on the minimum evaporation rates of sample droplets at specific environmental conditions; these values are not yet known.

A.2. System configurations

There are three different configurations possible on the basis of the constraints and requirements mentioned in the previous section. The three configurations only vary in measurement position and mea-

surement orientation. They have not yet considered the environmental conditions needed to slow down the evaporation rate of the sample.

Assumption: The rotation represented in 2d is sufficient for system identification, the rotation from the xy plane to the xz or yx plane results in equivalent systems.

	Measurement position =	Orientation of EM grid while measuring =
V1	At plunge position	Vertical
V2	Not at plunge position	Vertical
V3	Not at plunge position	Horizontal

Figure A.3: Three possible configurations.

First configuration:
The measurement position is the same as the plunge start position. Thickness measurement is done on a vertical EM grid. Rotation of the EM grid occurs before the measurement step.

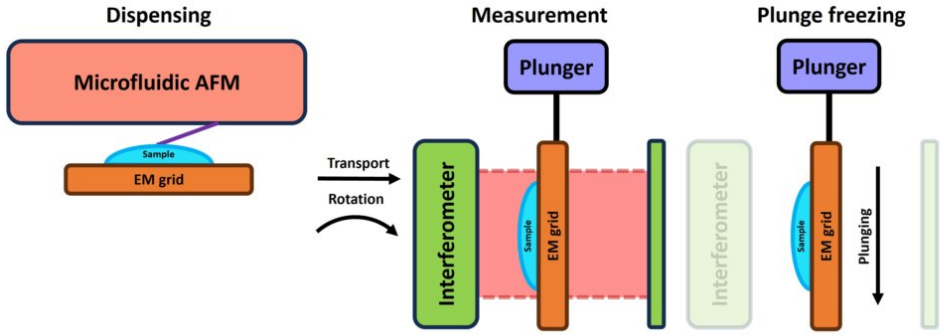

Figure A.4: Configuration 1

Second configuration:
The measurement position is not the same as the plunge start position. Thickness measurement is done on a vertical EM grid. Rotation of the EM grid occurs before the measurement step.

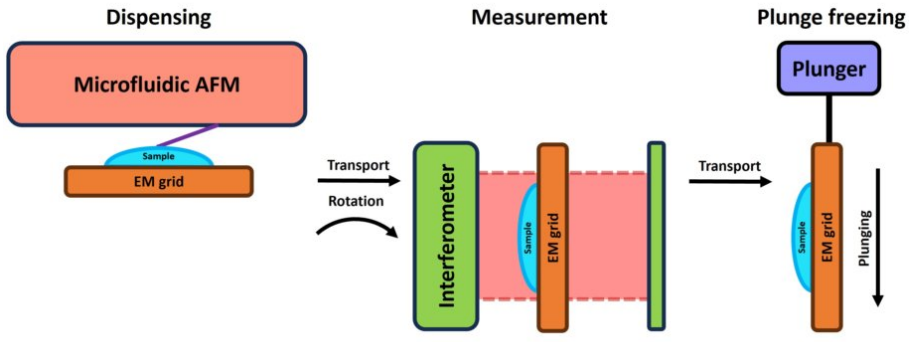

Figure A.5: Configuration 2

Third configuration:
The measurement position is not the same as the plunge start position. Thickness measurement is done on a horizontal EM grid. Rotation of the EM grid occurs after the measurement step.

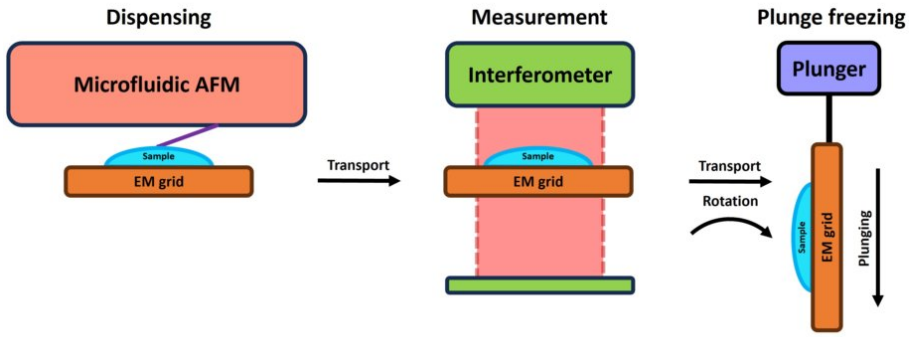

Figure A.6: Configuration 3

environmental control

The six reviewed systems used three different methods of environmental control. global control of humidity and temperature in a process chamber and local control of the temperature of the EM grid with a dew point stage (DP stage). All systems that used global humidity control operate the process chamber between 95% and 100% relative humidity, to bring the temperature of the dew point close to the global temperature. The AFM cannot operate at these humidity levels according to the constraint **CON-SD-07** that specifies a maximum relative humidity of 70%. This leaves a large enough temperature differential between the ambient temperature and the dew point temperature and requires active temperature control of the EM grid to compensate for this difference. Normal relative humidity in the test room is between 40% and 60%. So the real benefit of global humidity control would only be an increase of 10%. Therefore, the global humidity and temperature control are left out for the rest of this analysis and may be considered after the performance of the DP stage is known. The constraints and requirements for the implementation of a DP stage are listed below.

Constraints:

CON-DP-01 The DP stage position can be the same as the EM grid position.

CON-DP-02 The stage position of the dew point can be the same as the dispense position.

CON-DP-03 The DP stage position can be the same as the measurement position.

CON-DP-04 The DP stage position can be the same as the plunge start position.

CON-DP-05 The DP stage position cannot be the same as the plunge end position.

Requirements:

REQ-DP-01 The DP stage needs to lower the evaporation rate of the sample far enough to have no major volume loss due to evaporation.

REQ-DP-02 The temperature of the EM grid must be adjustable.

With the introduction of local temperature control of the EM grid, the number of possible system variants is increased to 18 of the EM grid. These configurations can be seen in Table A.7.

	Measurement position =	Orientation of EM grid while measuring =	Releasing EM grid form DP stage		
V1.1	At plunge position	Vertical	Before rotation	Before measuring	At dispense position
V1.2	At plunge position	Vertical	Before rotation	Before measuring	Between dispense and measure position
V1.3	At plunge position	Vertical	After rotation	Before measuring	Between dispense and measure position
V1.4	At plunge position	Vertical	After rotation	Before measuring	At measure / plunge position
V1.5	At plunge position	Vertical	After rotation	After measuring	At measure / plunge position
V2.1	Not at plunge position	Vertical	Before rotation	Before measuring	At dispense position
V2.2	Not at plunge position	Vertical	Before rotation	Before measuring	Between dispense and measure position
V2.3	Not at plunge position	Vertical	After rotation	Before measuring	Between dispense and measure position
V2.4	Not at plunge position	Vertical	After rotation	Before measuring	At measure position
V2.5	Not at plunge position	Vertical	After rotation	After measuring	At measure position
V2.6	Not at plunge position	Vertical	After rotation	After measuring	Between measure and plunge position
V2.7	Not at plunge position	Vertical	After rotation	After measuring	At plunge position
V3.1	Not at plunge position	Horizontal	Before rotation	Before measuring	At dispense position
V3.2	Not at plunge position	Horizontal	Before rotation	Before measuring	Between dispense and measure position
V3.3	Not at plunge position	Horizontal	Before rotation	Before measuring	At measure position
V3.4	Not at plunge position	Horizontal	Before rotation	After measuring	At measure position
V3.5	Not at plunge position	Horizontal	Before rotation	After measuring	Between measure and plunge position
V3.6	Not at plunge position	Horizontal	After rotation	After measuring	Between measure and plunge position
V3.7	Not at plunge position	Horizontal	After rotation	After measuring	At plunge position

Figure A.7: 18 Possible variants.

The thickness of the sample needs to be reduced in a controlled way while measuring the thickness in real time. This is possible if the DP stage is used to control the temperature off the EM grid during the measurement step. The functionality of EM grid temperature control during the measurement step is introduced as a system level requirement.

requirement:

REQ-SY-04 The temperature of the EM grid has to be adjustable during the thickness measurement.

This reduces the total number of variations to 8. Each of these variants has specific advantages and disadvantages that must be considered. The remaining variants are listed in figure A.8 and for of them have their schematic representation shown in figure A.9.

	Measurement position =	Orientation of EM grid while measuring =	Releasing EM grid form DP stage		
V1.5	At plunge position	Vertical	After rotation	After measuring	At measure / plunge position
V2.5	Not at plunge position	Vertical	After rotation	After measuring	At measure position
V2.6	Not at plunge position	Vertical	After rotation	After measuring	Between measure and plunge position
V2.7	Not at plunge position	Vertical	After rotation	After measuring	At plunge position
V3.4	Not at plunge position	Horizontal	Before rotation	After measuring	At measure position
V3.5	Not at plunge position	Horizontal	Before rotation	After measuring	Between measure and plunge position
V3.6	Not at plunge position	Horizontal	After rotation	After measuring	Between measure and plunge position
V3.7	Not at plunge position	Horizontal	After rotation	After measuring	At plunge position

Figure A.8: 8 Possible variants that release the EM grid from the DP stage after measuring the thickness.

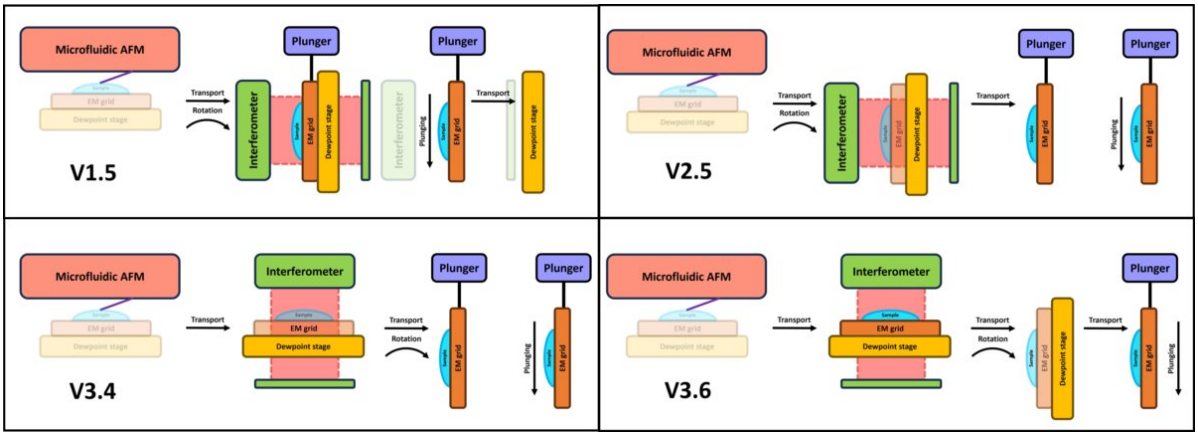

Figure A.9: Schematic representation of four variants to illustrate the differences.

The design considerations listed below were used to evaluate the eight remaining variants, the benefits and challenges associated with each option are discussed and finally summarised in the comparison table shown in figure A.10.

Measurement position

The measurement position can be before rotating the EM grid or after rotating the EM grid.

measuring before rotation:

advantages: The dispensing step and the measurement step are carried out in the same coordinate frame. This allows for the use of the same xy movement stage to position the EM grid and sample during both steps. The precise location of the sample on the EM grid is known and can be used to position the sample inside the field of view of the interferometer.
Challenges: Transport from measurement position/orientation to plunge start position includes at least one rotation. The rotation time is added to the process time between the finished thickness measurement and plunge freezing.

measuring after rotation:

Advantages: The rotation time is not added to the process time between the finished thickness measurement and plunge freezing. transport time from measurement position to plunge start position is at minimum 0 seconds.
Measurement on a vertical EM grid means that the interferometer can be built in the horizontal plane; this is the same as the previous test setup for the interferometer.
Challenges: Dispensing and measurement do not happen in the same coordinate system. they share at most one axis of movement. This means that at least one DoF with precise positioning needs to be added to position the sample in the field of view of the interferometer.
The precise location of the sample on the EM grid is no longer known.this would require an additional optical system to locate the sample after rotation with some form of image-processing software before the measurement can begin.

Releasing EM grid form Dew-point stage

The presence of the DP stage after measurement must be considered, the main consideration is when to remove the EM grid from the DP stage, before or after rotation?

Release DP stage before rotation:

Advantages: The dew-point stage does not have to rotate, therefore simplifying the mechanical complexity and its design.
Challenges: At least one rotational movement is needed to position the EM grid at the plunge start

position. Rotation time is added to the process time between the removal of the DP stage and plunge freezing.

Release DP stage after rotation:
Advantages: The EM grid is temperature controlled during the rotation. With this the rotation time is less critical.
Challenges: Adding the ability to rotate to the DP stage makes it more challenging to design and build.

	Image processing challenge	Mechanical challenges		Minimum hardware complexity	
	Sample droplet localization on EM grid before thickness measurement	Design of a rotating dewpoint stage	Rotation time is critical and needs to be minimized	Minimum number of position accurate motion stages	Minimum number of microscopes
V1.5	Yes	Yes	No	3	2
V2.5	Yes	Yes	No	3	2
V2.6	Yes	Yes	No	3	2
V2.7	Yes	Yes	No	3	2
V3.4	No	No	Yes	2	1
V3.5	No	No	Yes	2	1
V3.6	No	Yes	No	3	1
V3.7	No	Yes	No	3	1

Figure A.10: Comparing complexity based on the design considerations.

The decision to measure before or after rotation has a major impact on the engineering field the challenges are places in. An image processing challenge is introduced for all variants that measure after rotation. Also at least one additional precision accurate movement axis is needed to position the sample in the field of view of the interferometer, all variants that measure before rotation gain a mechanical design challenge in minimising the time it takes to rotate the EM grid. Measurement before rotation is considered to be less complex to design.

removing the EM grid before rotation reduces the design complexity of the DP stage but shifts the challenge to designing a fast rotation mechanism. The Cryowriter system shows at least one mechanical solution to this challenge. The rotation DP stage in the current AFM4CryoEM system has shown that it is difficult to get it working properly due to the limited space available between the AFM and the microscope. Not rotating the DP stage is considered to be less complex to design.

A.3. Recommended system configuration

Variant **V3.4** and **V3.5** have the lowest complexity and are recommended as alternative system configurations for the AFM4CryoEM system. The only difference is the exact release point of the DP stage. A systematic kinematic configuration analysis for these systems can be found in Appendix B.

B. Kinematic Configuration Analysis

Variant **V3.4** and **V3.5** can be implemented in several different kinematic configurations. The constraints and requirements listed in A, along with an assumption, are used to narrow down the possible kinematic configurations to four.

Assumption: The grid needs to exit the dew-point stage with a motion co-planar to its orientation, assuming it is held down with a spring clip of some sort. Note that this is similar to the current hardware of the AFM4CryoEM system but different from the implementation in the Cryowriter system. This assumption may need to be reconsidered during the detailed design.

The following four design options must be considered:

EM Grid Transfer to the Tweezers

Pick up the EM grid with tweezers somewhere in the process

Advantage: Further development in automation can be achieved if the pick-up of the EM grid is automated somewhere in the system (as with the Linkham plunger and Vitrojet systems). **Challenge:** Adding automated EM grid pick-up adds mechanical and control complexity.

Have the tweezers attached to the EM grid throughout the whole process

Advantage: Handling of the EM grid can always be done by manipulating the tweezers. No additional handling systems are needed, thus simplifying the design. **Challenge:** Automating the preparation of multiple EM grids may be more challenging in future developments.

Tweezers Transfer to the Plunge-Freeze Mechanism

Attach the tweezers to the plunge-freeze mechanism at some point in the process

Advantage: - **Challenge:** The transfer from the tweezers to the plunge mechanism adds to the mechanical and control complexity.

Have the tweezers attached to the plunge-freeze mechanism throughout the process

Advantage: No transfer mechanism is needed, thus minimizing mechanical and control complexity. **Challenge:** Implementation may be challenging due to space constraints that the design must fit.

For this analysis, systems with minimum mechanical and control complexity are considered. These are the systems that have the EM grid attached to the tweezers throughout the process and the tweezers attached to the plunge mechanism throughout the process.

The next two design options cannot be evaluated yet. This leaves four possible kinematic configurations. The associated advantages and challenges of these four options need to be evaluated further once more physical details and space constraints are defined in preparation for the detailed design.

Releasing the EM Grid from the Dew-Point Stage

Options: Move the EM grid **or** move the DP stage?

Placement of the Rotation Point

Options: Rotate the EM grid with a hinge in the plunge arm **or** rotate the entire plunge mechanism?

B.1. Possible Kinematic Configurations

The figures below show the four possible kinematic configurations. The aspiration step and the dispensing step are omitted in the figures because they are the same for each option. The figures show the movements from the moment the measurement system measures the correct thickness.

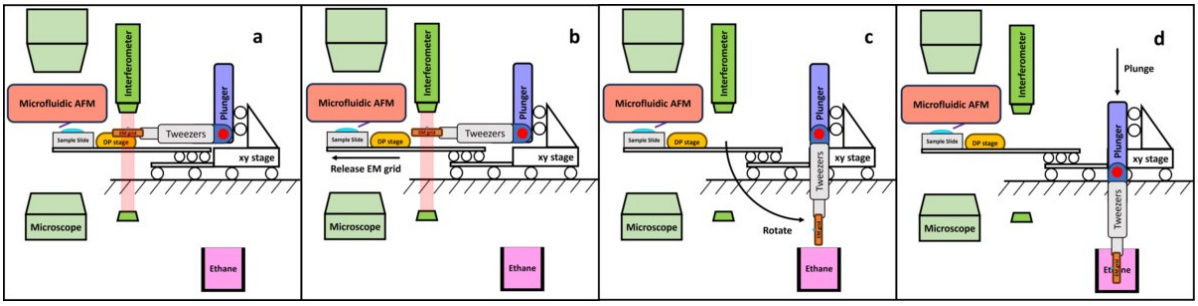

Figure B.1: a: The interferometer measures the correct thickness. **b:** The EM grid is released by moving the DP stage. **c:** EM grid and tweezers rotate on a hinge located in the plunge arm. **d:** Plunge freezing.

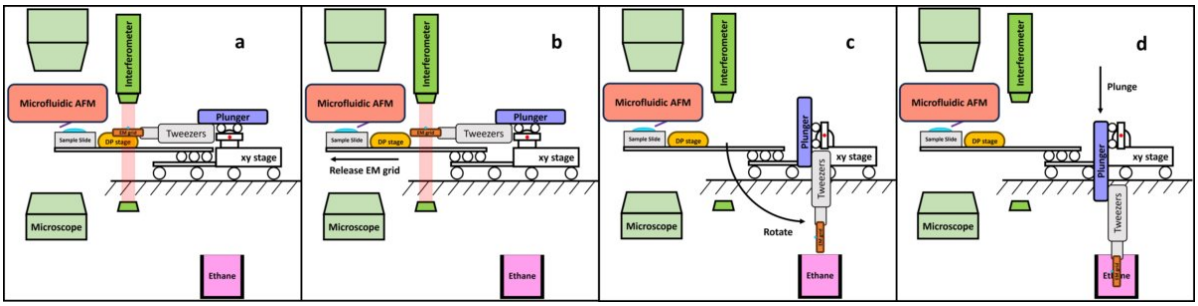

Figure B.2: a: The interferometer measures the correct thickness. **b:** The EM grid is released by moving the DP stage. **c:** The entire plunge mechanism, including EM grid and tweezers, rotates from horizontal to vertical. **d:** Plunge freezing.

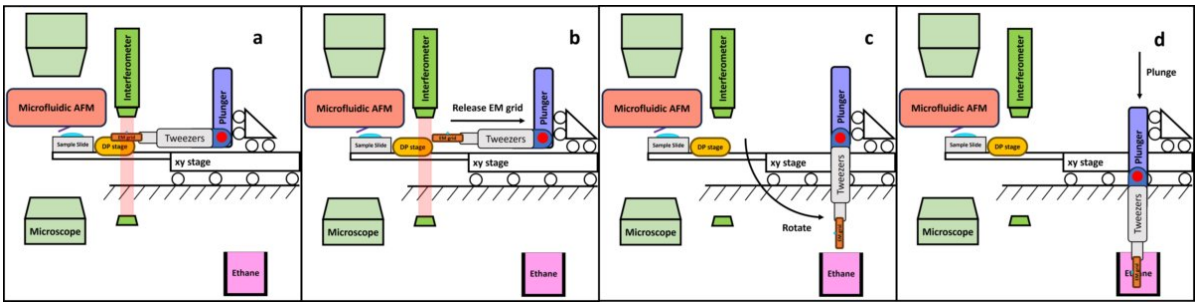

Figure B.3: a: The interferometer measures the correct thickness. **b:** The EM grid is released by moving the whole plunge mechanism. **c:** EM grid and tweezers rotate on a hinge located in the plunge arm. **d:** Plunge freezing.

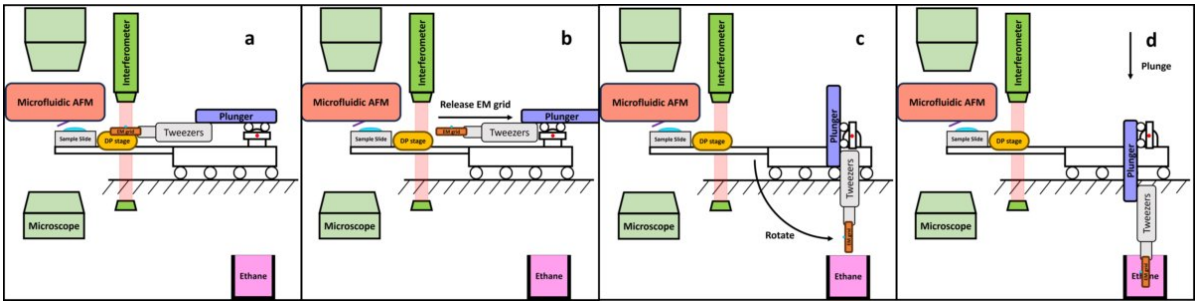

Figure B.4: a: The interferometer measures the correct thickness. **b:** The EM grid is released by using the movement axis of the plunge mechanism. **c:** The entire plunge mechanism, including EM grid and tweezers, rotates from horizontal to vertical. **d:** Plunge freezing. **Note:** This system has one movement axis less than the rest; however, it requires a plunge mechanism that can move in two directions.

C. List of supplementary videos

Link to playlist:

https://www.youtube.com/playlist?list=PL1UdBRxw2tWEVDsuggh17qFTX6aLvsxuF

(1) **Working principle of the plunging mechanism**

https://youtu.be/hdYXave2nUo

The intended functionality of the designed mechanism is demonstrated with a CAD animation.

(2) **Demonstration of the plunge freeze sequence**

https://youtu.be/nRzBYDpheQw

This video demonstrates the plunge freeze action. The EM grid is transported through ambient conditions from the temperature-controlled grid holder to the plunge start position. The end rotation triggers the plunge motion. The entire process takes $260\,\mathrm{ms}$.

(3) **Plunge freezing action in slow motion**

https://youtu.be/LXSiqtzeDhc

Slow motion footage was used to measure the position of the tweezer tip and EM grid during the motion sequence. The mechanical performance of the system was evaluated based on these data points.

(4) **A nL-sized droplet on a glass surface with a temperature equal to the measured dew point**

https://youtu.be/G2axm86OZD4

This video shows a time-lapse of an evaporating water droplet. The total evaporation time is 49 minutes.

(5) **Droplet dispensed on hydrophobic EM grid with a temperature 1 degree above the measured dew point**

https://youtu.be/BcxG1l7Mvr4

This video shows the evaporation speed of a pL-sized droplet when the temperature of the EM grid is 1 degree above the measured dew point. There is not enough time to perform thickness measurements when the grid temperature is higher than the measured dew point.

(6) **Droplet dispensed on a hydrophobic EM grid**

https://youtu.be/mMxTvGMl3iA

The droplet is dispensed with a $200\,\mu\mathrm{m}$ long microfluidic cantilever with an aperture of $8\,\mu\mathrm{m}$. The grid spacing is $100\,\mu\mathrm{m}$. The grid temperature is set to be 3 degrees below the measured dew point.

(7) **Fringe pattern of a pL-sized droplet on a hydrophobic EM grid**

https://youtu.be/NeOb_w2CDXU

This video shows the fringe pattern recorded during the evaporation of a droplet on an EM grid with a temperature 3 degrees below the measured dew point.

(8) **Dispensing of multiple droplets on a plasma-treated EM grid**

https://youtu.be/vo5M3IAT49A

This video shows the manual positioning and dispensing of multiple droplets. The real-time thickness measurement of the last dispensed droplet just before plunge freezing was validated with a CryoEM thickness measurement.

(9) **Fringe pattern of a droplet on a plasma-treated EM grid**

`https://youtu.be/nTRn7GI0S18`

This video shows the last section of fringe pattern measurements before plunge freezing. The height information obtained from the data points just before plunge freezing was validated with a CryoEM thickness measurement.

(10) **Demonstration of all manual operations in one complete test procedure**

`https://youtu.be/Up-BQSS3WIQ`

This video shows all manual operations that are described in the user manual of the system. The footage shown is not from a real test sequence; it was recorded for demonstration purposes. A real test sequence may include a real-time thickness measurement step that takes several minutes before the plunge freeze mechanism is activated.

D. User Instructions Test Setup

D.1. Software

Matlab

The real-time thickness measurement is done with a Matlab script. It measures roughly 5 times a second and displays the resulting height profile and the measured fringe pattern.

TEC Control Software

Software (TEC Service Software v5.10) is provided by the manufacturer and is free to download. Key features include:

1. Stores configuration locally. If a new PC is connected for the first time, press the ”Read Config” button to retrieve the settings stored in the device.
2. NTC temperature settings. The calibration curve of the NTC sensor is set with 3 data points, as given in the datasheet of the sensors. The sensor characteristics can be found in the ”Advanced” tab under the subtab ”Temperature Conversion”.
3. Storing data. Data can be stored in a CSV file. This can be done in the ”Maintenance” tab.
4. Auto tune. The system has an autotune function, which can be found in the ”Auto Tuning” tab.
5. TEC characteristics and failsafe temperatures. The characteristics of the TEC can be set in the ”Temperature Control” tab. It is also possible to set thermal limits. If for some reason the water cooling loop is not turned on and the TEC hot side reaches the set upper limit of 40°C, the system turns itself off automatically.

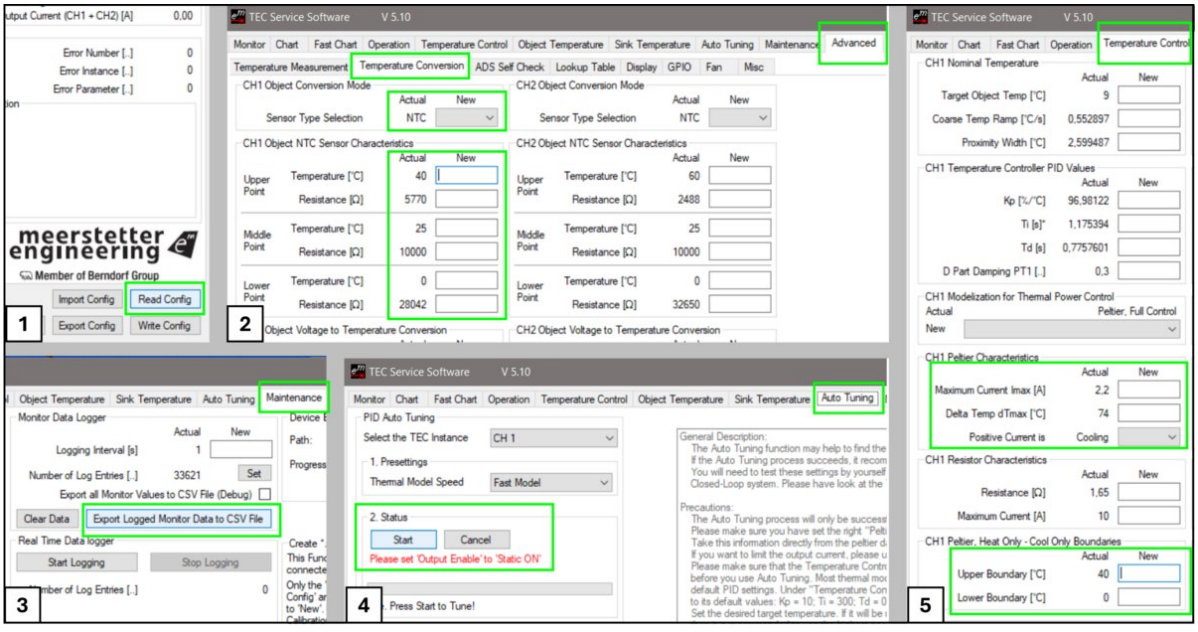

There is also the option to read and write data with a LabView script. This could be used for automation in the future.

Dewpoint Sensor Software

Software (1.7.4.0 Sentax64) is provided by the manufacturer at the time of purchase. It is possible to log the data. There is also the option to read the data with a LabView script, which could be used for automation in the future.

Pressure Controller Software
The pressure controller software (CORA) is installed on the desktop PC located next to the test setup.

USB Camera App
The USB camera app can be downloaded from the Play Store. It is used to view and record the output of the USB microscope. This is done on a separate device due to some USB port conflict in MATLAB; it does not work if two USB microscopes are connected.

D.2. Test Setup
Interferometer Adjustments
Start the real-time thickness measurement script to get a preview window with the live feed from the CCD.

Aligning Each Beam Path to Hit the CCD in the Middle:

1. Block the path of the beam that does not pass through the EM grid.
2. Use a small white card and hold it in front of the CCD. Manually adjust the angles of the second beamsplitter to aim the beam roughly to the middle of the CCD.
3. Remove the white card and look at the preview window. For one axis at a time, rotate to observe intensity changes in the image. Find the brightest setting and repeat for the other axis.
4. Block the path of the beam that goes through the EM grid. Use the white card again and the 45-degree mirror to align the beam to hit the CCD roughly in the middle. Repeat the previous step.

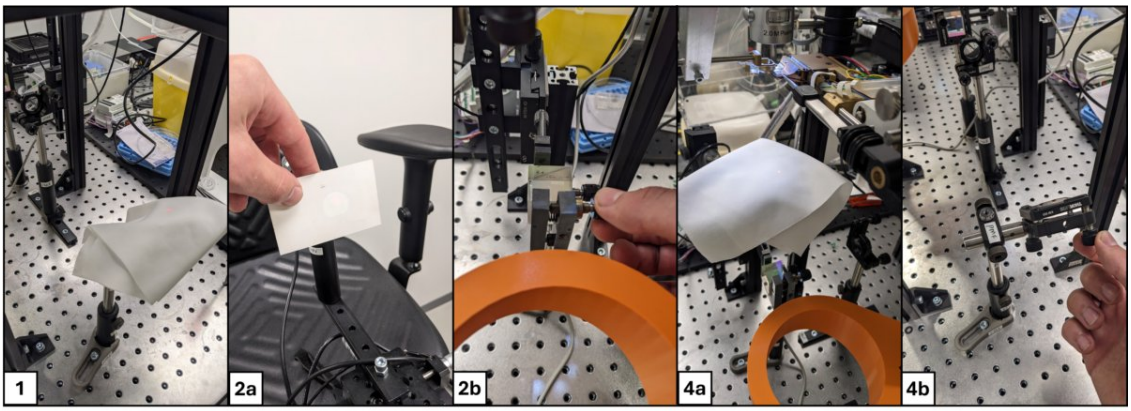

Getting the EM Grid Bars in Focus:

1. Block the path that does not cross the EM grid. Move the lens up or down with the linear stage to get the edge of the grid bars in focus.

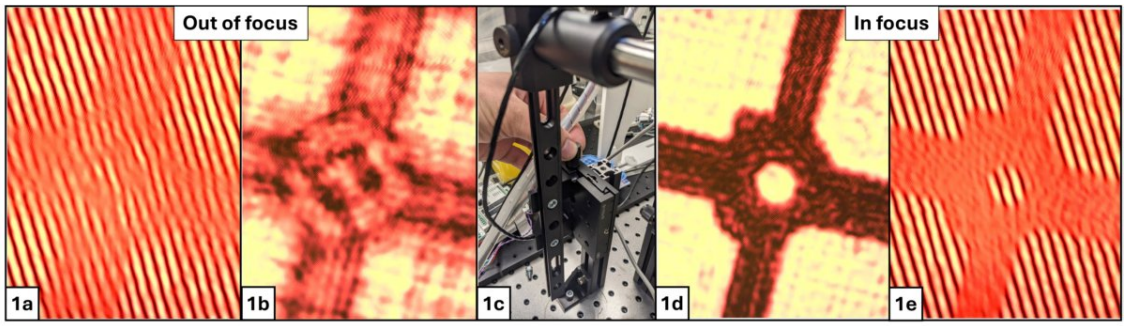

2. Check if the distance of both lenses to the beamsplitter is roughly the same, within 10mm difference. If necessary, move the other lens to compensate, which may result in a misalignment of the beam again.

3. The interferometer should be adjusted to give at least 15 to 20 fringe lines across one grid square. More careful alignment of the optical elements is needed beforehand to make the fringe pattern more predictable and controllable.

D.3. Step by Step Test Procedure

This section will list all the steps needed to turn on the system, prepare the system for a sample preparation sequence, and perform a sample preparation sequence. There is also a shutdown procedure. Video (10) all the manual operations to complete one test procedure.

System Start-Up Steps

1. Turn on the laser. It takes a few minutes to warm up and turn on.
2. Turn on the DPstage control box. There is a power switch next to the mains power cord input.
3. Turn on the plunge mechanism controller (Controlino). This is done by turning on the power distribution block that it is plugged into.
4. Connect the USB hub to the laptop. It connects the control box, the DP sensor, and the USB microscope CCD sensor of the interferometer to the laptop.
5. Connect a smartphone with the USB camera app on it to the USB microscope used for dispensing.

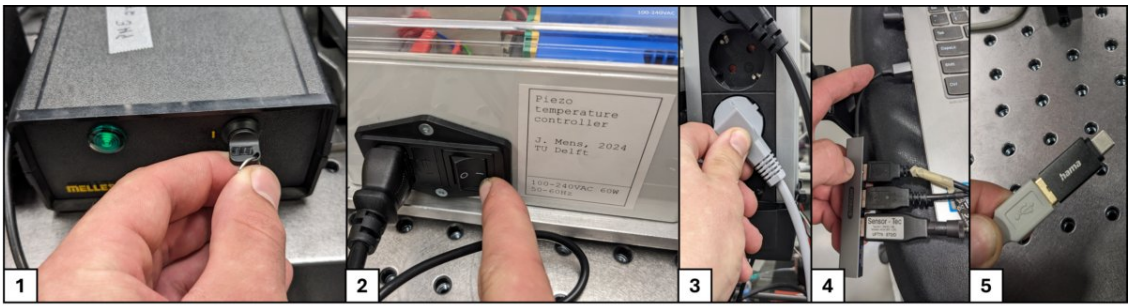

6. Turn on the PC that is connected to the pressure controller.
7. Turn on the pressure controller and the base station to which it is connected.
8. Start the pressure controller software CORA.

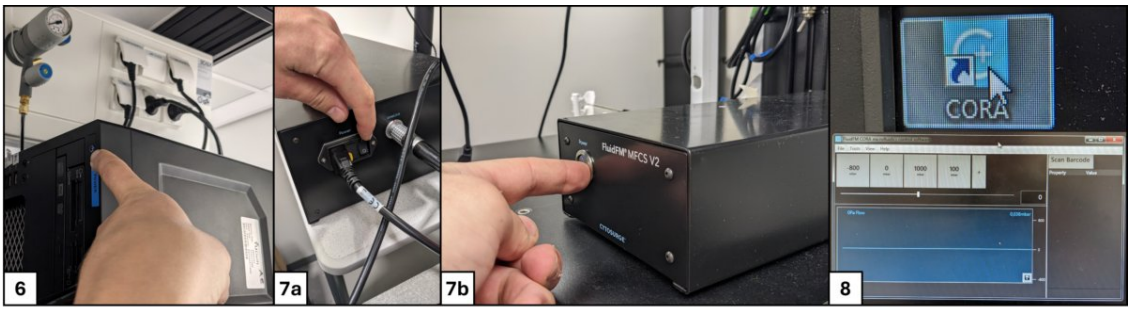

9. Start Matlab, TEC controller software, and DP sensor software.

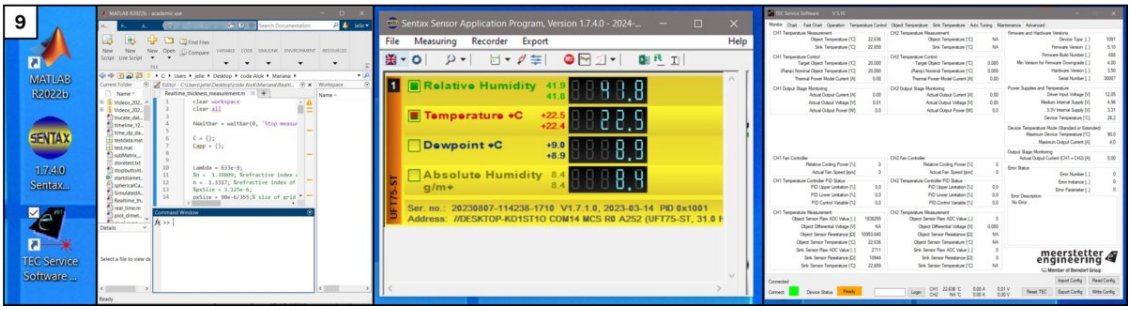

10. Connect the pressure line to a microfluidic cantilever.
11. Load the cantilever on the cantilever holder. It clips on and can slide over the holder 90 degrees, then rotate to its final position. When it is clipped on, rotate to the final position.
12. Start the data logging in the DP sensor software by pressing the T button and creating a save file.

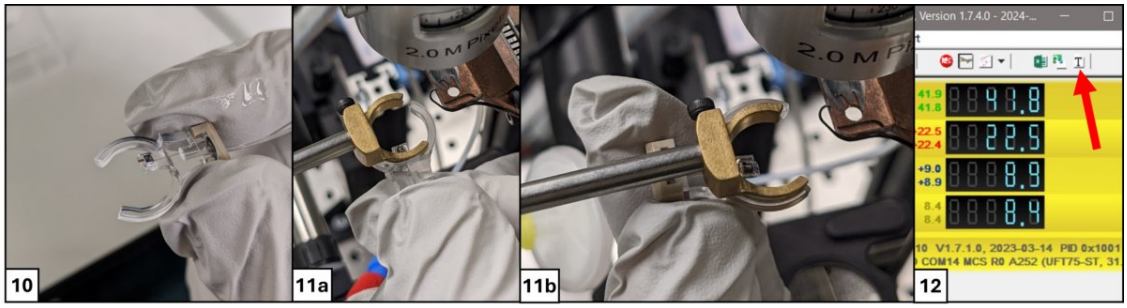

Test Setup Preparation Steps

1. Load an EM grid in the tweezers.
2. Rotate the height adjust wheel so it moves up. This ensures the grid does not touch the grid holder when the tweezers are installed.

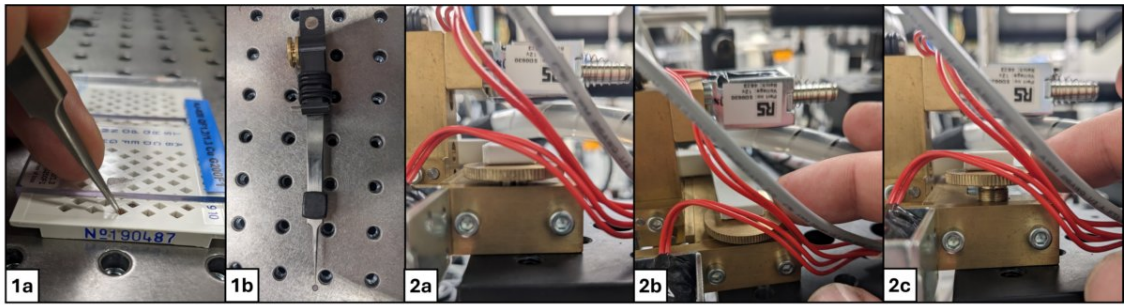

3. Put the plunger into the armed position by pushing against the solenoid that actuates the DPstage and rotation release. Push the plunger all the way up, push in the trigger solenoid to clear the trigger with the trigger toe, release the trigger solenoid, and the plunger is retained by the trigger mechanism. Let go of the release solenoid.
4. Unscrew the thumbwheel that locks the retaining pin in place, and rotate the retaining pin to the open position.

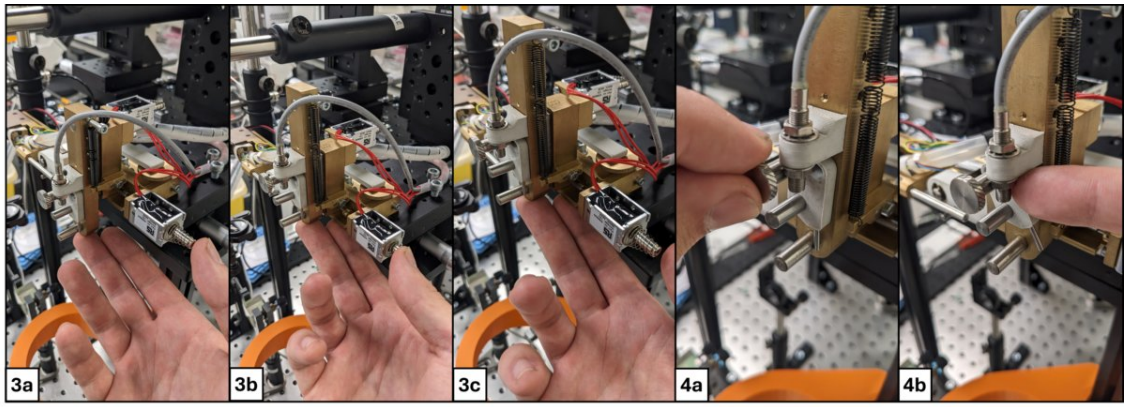

5. Install the tweezers on the plunger. Push the tweezer holder in an almost vertical position, all the way onto the rotation pin, and rotate the retaining pin back so it falls into the slot of the tweezer holder to prevent the tweezers from sliding off. Tighten the thumbwheel to secure the locking mechanism. The tweezers are now in the plunge start position.

6. Rotate the grid clip into the open position.

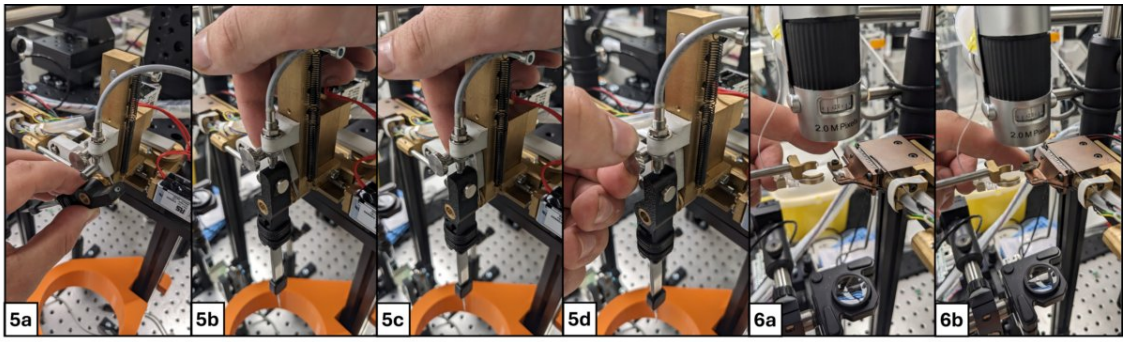

7. Push in the release solenoid again and rotate the tweezers up until the grid is some centimeters above the grid holder. Release the solenoid again to position the grid holder below the EM grid and lower the tweezers until they rest on the release pin.

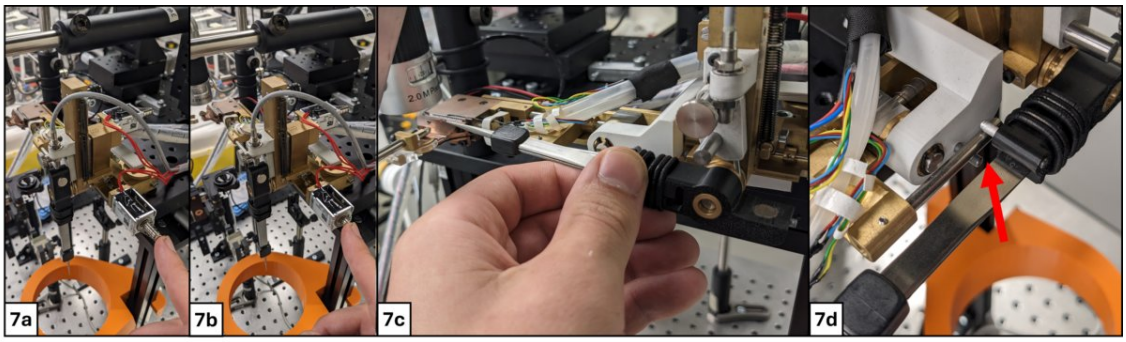

8. Use the height adjust wheel to lower the grid onto the grid holder. Shift the tweezers in its holder if the side-to-side or front-to-back position is not correct. There is room built into the tweezer holder to allow for this adjustment.
9. Rotate the grid clip to the closed position onto the EM grid.
10. Place the ethane cup in the holder below the plunger.

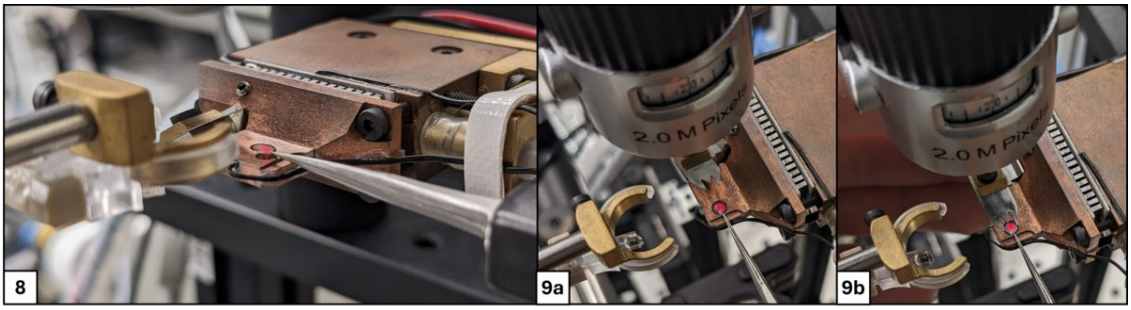

Step by Step Test Sequence

1. Go to the DP sensor software to see what the dew point is.
2. Press the water pump and fan buttons on the control box to turn on the water cooling loop.
3. Go to the TEC controller software, to the tab temperature control and manually type in the desired setpoint.
4. Go to the operations tab and select ”static on” in the drop-down menu in the CH1 output enable section.
5. Press the write config button in the lower right corner. This turns on the temperature controller and it will start cooling to the given setpoint.

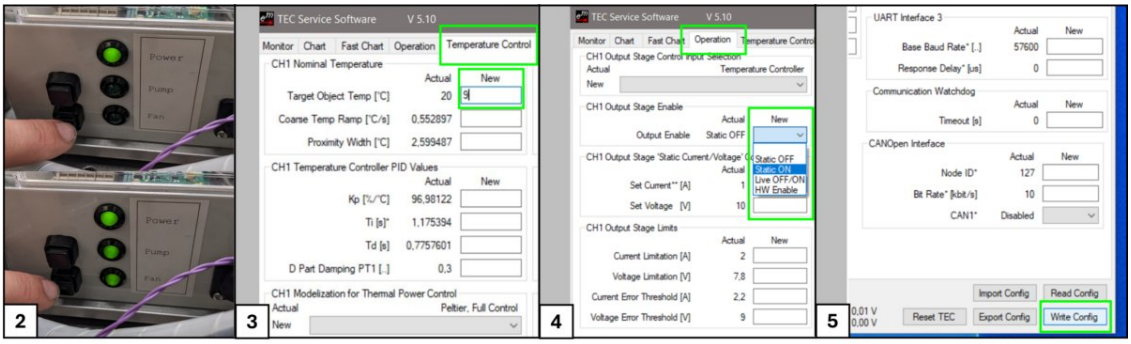

6. Run the real-time thickness measurement Matlab script. A preview window with a live feed of the interferometer data appears.
7. Use the preview window to position a grid square in the middle of the field of view. Make sure the exact grid location is noted based on the finder grid features. The interferometer may need adjusting if it is not properly aligned or out of focus. See the interferometer adjustment section on how to proceed.
8. **Turn off** the fan and pump again on the control box and wait for the interferometer image to stabilize.
9. Type a ”1” into the command line of Matlab and press enter to save the reference frame.
10. **Turn on** the water pump and fan again.
11. Follow the directions in Matlab. Give two points for the rotation and draw a square to crop the image, crop some distance away from the grid bars.

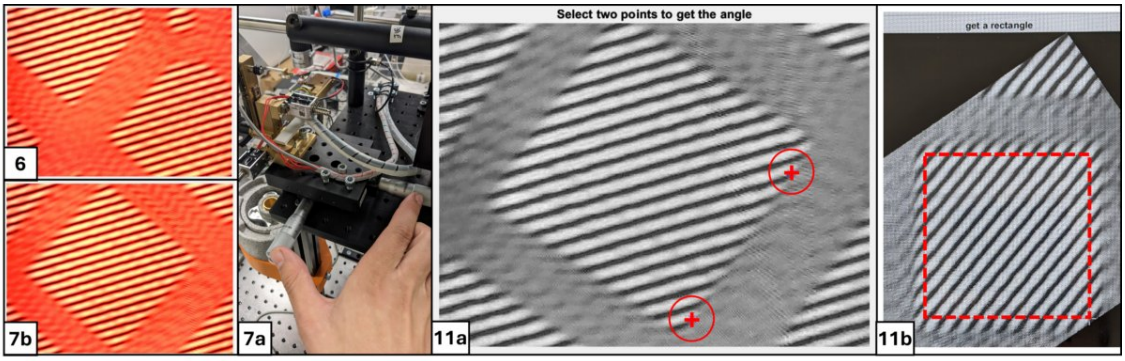

12. Move the USB camera to the position above the EM grid with the XYZ stage and use the Z stage to focus the camera on the grid.
13. Use the XYZ stage to move the cantilever into the field of view of the microscope, position the cantilever above the grid that was chosen before taking the reference frame. Do this with the cantilever XYZ stage **AND NOT** the XY stage of the mechanism!

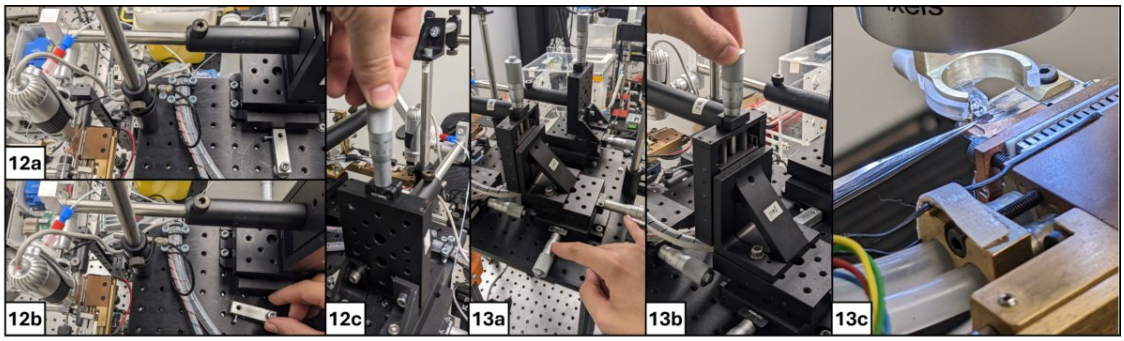

14. Lower the cantilever with the Z stage until it becomes sharp by entering into the focal plane of the microscope, adjusting in X and Y if needed to get the tip in the middle of the grid.

15. Turn off the fan and water pump again.
16. Start the recording in the USB camera app.
17. Dispensing: Lower the cantilever slowly until the cantilever bends down and touches the carbon film. Use the pressure controller to dispense some liquid. Use the Z stage to move the cantilever up and the X stage to move the cantilever as fast as you can, far enough that it will not be hit by the grid clip when it is moved to the open position before plunging.
18. Push the camera away and secure it with the stop lever.

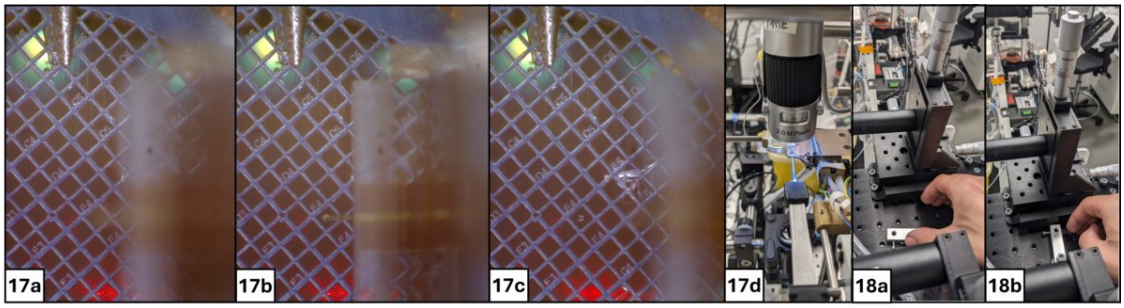

19. Type 1 in the Matlab command window and press enter. This starts the real-time thickness measurement.
20. Stop the recording in the USB camera app.
21. Monitor the measured thickness until a desired threshold is measured.
22. Start plunging procedure: Rotate the grid clip into the open position. Use one hand to push down the styrofoam ring around the ethane cup to clear the path of the tweezers during rotation. Use your other hand to push the green button to activate the plunging sequence.

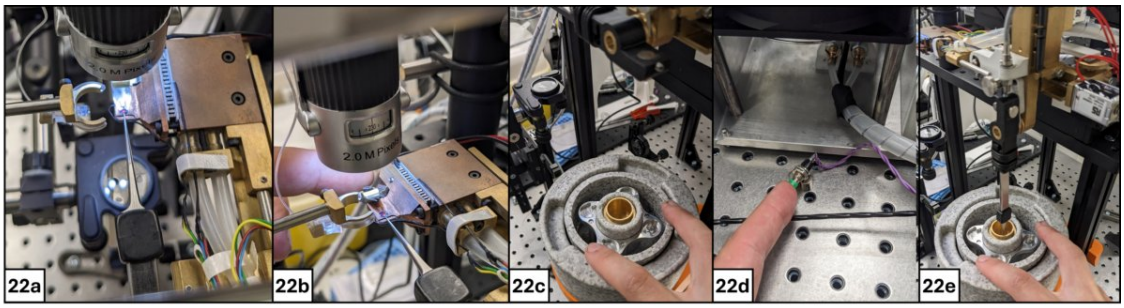

23. Release the styrofoam ring.
24. Press the cancel button in Matlab to stop the measurement (needs to be changed to a button that says stop at some point). Matlab will print that it is storing data and will also tell when it is finished storing data.
25. Turn on the pump and fan again (do not forget this!).

EM Grid Transfer to Storage

1. Unlock the thumbscrew and rotate the retaining pin to the side to free the tweezer holder.
2. Slide the plastic clip on the tweezers up while keeping the tweezers closed by hand.
3. Use one hand to move the plunger up and the other to rotate the tweezers to the side and lower the plunger again to drop the EM grid in the liquid nitrogen.
4. Slide the tweezers from the rotation pin.
5. Proceed with placing the grid into the storage unit.
6. A new test can be performed by starting again with step 1 of the test setup preparation steps.
7. Go to the shutdown procedure at the end of the last test.

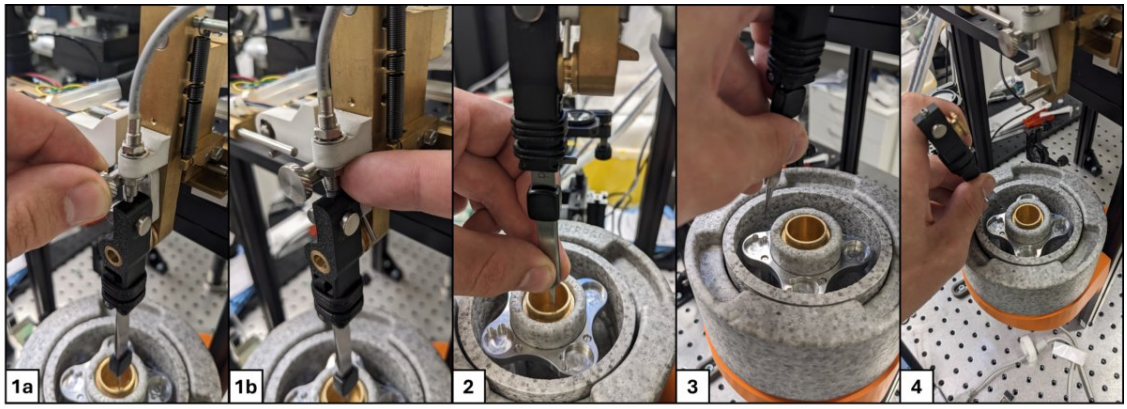

Shutdown Procedure

1. Go to the Maintenance tab in the TEC control software. Press the ”Export logged Monitor data to CSV file” button to export the data taken during the performed tests.
2. Go to the operations tab in the TEC control software. Select ”static off” in the drop-down menu in the CH1 output enable section.
3. Press Write Config in the lower right corner to turn off the DP stage.

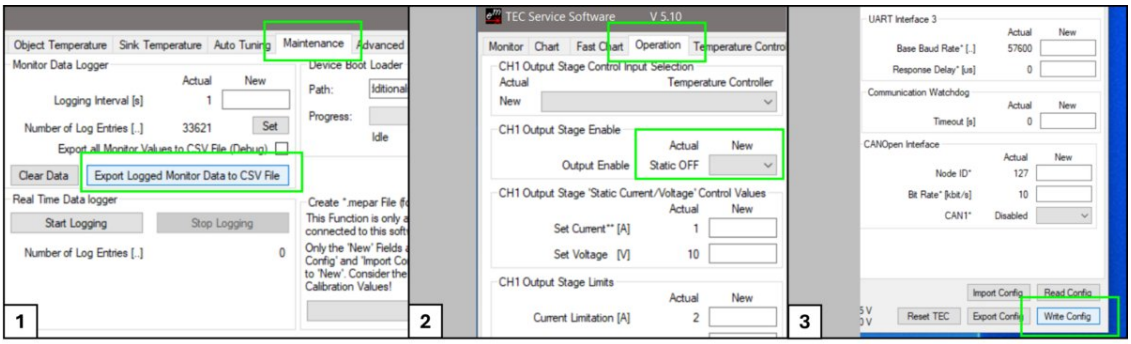

4. Turn off the pump and fan, and then turn off the control box. It may take some time to shut down due to the output capacity of the power supply; you can turn the fan briefly on to speed up the process.
5. Close the TEC control software (only if you are sure you stored the data!).
6. Go to the DP sensor software and press the T icon again. This stops the data logging. The data is stored in the .txt file that was created.
7. Close the DP sensor software.
8. Check if Matlab has finished storing the last data set and close Matlab.
9. Turn off the laser.
10. Close the pressure controller software and shut down the PC.
11. Turn off the pressure controller and its base station.
12. Disconnect the USB hub from the laptop.
13. Disconnect the phone from the USB microscope.
14. Make sure the plunger is left in the down position.
15. Cut the power to the plunge mechanism controller.

D.4. Recommendations

The following list of recommendations is given to improve the usability of the system:

1. Use a CCD that **does not** have an automatic brightness correction built-in. This would resolve the following issues:
   (a) Aligning the laser beams can be done more easily and precisely, because you do not have to be faster than the internal brightness correction anymore.
   (b) It can be seen in the raw measurement footage that the brightness control is constantly compensating, resulting in intensity changes over the entire field of view. This changes the grayscale values at places where there is no droplet and probably contributes to the noise in the measurement results.
2. Rewrite the Matlab code to have some user interface with simple buttons. The ”type 1 and press enter routine” adds more steps to an already complicated sequence of actions.
3. Rewrite the Matlab script to timestamp the raw data instead of recording the time passed since the start of the measurement. This would make the alignment of the DP sensor data, TEC controller data, and thickness measurement data a lot easier.
4. Change the tweezer position adjustment. There is only a fine-feed knob for adjusting the Z position of the grid and tweezers. The X and Y adjustments have to be made by manually wiggling the tweezers to the right position. This is somewhat difficult due to slip-stick effects. An adjustment system that can affect the X and Y position of the tweezers independently from each other would be much easier to use.
5. Add a quick retract style motion to the X axis of the cantilever XYZ stage, similar to the one used in the microscope. Retracting the cantilever far enough to clear the grid clip takes several seconds, making measurements of faster evaporating droplets nearly impossible.